NONDESTRUCTIVE EVALUATION OF ROCKET MOTORS; FINITE ELEMENT ANALYSIS OF SOLID PROPELLANT FAILURE

By
Scott A. Mullin
P. A. Cox
Charles E. Anderson, Jr.

SwRI Report 7958/802/1

July 1986

SOUTHWEST RESEARCH INSTITUTE
SAN ANTONIO HOUSTON

Unclassified
SECURITY CLASSIFICATION OF THIS PAGE

A192890

REPORT DOCUMENTATION PAGE

1a. REPORT SECURITY CLASSIFICATION Unclassified	1b. RESTRICTIVE MARKINGS None
2a. SECURITY CLASSIFICATION AUTHORITY	3. DISTRIBUTION / AVAILABILITY OF REPORT Unlimited
2b. DECLASSIFICATION / DOWNGRADING SCHEDULE	
4. PERFORMING ORGANIZATION REPORT NUMBER(S) 7958/802/1	5. MONITORING ORGANIZATION REPORT NUMBER(S)
6a. NAME OF PERFORMING ORGANIZATION Southwest Research Institute 6b. OFFICE SYMBOL (If applicable)	7a. NAME OF MONITORING ORGANIZATION Naval Surface Weapons Center
6c. ADDRESS (City, State, and ZIP Code) 6220 Culebra Road San Antonio, TX 78284	7b. ADDRESS (City, State, and ZIP Code) China Lake, CA 93555
8a. NAME OF FUNDING / SPONSORING ORGANIZATION Defense Logistics Agency 8b. OFFICE SYMBOL (If applicable) DTIC-DF	9. PROCUREMENT INSTRUMENT IDENTIFICATION NUMBER DLA900-84-C-0910, CLIN 0001AA
8c. ADDRESS (City, State, and ZIP Code) DTIC, Cameron Station Alexandria, VA 22314	10. SOURCE OF FUNDING NUMBERS PROGRAM ELEMENT NO. / PROJECT NO. / TASK NO. / WORK UNIT ACCESSION NO.

11. TITLE (Include Security Classification)
Nondestructive Evaluation of Rocket Motors; Finite Element Analysis of Solid Propellant

12. PERSONAL AUTHOR(S)
Scott A. Mullin, P. A. Cox, Charles E. Anderson, Jr.

13a. TYPE OF REPORT	13b. TIME COVERED	14. DATE OF REPORT (Year, Month, Day)	15. PAGE COUNT
Interim	FROM 9-85 TO 7-86	86-7-31	84

16. SUPPLEMENTARY NOTATION
Performed as a special task for the Nondestructive Testing Information Analysis Center

17. COSATI CODES		
FIELD	GROUP	SUB-GROUP

18. SUBJECT TERMS (Continue on reverse if necessary and identify by block number)
Nondestructive Evaluation, Shrike,
Cookoff, Peel Test
Finite Element Analysis,

19. ABSTRACT (Continue on reverse if necessary and identify by block number)
A linear elastic finite element model of the Shrike missile was developed and run in a series of parametric studies to determine the effect of a cookoff-induced gas bubble upon the missile case and propellant. A series of case-to-liner peel tests were also modeled in order to obtain fracture toughness values of the case-liner interface. The model identified the critical gas bubble pressures to rupture the case or propellant, and evaluated the peel tests for their worthiness in the cookoff situation.

Keywords:

20. DISTRIBUTION / AVAILABILITY OF ABSTRACT ☒ UNCLASSIFIED/UNLIMITED ☐ SAME AS RPT ☐ DTIC USERS	21. ABSTRACT SECURITY CLASSIFICATION Unclassified
22a. NAME OF RESPONSIBLE INDIVIDUAL Charles E. Anderson, Jr.	22b. TELEPHONE (Include Area Code) (512) 522-2313 22c. OFFICE SYMBOL

DD FORM 1473, 84 MAR
83 APR edition may be used until exhausted.
All other editions are obsolete.

SECURITY CLASSIFICATION OF THIS PAGE
UNCLASSIFIED

NONDESTRUCTIVE EVALUATION OF ROCKET MOTORS; FINITE ELEMENT ANALYSIS OF SOLID PROPELLANT FAILURE

By
Scott A. Mullin
P. A. Cox
Charles E. Anderson, Jr.

SwRI Report 7958/802/1

July 1986

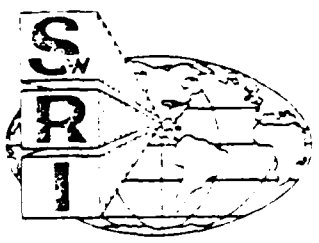

SOUTHWEST RESEARCH INSTITUTE
SAN ANTONIO HOUSTON

TABLE OF CONTENTS

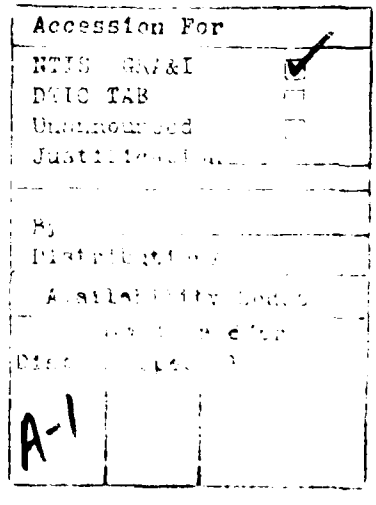

LIST OF FIGURES

LIST OF TABLES

I. INTRODUCTION

A hypothesis for one of the failure mechanisms of a rocket motor case is heat transfer through the outer case of the rocket causing the liner between the propellant and case to degrade. Pyrolysis of the liner then occurs, resulting in a pressurized bubble which may be of sufficient magnitude to cause the propellant to tear or rupture. This tearing or rupturing will expose more propellant to hot gases, thereby giving more surface area to burn. If the propellant ignites, it could cause a violent, uncontrolled reaction. The scope of work for this task was to perform a structural analysis on the rocket in the cookoff scenario, to determine what stresses and strains occur in the propellant and motor case, and to evaluate the bubble hypothesis as a cause of violent reactions.

II. DESCRIPTION OF ANALYSIS APPROACH

A. Rocket Motor

The rocket motor can be a complex analysis problem, with a thin outer case of a strong material (steel or aluminum), a liner/insulator material which is usually rubber-like in behavior, and a thick inner core of propellant, which also generally behaves in a nonlinear, rubber-like fashion. The analysis approach used in this report was to construct an accurate finite element model of the rocket geometry and material properties. A finite element model is a very convenient form in which to do parametric studies, where one parameter can be changed (such as propellant thickness) and the resulting effect can be determined.

A typical rocket motor configuration is shown in Figure 1, with a section view showing the different propellant thicknesses of the core interior. Also included in Figure 1 is a figure illustrating the bubble hypothesis. The finite element model was based upon the geometry in Figure 1, with the actual dimensions and material properties coming from the Shrike, a typical missile involved in the cookoff problem. The model contains the steel case, the liner, and the propellant.

The structural analysis was performed with TEXGAP, a linear finite element code which was written for solid propellant applications. The TEXGAP code contains a reformulated element (to avoid locking) for use with rubber-like materials, i.e., materials with a Poisson ratio close to 0.5. This code also contains an element formulated for a bimaterial crack singularity.

A two dimensional, axisymmetric, linear model of the rocket configuration was used in the analysis. This model is a first approximation to the problem. The two dimensional model is a simulation of a pressurized, radially symmetric bubble between two layers of a flat, circular plate. This model ignores curvature effects, but was chosen for three reasons. First, it was desired to get a feel for both the problem and the tendencies of TEXGAP using the simplest representative problem. Second, a two dimensional model is cheaper than a full three dimensional model due to the smaller number of degrees of freedom. Third, the two dimensional model was expected to give answers that were reasonably accurate, especially when the bubble size is

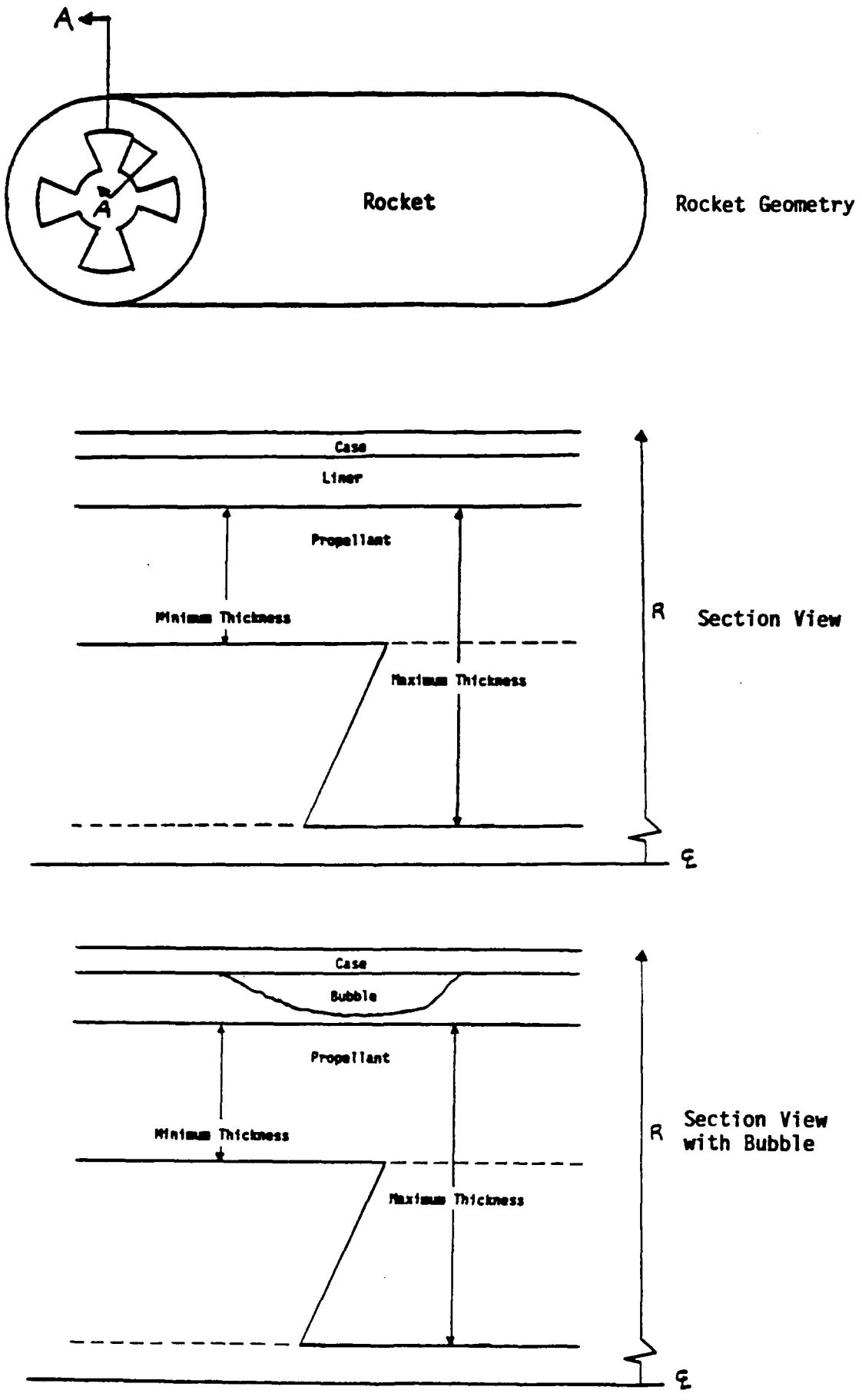

Figure 1. Rocket Motor Configuration

small compared to the rocket diameter. The linear analysis was chosen over a nonlinear analysis because a nonlinear model requires biaxial stress-strain material data, which is nonexistent in the open literature for the propellant and liner.

The model was composed of quadratic elements. The thickness of propellant was designed to be easily changed from the minimum thickness, between the webs, to the maximum thickness, including the webs. In this way a parametric study on the effects of propellant thickness could be performed. Since the linear code requires material input of only the elastic modulus E, and Poisson's ratio ν, the liner and propellant were modeled as one material since they have nearly the same E and ν. The material properties used in the model are shown in Table 1, from References 1 and 5.

Table 1. Rocket Model Material Properties

Material	E(psi)	ν
Steel (4340)	29.0×10^6	.30
Propellant	1100.	.49
Liner	1100.	.49

The bubble was modeled as a crack between the case and the liner/propellant interface. When a pressure is applied to this surface, it opens up as a pressurized bubble would. The model was designed so that the crack length could be changed easily for parametric studies. Figure 2 shows the finite element model for the minimum thickness of propellant, and Figure 3 gives a close-up of the crack tip region. This representation of the bubble was felt to be the most accurate, based upon engineering judgement of the situation.

For several of the procedures being studied to mitigate the cookoff event, it is likely that one area of the motor case would heat faster than surrounding areas, causing localized bubble formation. Adjacent areas to the bubble, which had not been heated sufficiently to cause degradation of the liner, would still maintain the bond between case and liner. The steel case and the thick propellant would offer resistance against the bubble's growth, so it is most likely that a thin, elliptical bubble would result. This type of bubble would have very thin, crack-like edges to it, which would be areas

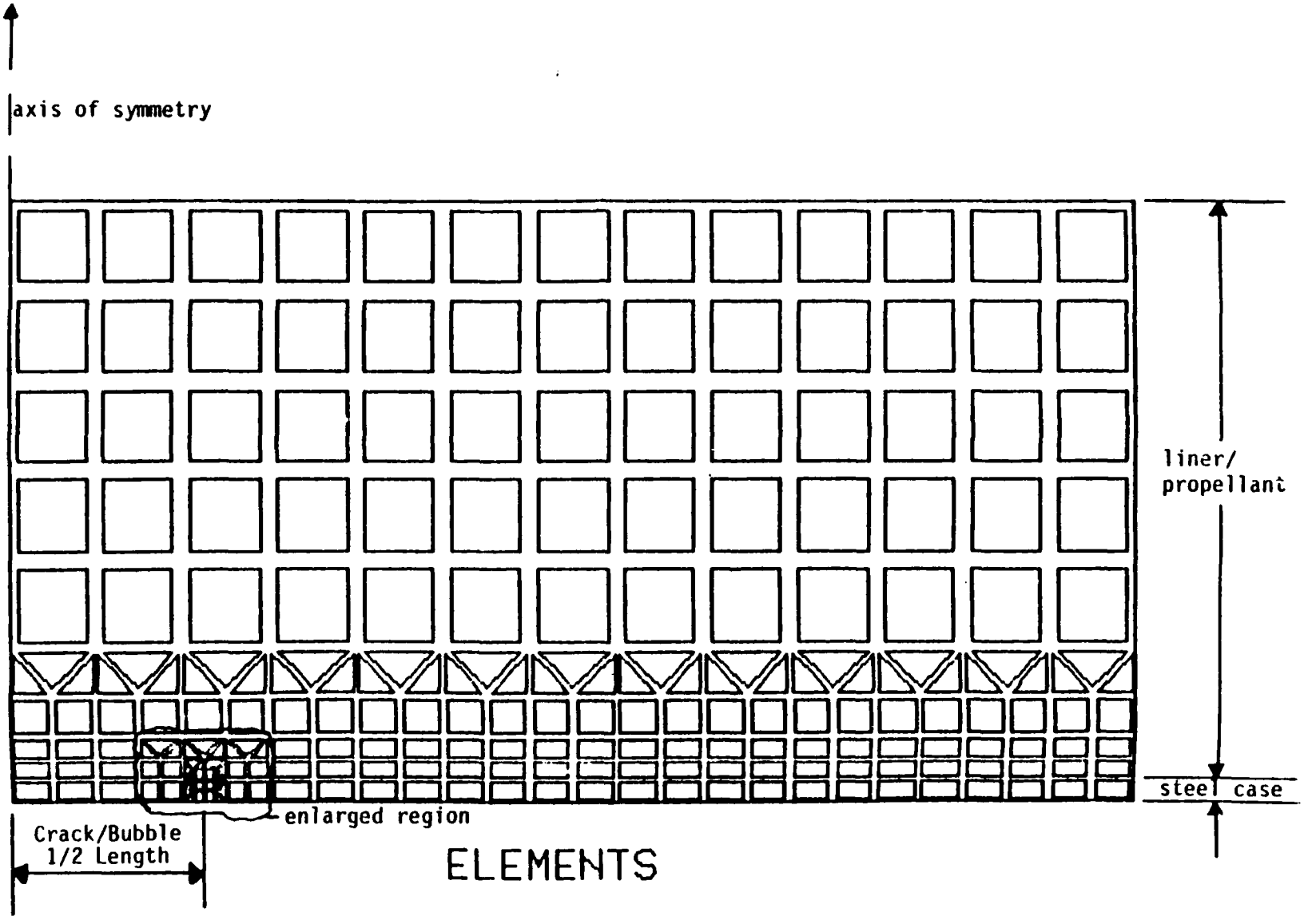

Figure 2. Flat Plate Two Dimensional Axisymmetric Rocket Model

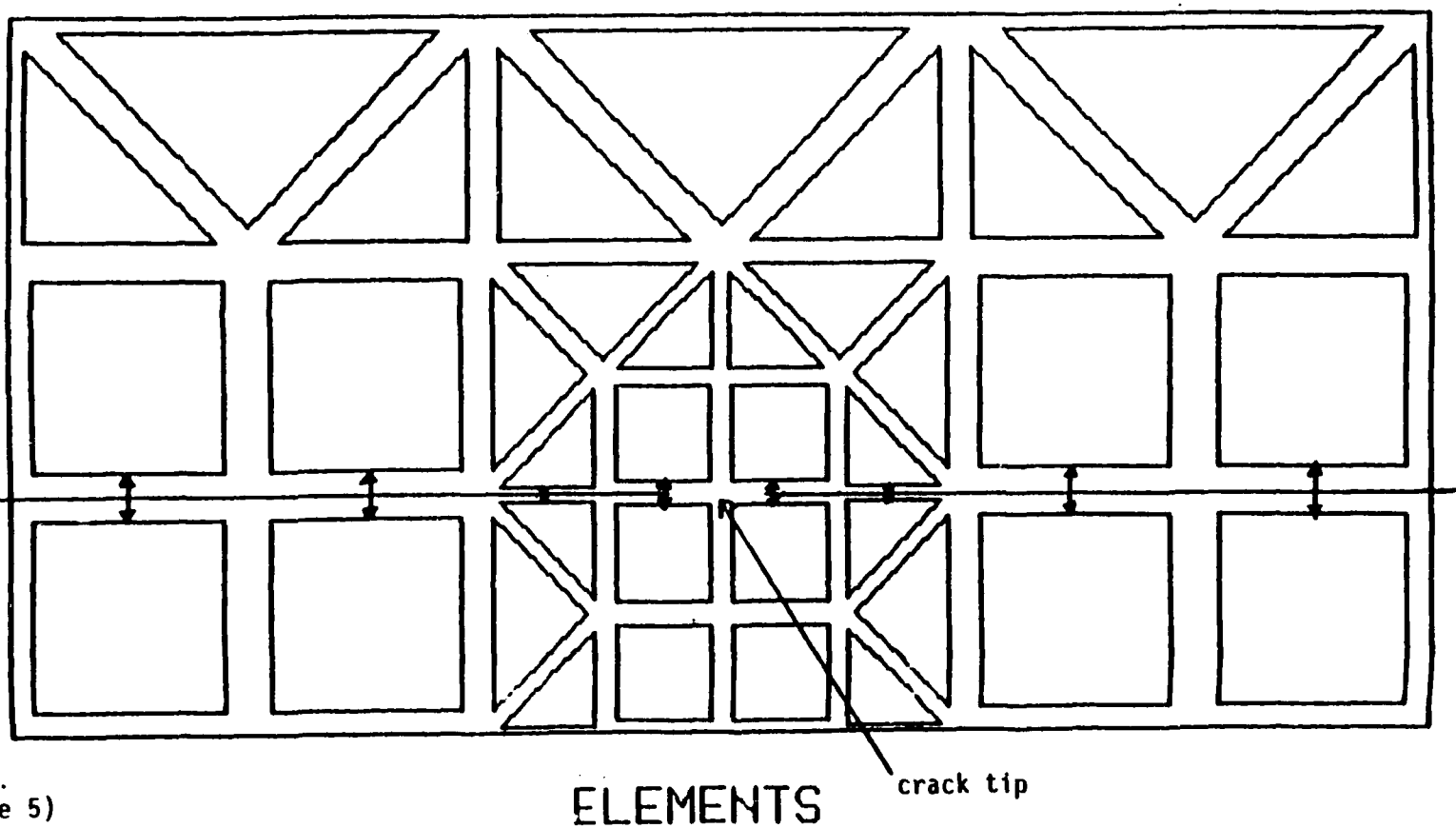

Figure 3. Enlargement of Figure 2

of stress concentrations. In the limit, these stress concentrations become singularities where the stresses go to infinity. This type of stress problem cannot be resolved with normal finite elements. To be able to model those types of singularities, the crack tip and crack type elements have been used.

The pressure loads occurring in the bubble have not been defined at this time. They must be determined experimentally or by a coupled heat transfer/ mechanical model that treats liner pyrolysis and the mechanical distortions in the case, liner and propellant (this point is discussed in more detail in Section V). However, in a linear elastic analysis, all of the displacements, strains, and stresses will scale linearly with the load. This allows a single load to be chosen to obtain the stresses, strains, etc. A different loading will change the results by the ratio of loading valves. The load chosen to determine the performance of the model was 100 psi, applied internally along the crack face. The boundary conditions and size of the model were chosen to isolate the effects of the bubble upon the model. Figure 4 shows the deformed model and the boundary conditions. A close-up of the deformed crack tip region is shown in Figure 5.

The output from the model includes stresses, strains, and K_I and K_{II} stress intensity factors at the crack tip. The stress intensity factors are a measure of the crack's potential to grow. They are computed, then compared to the material property called fracture toughness, just as stress is computed and compared to the yield or ultimate strength of the material. K_I is the stress intensity factor which is associated with a crack opening motion, and K_{II} is associated with a crack sliding motion. The numerical results indicated that there were no severe element distortions occurring, and that there were no areas of unusually high stress or strain caused by improper boundary conditions.

The analysis approach for the rocket model involved varying the parameters of crack length and propellant thickness for the given load of 100 psi. For each case analysed, the finite element results were examined to determine the locations of maximum stress, and the stress intensity factors at the crack/bubble tip were noted. Variations in propellant thickness were made to determine the effects the inner core webs would have upon the results. The crack/bubble length was increased to see what effect an increase in bubble size would have upon the stresses and stress intensity factors. Maximum stresses in the model were compared to manufacturer's data on the ultimate

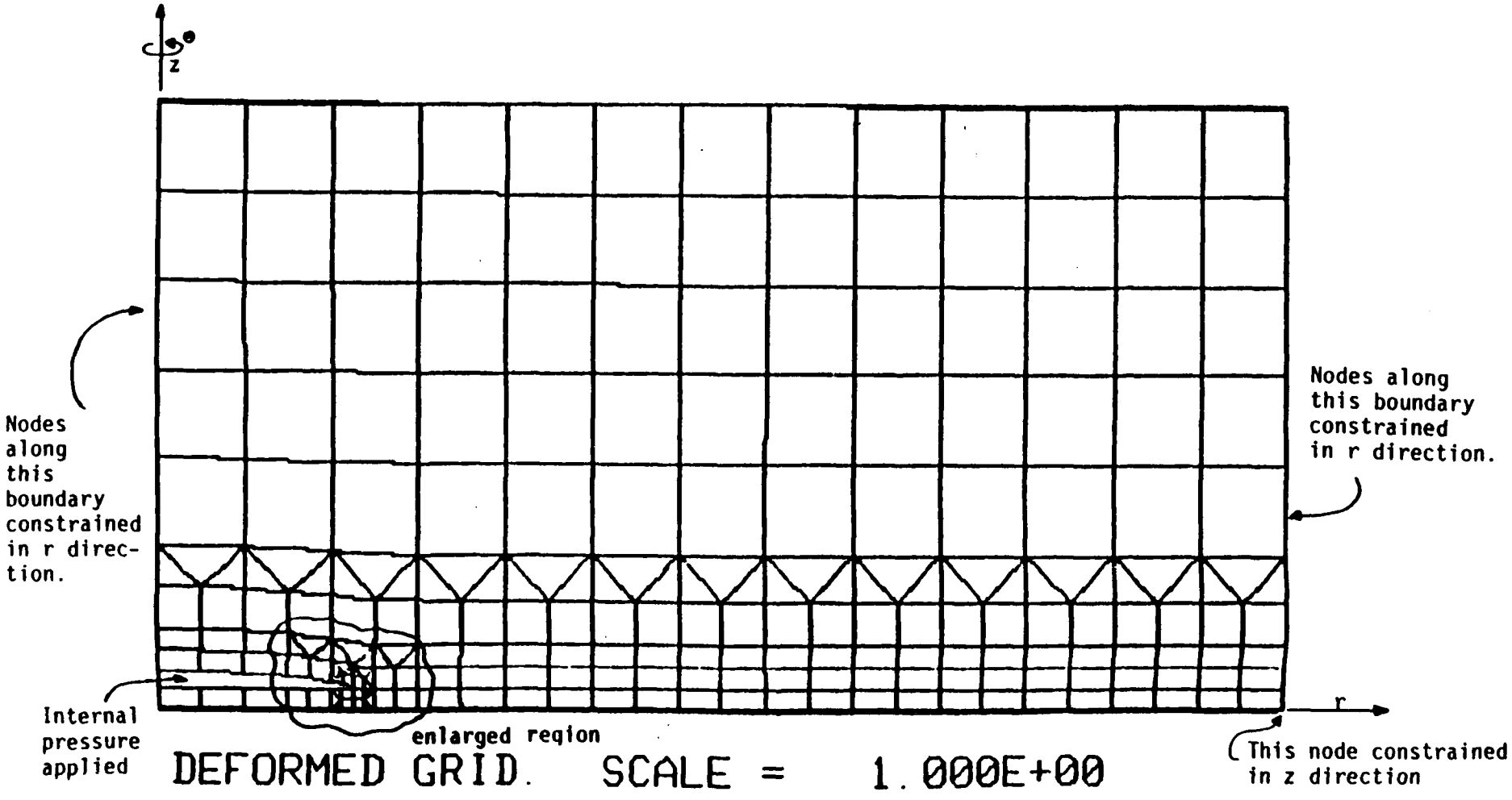

Figure 4. Deformed Rocket Geometry P = 100 psi

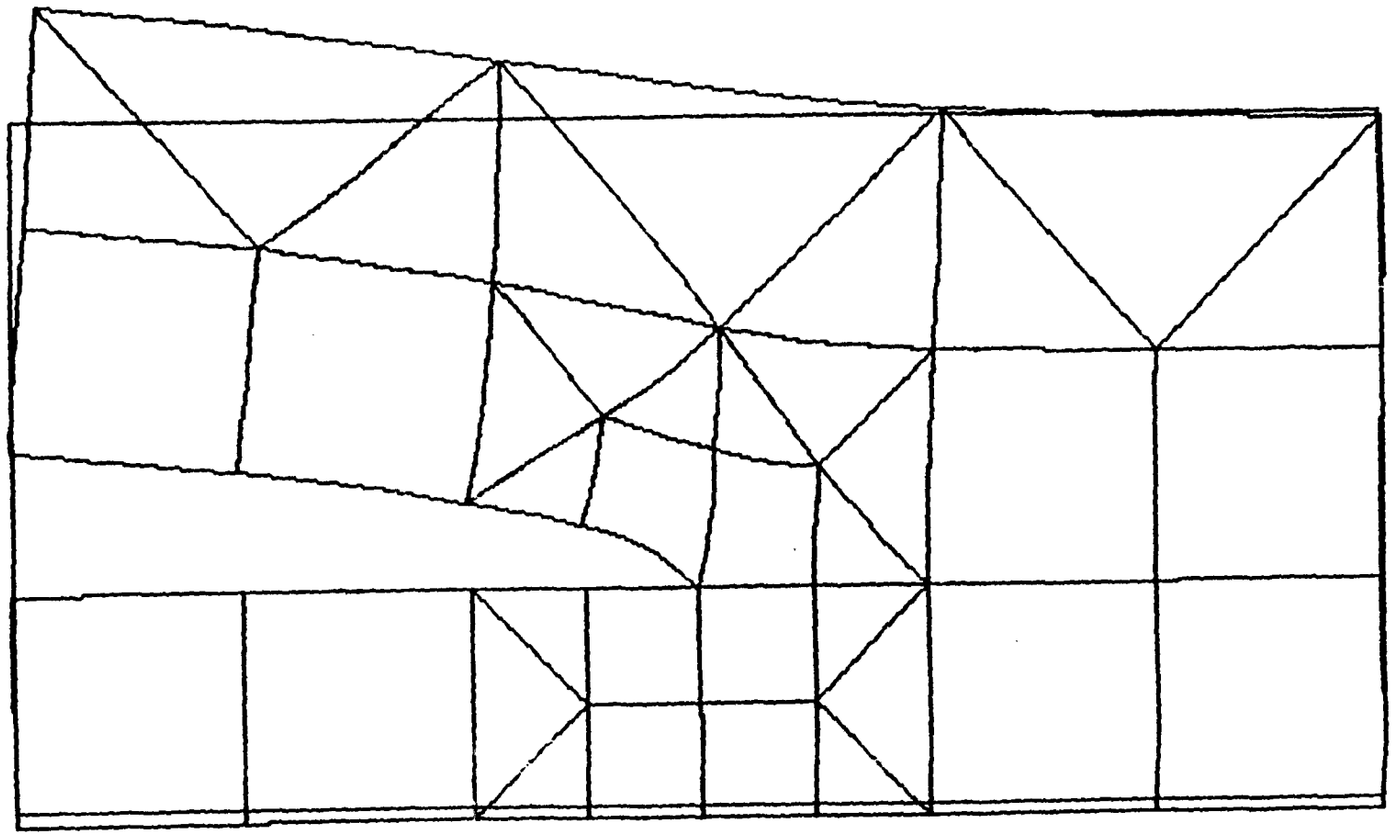

Figure 5. Enlargement of Figure 4

uniaxial strength of the propellant. A fracture toughness value, for comparison to the stress intensity factors, was not available in the literature, so finite element modeling of liner-case peel tests was undertaken to establish the fracture toughness for the liner-case bond. The analysis description of the peel tests is presented in the next section. A complete discussion of the results appears in Section III.

No temperature effects were included in the model. The reason for this was mainly the lack of high temperature data for the material properties of propellant and liner, and the lack of high temperature peel test, or similar unbonding type test data.

B. Peel Tests

In addition to a failure criteria for the propellant, the fracture toughness of the liner-case interface has to be determined in order to have comparison figures for the K_I and K_{II} stress intensity factors which occur at the rocket model crack tip. In order to obtain representative numbers for the peel strength of the liner-case interface, a series of tests were performed at five different peel angles (Ref. 2). The test specimen, test fixture and peel parameters are shown in Figure 6 reproduced from Reference 2. The approach taken here was to model the peel tests in TEXGAP; this modeling was similar to that of the pressurized bubble between the propellant and the motor casing. Values of K_I and K_{II} were computed by the finite element model for each peel angle. These values of K_I and K_{II} define a curve in K_I - K_{II} space. Since the peel loads used to determine the K_I and K_{II} values are the loads required to fail the bond, the curve they map out would be a region of facture toughness states. Thus, if a numerical simulation using the rocket model produces a K_I - K_{II} point inside the curve, the crack will not propagate; if the point lies outside the curve, the fracture toughness is exceeded and the crack will run.

A number of models were constructed and tested before a final model configuration was selected. In order to be comparable with the rocket motor analysis, a linear model was constructed. The loads, from the mean peel strength data given for each peel angle in Figure 6, caused severe element distortions in the model. Since the analysis was linear, the peel loads were divided by ten to give scaled results with less element distortion.

Peel Parameters.

Position	Peel angle, deg	Peel speed, V_{PS}, in/min	Test bed speed, V_{TB}, in/min
1	49	5.62	2
2	73	7.30	5
3	90	5.00	5
4	110	3.62	5
5	133	2.85	5

Averaged Peel Strength Data.

Missile insulation	Position	Average loads, lb/in			Mean load, lb/in	Standard deviation
Shrike, Mods 4 and 7	1	169	166	163	166	3.00
	2	76.6	82.3	77.8	78.9	3.00
	3	54.0 54.0	49.7	49.0	51.7	2.70
	4	41.1 41.4	40.0	42.4	41.2	0.99
	5	38.3	38.4	38.7	38.5	0.21

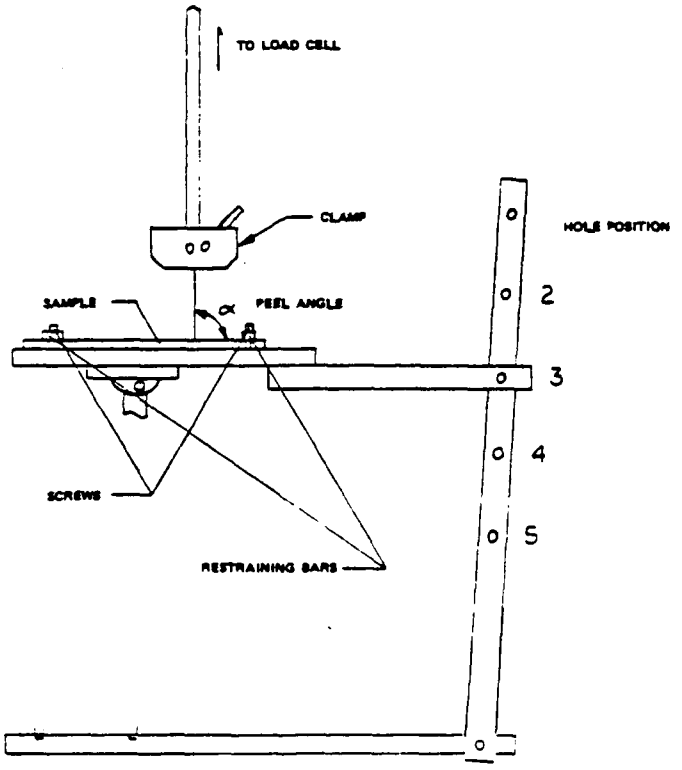

Variable Peel Angle Test Fixture.

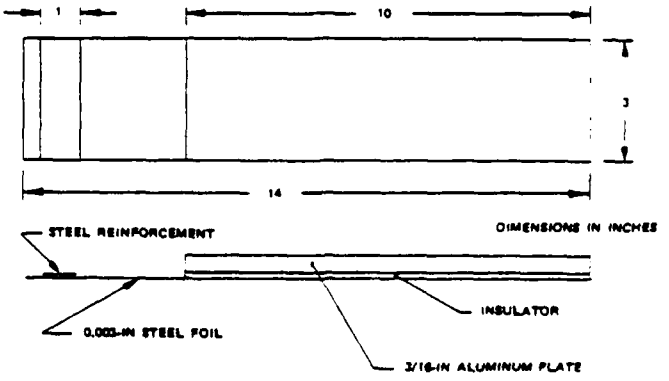

Peel Test Specimen.

Figure 6. Peel Test Description

The actual peel test was arranged to maintain a constant peel angle while the liner was peeled from the casing material (Ref. 3). The finite element model was required to follow this type of behavior. Boundary conditions were applied to the finite element model to maintain constant peel angle in the model.

The peel test finite element model finally chosen is shown in Figure 7, with a close-up of the crack tip region shown in Figure 8. As mentioned previously, the model material behavior was assumed to be linear. The material properties used in the model are shown in Table 2 from References 1 and 5. The model was solved with a plane strain assumption, which is warranted by the width of the test specimens. The elements were quadratic. The aluminum plate and the liner material shown in Figure 6 were modeled; but the steel foil was not, due to its thinness. The steel foil provided the means for transferring the peel load to the insulator/liner. It is very strong, compared to the liner, in the longitudinal pull mode, but due to its thinness it provides virtually no bending moment. The action of the steel foil was introduced to the model by adding tie elements to the top surface of the liner. These elements constrain the nodes to slide together, simulating the steel foil action. These tie elements also acted as a boundary condition to keep the deformation of the model along the original peel angle, simulating the results of the actual peel tests. The mean peel load, divided by ten to reduce distortion, was applied to the section of the model which simulated a portion of the already peeled liner. The mean peel load remained almost constant during the tests (Ref. 3), which indicated that the fracture toughness of the liner-case interface remained constant as the liner was peeled off.

Table 2. Peel Test Model Material Properties

Material	E(psi)	ν
Aluminum	10.0×10^6	.32
Liner	1100.	.49
Steel (Tie elements)	29.0×10^6	.30

The radius of curvature was made equal to the liner thickness to give a smooth transition between the horizontal portion of the model and the portion of the model which lays along the peel angle. The thickness of the aluminum

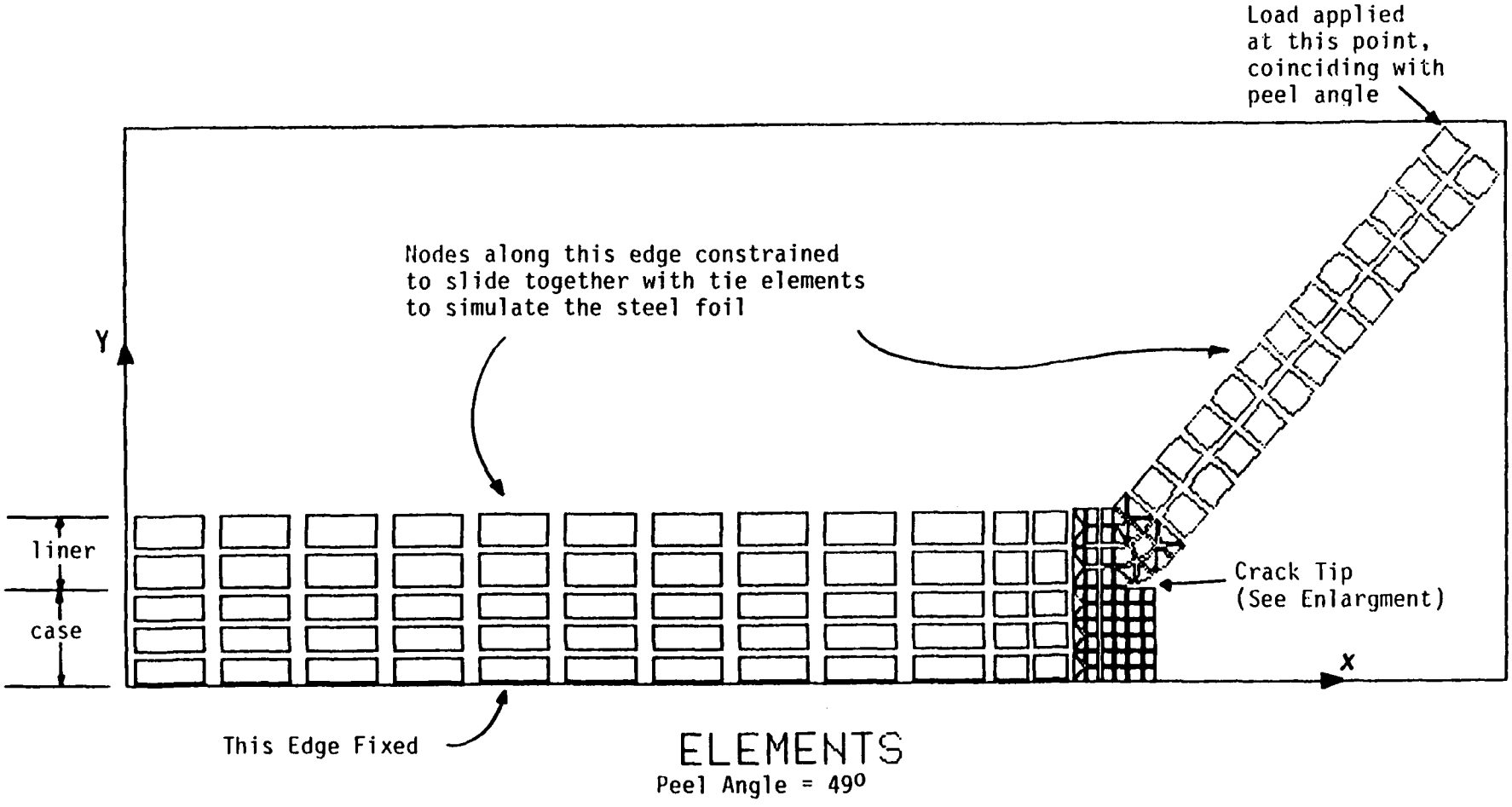

Figure 7. Peel Test Plane Strain Model

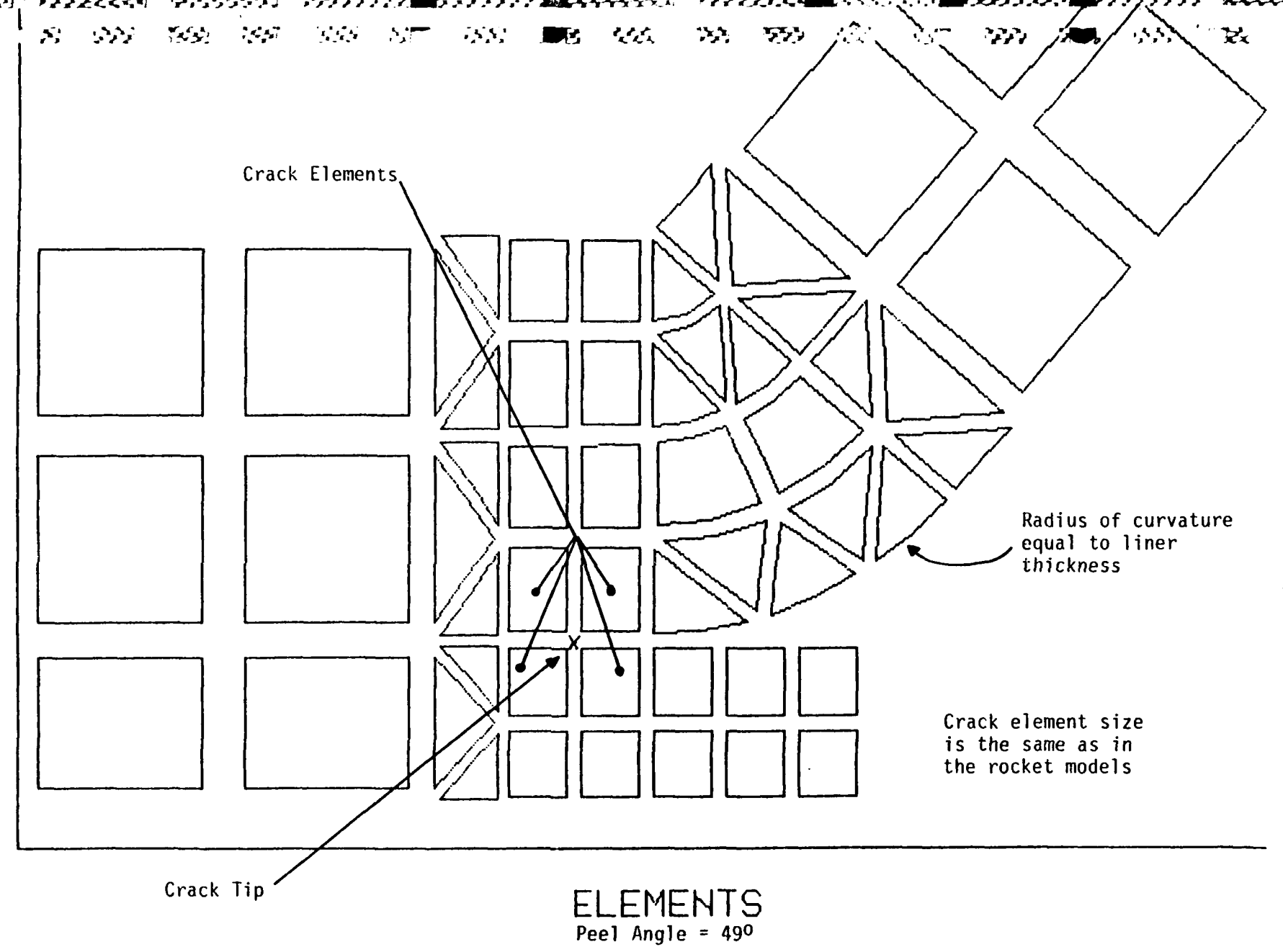

Figure 8. Enlargement of Figure 7

plate came from the actual peel test configuration, and the thickness of the liner was based on the Shrike rocket configuration, since it was not given in Reference 2.

The stress intensity factors, K_I and K_{II}, are computed in TEXGAP through a special contour integral which numerically integrates along the perimeters of the crack elements. For this reason, the size of the crack elements can affect the stress intensity factor calculations. If the crack elements are too small, or large, the answers they give may be severely distorted also. In order to eliminate any possible discrepancy, the size of the crack elements in the rocket model and the peel test model were made the same. A sensitivity analysis was performed with the peel test model, using crack element sizes twice as large and half as small as the current size. The results showed a variation of less than 10 percent, indicating that the current crack element size is valid.

The location of the crack in the model was another important consideration. From a qualitative point of view, the tip of the crack would be expected to be right at the point where the curved portion of the model connects to the flat portion. A requirement of the crack element, however, is that its sides have to be straight. Also, the stress intensity factor calculation is formulated for a slit type crack surrounded by crack elements, which has an opening of zero degrees. Since the crack elements have to surround the crack tip, it would be impossible to satisfy the above criteria while placing the crack tip right at the point where the curved and flat portions meet. The decision was made to move the crack back one element length (.028 in) in order to overcome these problems (see Figure 8). Since this distance is small, the model did not display any unusual behavior. The results of the peel test model will be discussed in Section III.

III. RESULTS

A. Rocket Model

The rocket model described in Section IIA was run in a number of different configurations. The internal pressure load applied to all the different models was 100 psi, which was used as a test value, rather than a specific cookoff-determined valve. Since the internal geometry of the rocket propellant can vary between a minimum and maximum thickness, as shown in Figure 1, the effect of propellant thickness was determined by running two different thicknesses. These thicknesses correspond to the minimum and maximum propellant thicknesses of the Shrike rocket. These runs were intended to give bounds upon the stress, strain, and stress intensity factor values.

To determine the effect of a growing bubble upon the stresses developed in the rocket, the crack/bubble length was varied in the models. The lengths chosen were ½ inch and 1 inch. These lengths would correspond to bubble diameters of 1 and 2 inches, respectfully. Both of these lengths were used in all models to determine the trends.

The thin and thick propellant models described above do not reflect the fact that a significant portion of the liner material may be removed (turned into a gas, creating the bubble) in the cookoff process. It is not currently known how much liner material would degrade and pyrolysize during the cookoff process. In order to examine the effect of the removal of some of the liner material, two models with some of the liner elements deleted were run to determine trends. Both of these models had the minimum propellant thickness, with crack/bubble lengths of ½ and 1 inch. The different model configurations are summarized in Table 3. Plots of the initial and deformed geometries of all the cases described above are given in Appendix A.

The failure criteria of the rocket propellant are based upon maximum stress and strain room temperature values for the Shrike rocket propellant from Reference 1. These values are reproduced in Table 4, along with ultimate stress and strain data for the case from Reference 5. It is believed that these results come from uniaxial stress tests.

Table 3. Rocket Model Configurations

Crack/Bubble Length (in)	Minimum Propellant Thickness	Maximum Propellant Thickness	Some Liner Removed*
½	X	X	X
1	X	X	X

*These models used the minimum thickness propellant

Table 4. Rocket and Case Mechanical Properties

Material	E(psi)	σ_m(psi)	ε_m (in/in)
Propellant	1100	160.	.21
Steel (4340)	29.0×10^6	160,000.	.16

The state of stress and strain in the rocket model is triaxial. (There are r, z, and θ components. The theta component is due to the axisymmetric analysis.) In order to compare the rocket stresses and strains with those in Table 4, the principal stresses and strains at each node are noted, and a von Mises stress and strain is also computed using these principal values. The von Mises criteria is usually used to define the yield point for linear elastic materials. We have used the von Mises criteria in this analysis to define the failure point, which is a valid approach because the model is linear elastic. In that manner, the maximum value of stress for comparison to the failure values at a node will either be one of the principal values, or the von Mises stress. Shear stresses and strains are not used as failure criteria because material failure values for comparison do not exist. The von Mises stresses and strains are computed from the following formulas, where the 1, 2, and 3 subscripts represent the principal values.

$$2\sigma_{vm}^2 = (\sigma_1 - \sigma_2)^2 + (\sigma_1 - \sigma_3)^2 + (\sigma_2 - \sigma_3)^2$$

$$2\varepsilon_{vm}^2 = (\varepsilon_1 - \varepsilon_2)^2 + (\varepsilon_1 - \varepsilon_3)^2 + (\varepsilon_2 - \varepsilon_3)^2$$

The following figures and tables show selected values of the r, z and θ components of stress and strain, the principle stresses and strains, and a von Mises stress and strain for each of the rocket models in Table 3. The stress intensity factors, K_I and K_{II}, are also reported on these figures. Results are given for the propellant and the case, and also for the liner. The areas of principle concern for failure in the rocket are the propellant and the case. The liner values are given only for comparison to peel test valves, and to show trends in the stress/strain patterns. A failure in the liner alone would not significantly influence the cookoff problem. The primary failure mode investigated for the liner would be the ability of the bubble to advance down the liner-case interface. This will be determined by examining the stress intensity factor values at the edge of the bubble (crack tip), and comparing them to the peel test model results, which are reported next.

Location Guide For Stress and Strain
Minimum Thickness Propellant Rocket Models

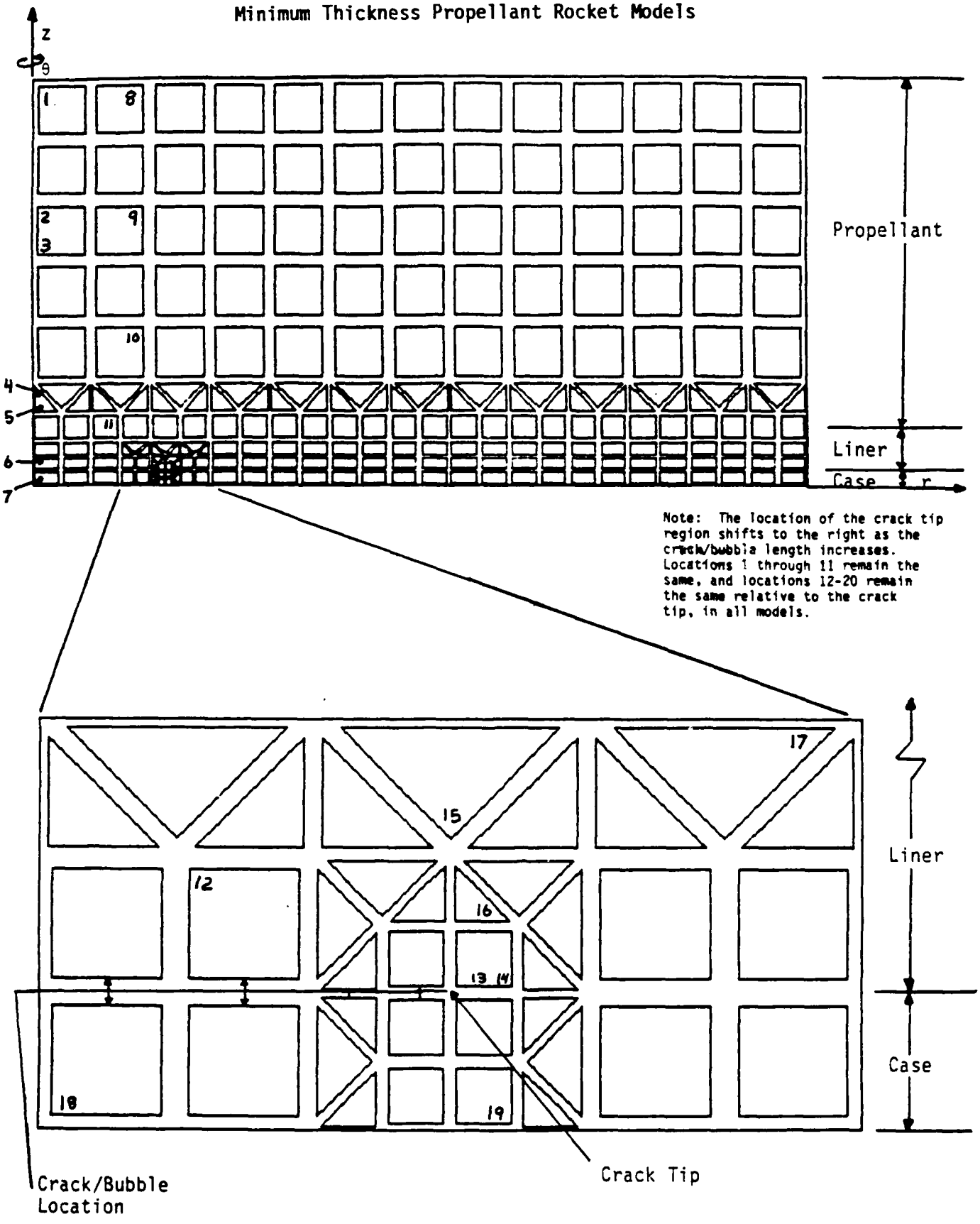

Figure 9

Table 5. Output Values From Minimum Thickness Propellant Models

Crack/Bubble Length = ½ inch

K_I = 212.9 psi. √in. K_{II} = 313.7 psi. √in.

(All stress values in psi, positive denotes tensile value)

Location	σ_r	σ_z	σ_θ	σ_1	σ_2	σ_3	σ_{vm}
1	9.3	0	9.3	9.3	0.4	9.3	8.9
2	3.4	-7.4	3.4	3.4	-7.4	3.4	10.8
3	2.8	-18.4	2.8	2.8	-18.4	2.8	21.2
4	-8.2	-74.9	-8.2	-8.2	-74.9	-8.2	66.7
5	-26.0	-89.0	-26.0	-26.0	-89.0	-26.0	63.0
6	-76.5	-100.2	-76.5	-76.5	-100.2	-76.5	23.7
7	11320	24.1	11320	11320	24.1	11320	11296
8	5.5	0	6.5	5.5	0.1	6.5	6.0
9	1.0	-3.5	2.6	4.1	-6.6	2.6	10.0
10	-5.0	-13.3	3.5	6.0	-24.3	3.5	29.1
11	-14.6	-58.5	-8.4	1.9	-75.0	-8.4	72.3
12	-31.9	-97.6	-49.1	-29.6	-99.9	-49.1	62.9
13	187.5	195.3	187.4	199.3	183.5	187.4	14.3
14	108.4	114.3	108.2	117.0	105.7	108.2	10.3
15	-17.4	67.6	34.2	91.4	-41.1	34.2	115.1
16	17.3	161.5	77.3	166.0	12.8	77.3	133.2
17	5.5	20.1	15.3	23.2	3.3	15.3	17.4
18	6846	-5.6	8679	6859	-18.5	8679	7945
19	575	23.6	4972	589	9.9	4972	4699

Table 5. Output Values From Minimum Thickness Propellant Models (Cont'd)

Crack/Bubble Length = ½ inch

K_I = 212.9 psi √in. K_{II} = 313.7 psi √in.

(All stress values in psi, positive denotes tensile value)

Location	ε_r	ε_z	ε_θ	ε_1	ε_2	ε_3	ε_{vm}
1	0	-.0078	0	.0043	-.0078	0	.011
2	0	-.0096	0	.0049	-.0096	0	.013
3	0	-.019	0	.0093	-.019	0	.025
4	0	-.061	0	.029	-.061	0	.080
5	0	-.058	0	.026	-.058	0	.074
6	0	-.024	0	.0075	-.024	0	.029
7	0	-.0002	0	.0003	-.0002	0	.0004
8	.0022	-.0051	.0034	.0022	-.0051	.0034	.0080
9	.0012	-.0047	.0034	.0054	-.0090	.0034	.014
10	-.001	-.012	.010	.014	-.0027	.010	.015
11	.017	-.042	.025	.039	-.064	.025	.097
12	036	-.052	.013	.039	-.056	.013	.085
13	.00002	.010	-.0002	.016	-.0054	-.0002	.019
14	.00001	.0080	-.0002	.012	-.0036	-.0002	.014
15	-.058	.056	.012	.089	-.090	.012	.16
16	-.078	.116	.0031	.122	-.084	.0031	.18
17	-.011	.0095	.0018	.012	-.014	.0018	.022
18	.0001	-.0002	.0002	.0001	-.0002	.0002	.0004
19	-.00003	-.00006	.0002	-.00003	-.00006	.0002	.0002

Table 6. Output Values From Minimum Thickness Propellant Models

Crack/Bubble Length = 1 inch

K_I = 249.9 psi $\sqrt{in.}$ K_{II} = 641.0 psi $\sqrt{in.}$

(All stress values in psi, positive denotes tensile value)

Location	σ_r	σ_z	σ_θ	σ_1	σ_2	σ_3	σ_{vm}
1	50.0	0	50.0	50.0	1.1	50.0	48.9
2	14.3	-23.2	14.3	14.3	-23.2	14.3	37.5
3	3.7	-45.5	3.7	3.7	-45.5	3.7	49.2
4	-37.8	-91.8	-37.8	-37.8	-91.8	-37.8	54.0
5	-57.8	-96.5	-57.8	-57.8	-96.5	-57.8	38.7
6	-94.1	-99.9	-94.1	-94.1	-99.9	-94.1	5.8
7	35500	31.8	35500	35500	31.8	35500	35468
8	35.0	0	39.0	35.0	0.7	39.0	36.5
9	9.4	-16.3	12.6	18.7	-25.7	12.6	41.7
10	-6.8	-57.5	-3.8	4.6	-68.9	-3.8	69.7
11	-50.5	-95.0	-52.2	-49.0	-96.5	-52.2	51.5
12	-3.2	-96.7	-40.9	1.7	-101.6	-40.9	89.9
13	362.0	376.0	361.5	376.5	361.5	361.5	15.0
14	228.7	240.1	228.2	240.1	228.6	228.2	11.7
15	13.3	167.5	91.5	203.3	-22.5	91.5	195.6
16	77.2	317.1	172.3	324.3	70.0	172.3	221.6
17	29.0	60.3	44.3	65.3	24.0	44.3	35.8
18	8038	-12.1	19610	8107	-8014	19610	24034
19	-5622	-18.5	11520	-185.3	-5622	11520	15113

Table 6. Output Values From Minimum Thickness Propellant Models (Cont'd)

Crack/Bubble Length = 1 inch

K_I = 249.9 psi $\sqrt{in.}$ K_{II} = 641.0 psi $\sqrt{in.}$

(All stress values in psi, positive denotes tensile value)

Location	ε_r	ε_z	ε_θ	ε_1	ε_2	ε_3	ε_{vm}
1	0	-.042	0	0.23	-.042	0	.057
2	0	-.033	0	.017	-.033	0	.044
3	0	-.045	0	.022	-.045	0	.059
4	0	-.050	0	.022	-.050	0	.064
5	0	-.037	0	.015	-.037	0	.046
6	0	-.0087	0	-.0009	-.0087	0	.0083
7	0	-.0007	0	.0008	-.0007	0	.0013
8	.015	-.032	.020	.015	-.032	.020	.050
9	.010	-.024	.014	.023	-.037	.014	.056
10	.021	-.048	.025	.036	-.063	.025	.094
11	.018	-.042	.016	.020	-.044	.016	.062
12	.059	-.067	.0080	.065	-.074	.0080	.12
13	.0002	.019	-.0005	.020	-.0005	-.0005	.020
14	.0002	.016	-.0005	.016	.0001	-.0005	.016
15	-.097	.11	.0084	.16	-.15	.0084	.27
16	-.13	.20	.0016	.21	-.14	.0016	.30
17	-.020	.022	.0004	.029	-.027	.0004	.049
18	.00007	-.0003	.0006	.00008	-.0003	.0006	.0008
19	-.0003	-.00007	.0005	-.00007	-.0003	.0005	.0007

Location Guide For Stress and Strain
Minimum Thickness Propellant Rocket Models

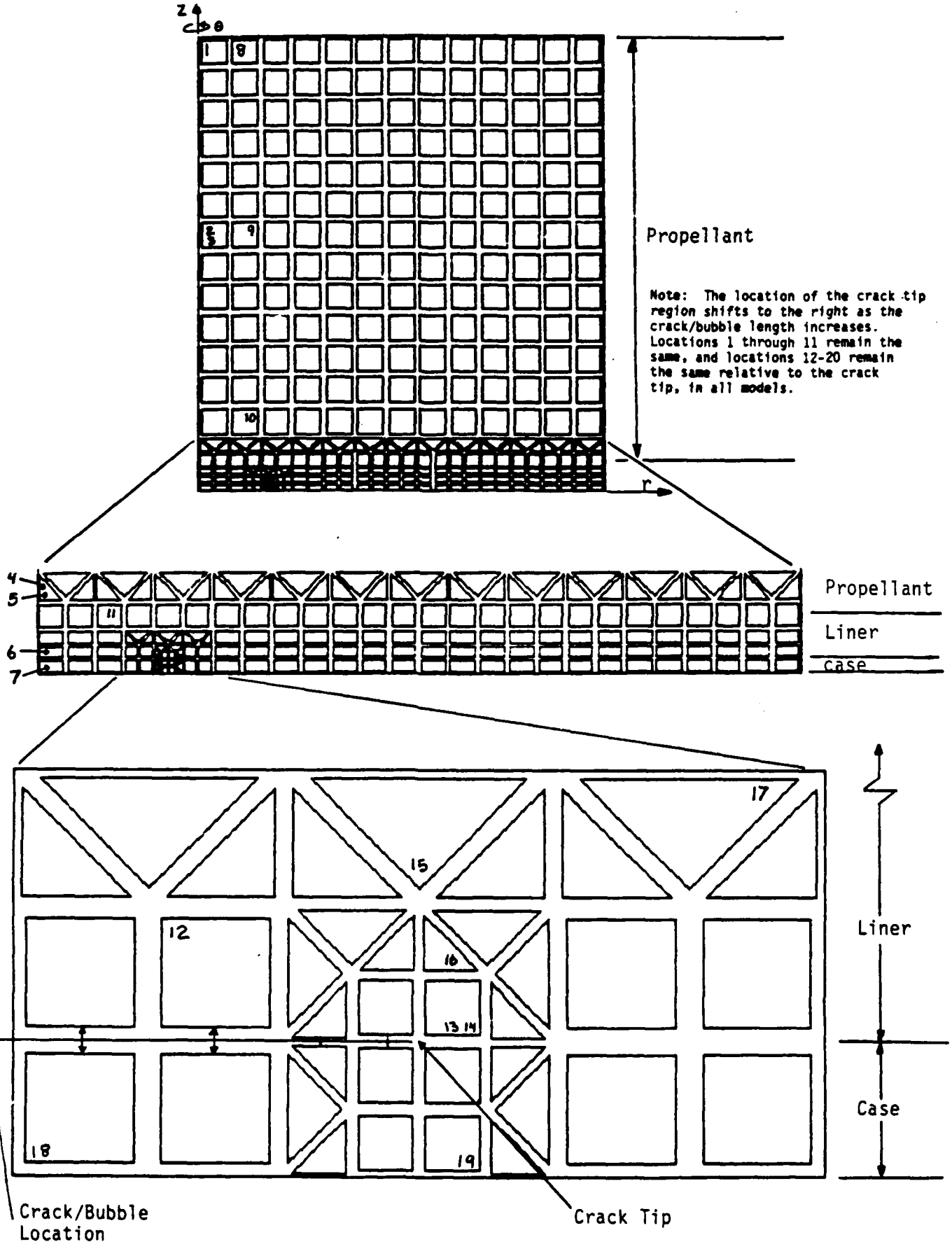

Figure 10

Table 7. Output Values From Maximum Thickness Propellant Models

Crack/Bubble Length = ½ in.

K_I = 228.3 psi √in. K_{II} = 351.1 psi √in.

(All stress values in psi, positive denotes tensile value)

Location	σ_r	σ_z	σ_θ	σ_1	σ_2	σ_3	σ_{vm}
1	0.7	0	0.7	0.7	.008	0.7	0.7
2	0.4	-1.7	0.4	0.4	-1.7	0.4	2.1
3	0.5	-2.7	0.5	0.5	-2.7	0.5	3.2
4	-8.8	-75.9	-8.8	-8.8	-75.9	-8.8	67.1
5	-26.4	-89.5	-26.4	-26.4	-89.5	-26.4	63.1
6	-76.1	-100.2	-76.1	-76.1	-100.2	-76.1	24.1
7	11840	24.1	11840	11840	24.1	11840	11816
8	0.6	0	0.6	0.6	.006	0.6	0.6
9	0.2	-1.3	0.3	0.4	-1.6	0.3	2.0
10	-5.7	-15.3	3.0	4.5	-25.5	3.0	29.3
11	-15.1	-59.4	-9.0	0.7	-75.2	-9.0	71.5
12	-32.7	-97.7	-49.5	-30.5	-99.9	-49.5	62.1
13	184.0	191.7	183.9	196.7	179.1	183.9	15.8
14	105.9	111.8	105.8	115.2	102.5	105.8	11.4
15	-18.3	65.3	32.6	88.5	-41.5	32.6	113.0
16	15.6	158.4	75.2	162.9	11.0	75.2	132.1
17	4.7	19.7	14.4	22.2	2.1	14.4	17.6
18	7368	-5.1	9201	7380	-17.0	9201	8456
19	1096	38.2	5494	1105	29.0	5494	5014

Table 7. Output Values From Maximum Thickness Propellant Models (Cont'd)

Crack/Bubble Length = ½ inch

K_I = 228.3 psi √in. K_I = 351.1 psi √in.

(All stress values in psi, positive denotes tensile value)

Location	ε_r	ε_z	ε_θ	ε_1	ε_2	ε_3	ε_{vm}
1	0	-.0006	0	.0003	-.0006	0	.0008
2	0	-.0019	0	.0009	-.0019	0	.0025
3	0	-.0029	0	.0014	-.0029	0	.0038
4	0	-.061	0	.029	-.061	0	.080
5	0	-.058	0	.026	-.058	0	.074
6	0	-.025	0	.0077	-.025	0	.030
7	0	-.0002	0	.0003	-.0002	0	.0004
8	.0002	-.0005	.0003	.0002	-.0005	.0003	.0008
9	.0006	-.0014	.0008	.0009	-.0017	.0008	.0026
10	-.0005	-.013	.012	.013	-.027	.012	.040
11	.017	-.042	.025	.038	-.064	.025	.096
12	.035	-.052	.013	.038	-.055	.013	.083
13	.000007	.013	-.0002	.017	-.0067	-.0002	.021
14	.000003	.0079	-.0002	.012	-.0046	-.0002	.015
15	-.057	.055	.016	.087	-.088	.016	.15
16	-.077	.12	.003	.12	-.083	.003	.18
17	-.011	.009	.002	.013	-.015	.002	.024
18	.0002	-.0002	.0002	.0002	-.0002	.0002	.0004
19	-.00002	-.00007	-.0002	-.00002	-.00007	-.0002	.0002

Table 8. Output Values From Maximum Thickness Propellant Models

Crack/Bubble Length = 1 in.

K_I = 320.7 psi $\sqrt{in.}$ K_{II} = 810.0 psi $\sqrt{in.}$

(All stress values in psi, positive denotes tensile value)

Location	σ_r	σ_z	σ_θ	σ_1	σ_2	σ_3	σ_{vm}
1	5.0	0	5.0	5.0	.06	5.0	4.9
2	2.0	-10.6	2.0	2.0	-10.6	2.0	12.6
3	2.3	-15.5	2.3	2.3	-15.5	2.3	17.8
4	-37.7	-95.4	-37.7	-37.7	-95.4	-37.7	57.7
5	-55.3	-98.3	-55.3	-55.3	-98.3	-55.3	43.0
6	-86.3	-100.0	-86.3	-86.3	-100.0	-86.3	13.7
7	37890	31.8	37890	37890	31.8	37890	37858
8	4.3	0	4.5	4.3	.05	4.5	4.4
9	1.0	-8.4	1.9	2.4	-9.8	1.9	12.0
10	-10.8	-66.4	7.7	-3.7	-73.5	7.7	76.1
11	-49.4	-96.8	-50.7	-48.8	-97.4	-50.7	47.7
12	-13.3	-97.4	-44.9	-9.7	-100.9	-44.9	79.7
13	335.6	349.8	335.0	357.1	328.2	335.0	26.2
14	210.5	221.7	210.0	227.7	204.5	210.0	21.0
15	3.2	149.3	78.6	180.3	-27.9	78.6	180.3
16	61.3	294.5	155.4	302.8	52.9	155.4	217.6
17	22.8	53.8	39.3	61.1	15.6	39.3	39.4
18	10420	-9.9	22000	10480	-62.6	22000	19113
19	-3245	-117.9	13920	-117.6	-3246	13920	15835

Table 8. Output Values From Maximum Thickness Propellant Models (Cont'd)

Crack/Bubble Length = 1 inch

K_I = 320.7 psi $\sqrt{in.}$ K_{II} = 810.0 psi $\sqrt{in.}$

(All stress values in psi, positive denotes tensile volume)

Location	ϵ_r	ϵ_z	ϵ_θ	ϵ_1	ϵ_2	ϵ_3	ϵ_{vm}
1	0	-.0043	0	.0024	-.0043	0	.0059
2	0	-.011	0	.0056	-.011	0	.015
3	0	-.016	0	-.0079	-.016	0	.014
4	0	-.054	0	.024	-.054	0	.069
5	0	-.041	0	.017	-.041	0	.052
6	0	-.016	0	.0028	-.016	0	.018
7	0	-.0008	0	.0009	.0008	0	.0009
8	.0019	-.0038	.0022	.0019	-.0038	.0022	.0059
9	.0038	-.0089	.0049	.0056	-.011	.0049	.016
10	.022	-.052	.027	.030	-.061	.027	.090
11	.019	-.044	.018	.020	-.045	.018	.064
12	.051	-.062	.0088	.056	-.066	.0088	.11
13	.0002	.019	-.0005	.029	-.0097	-.0005	.035
14	.0002	.015	-.0005	.023	-.0079	-.0005	.028
15	-.093	0.10	.0088	0.15	-0.13	.0088	.24
16	-0.12	0.19	.0020	0.20	-0.14	.0020	.30
17	-.021	.021	.0013	.031	-.031	.0013	.054
18	.0001	-.0003	.0006	.0001	-.0003	.0006	.0008
19	-.0003	-.0001	.0005	-.0001	-.0003	.0005	.0007

Location Guide For Stress and Strain
Minimum Thickness Propellant, Some Propellant Removed Rocket Models

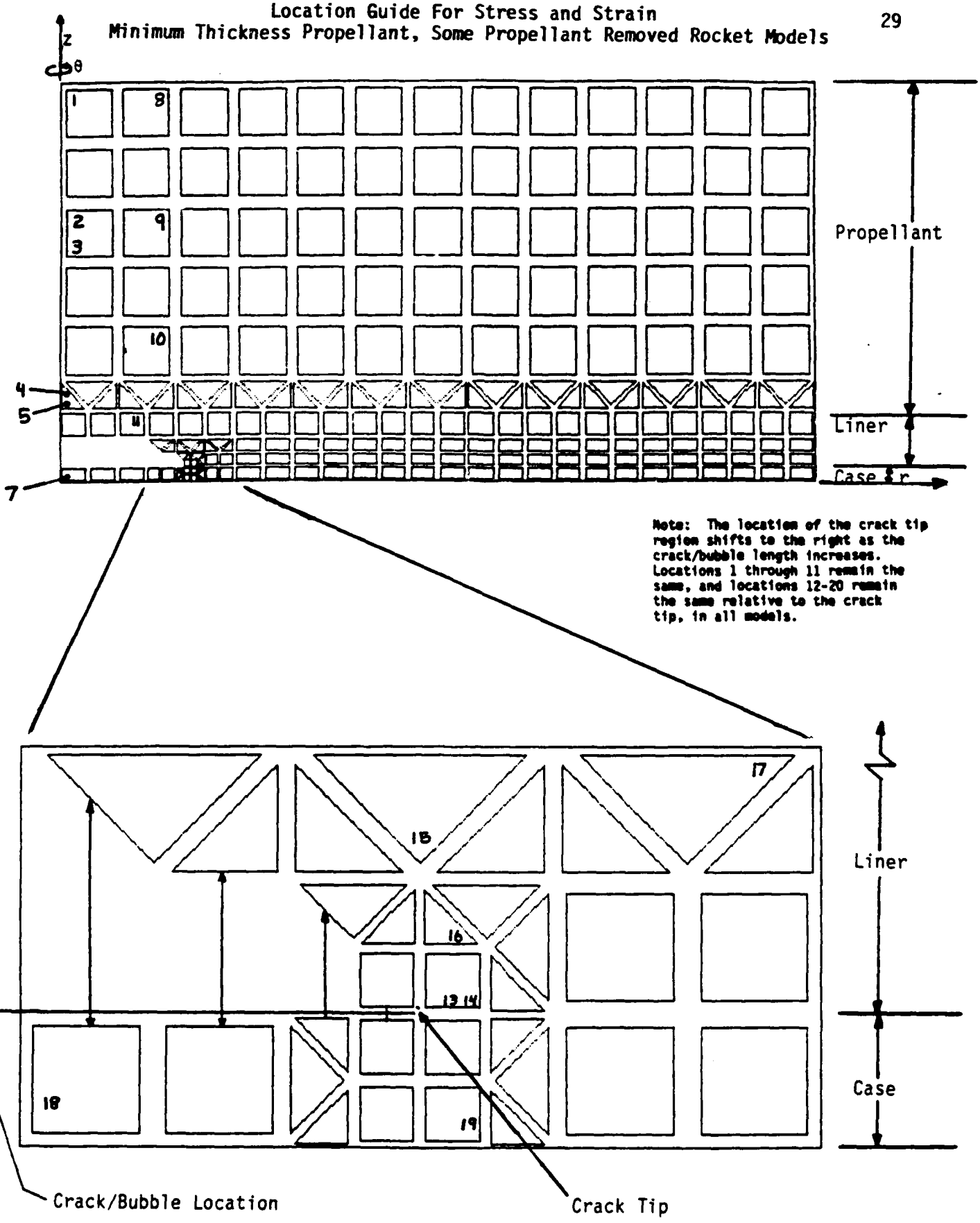

Figure 11

Table 9. Output Values From Minimum Thickness Propellant Models (Some Liner Removed)

Crack/Bubble Length = 1/2 in.

K_I = 212.0 psi $\sqrt{in.}$ K_{II} = 318.7 psi $\sqrt{in.}$

(All stress values in psi, positive denotes tensile value)

Location	σ_r	σ_z	σ_θ	σ_1	σ_2	σ_3	σ_{vm}
1	9.7	0	9.7	9.7	0.4	9.7	9.3
2	3.5	-7.7	3.5	3.5	-7.7	3.5	11.2
3	2.9	-19.2	2.9	2.9	-19.2	2.9	22.1
4	-9.2	-81.0	-9.2	-9.2	-81.0	-9.2	71.8
5	-31.4	-95.2	-31.4	-31.4	-95.2	-31.4	63.8
7	11410	24.1	11410	11410	24.1	11410	11386
8	5.7	0	6.7	5.7	0.1	6.7	6.2
9	1.0	-3.6	2.7	4.3	-6.8	2.7	10.4
10	-5.4	-13.4	3.7	6.3	-25.1	3.7	30.2
11	-22.4	-55.4	-8.3	-4.7	-73.2	-8.3	66.8
13	182.9	190.1	182.8	194.7	178.3	182.8	14.7
14	107.5	113.6	107.3	117.3	103.8	107.3	12.1
15	-17.3	71.4	36.4	92.8	-38.7	36.4	114.3
16	17.6	159.4	77.7	164.0	12.9	77.7	131.3
17	5.7	21.3	15.4	23.5	3.5	15.4	17.4
18	6935	-5.5	8768	6948	-18.2	8768	8032
19	655.7	26.7	5059	668.7	13.7	5059	4752

Table 9. Output Values From Minimum Thickness Propellant Models (Cont'd)
(Some Liner Removed)

Crack/Bubble Length = 1/2 inch

K_I = 212.0 psi $\sqrt{in.}$ K_{II} = 318.7 psi $\sqrt{in.}$

(All stress values in psi, positive denotes tensile value)

Location	ε_r	ε_z	ε_θ	ε_1	ε_2	ε_3	ε_{vm}
1	0	-.0080	0	.0044	-.0080	0	.011
2	0	-.010	0	.0051	-.010	0	.013
3	0	-.020	0	.0097	-.020	0	.026
4	0	-.066	0	.031	-.066	0	.086
5	0	-.059	0	.027	-.059	0	.076
7	0	-.0002	0	.0003	-.0002	0	.0004
8	.0022	-.0053	.0035	.0022	-.0053	.0035	.0082
9	.0012	-.0049	.0036	.0056	-.0093	.0036	.014
10	-.0013	-.012	.011	.014	-.028	.011	.041
11	.0069	-.038	.026	.031	-.061	.026	.090
13	.00002	.0097	-.0002	.016	-.0062	-.0002	.020
14	.00001	.0083	-.0002	.013	-.0049	-.0002	.016
15	-.060	.059	.012	.088	-.089	.012	.15
16	-.078	.11	.0032	.12	-.084	.0032	.18
17	-.011	.0098	.0019	.013	-.014	.0019	.024
18	.0001	-.0002	.0002	.0001	-.0002	.0002	.0004
19	-.00003	-.00006	.0002	-.00003	-.00006	.0002	.0002

Table 10. Output Values From Minimum Thickness Propellant Models (Some Liner Removed)

Crack/Bubble Length = 1.0 in.

K_I = 246.1 psi $\sqrt{in.}$ K_{II} = 652.8 psi $\sqrt{in.}$

(All stress values in psi, positive denotes tensile value)

Location	σ_r	σ_z	σ_θ	σ_1	σ_2	σ_3	σ_{VM}
1	52.8	0	52.8	52.8	0	52.8	52.8
2	14.6	-24.9	14.6	14.6	-24.9	14.6	39.5
3	3.1	-48.8	3.1	3.1	-48.8	3.1	51.9
4	-45.0	-95.6	-45.0	-45.0	-95.6	-45.0	50.6
5	-68.5	-99.0	-68.5	-68.5	-99.0	-68.5	30.5
7	35620	31.8	35620	35620	31.8	35620	35588
8	36.8	0	41.1	36.8	0.7	41.1	38.4
9	9.5	-17.3	12.9	19.6	-27.4	12.9	44.0
10	-8.1	-60.8	-5.2	4.1	-73.0	-5.2	72.9
11	-59.9	-98.2	-62.2	-59.2	-98.9	-62.2	38.3
13	350.3	367.8	349.8	377.8	340.3	349.8	33.8
14	228.5	242.5	228.0	346.2	224.7	228.0	119.9
15	25.0	168.5	98.6	206.1	-12.5	98.6	189.3
16	67.0	315.5	169.5	319.7	62.8	169.5	223.5
17	31.1	61.4	45.4	65.9	26.6	45.4	34.0
18	8160	-12.0	19740	8227	-79.0	19740	17238
19	-5498	-180.0	11650	-180.0	-5498	11650	15203

Table 10. Output Values From Minimum Thickness Propellant Models (Cont'd)
(Some Liner Removed)

Crack/Bubble Length = 1.0 inch

K_I = 246.1 psi $\sqrt{in.}$ K_{II} = 652.8 psi $\sqrt{in.}$

(All stress values in psi, positive denotes tensile value)

Location	ε_r	ε_z	ε_θ	ε_1	ε_2	ε_3	ε_{vm}
1	0	-.045	0	.025	-.045	0	.061
2	0	-.035	0	.018	-.035	0	.047
3	0	-.047	0	.023	-.047	0	.062
4	0	-.047	0	.021	-.047	0	.060
5	0	-.030	0	.011	-.030	0	.037
7	0	-.0007	0	.0009	-.0007	0	.0014
8	.015	-.033	.021	.015	-.033	.021	.051
9	.011	-.025	.015	.024	-.039	.015	.059
10	.022	-.049	.026	.038	-.066	.026	.099
11	.016	-.036	.012	.017	-.037	.012	.052
13	.0002	.024	-.0005	.037	-.013	-.0005	.045
14	.0002	.019	-.0005	.024	-.0048	-.0005	.027
15	-.091	-.10	.0081	.15	-.14	.0081	.25
16	-.14	.20	.0018	.20	-.14	.0018	.30
17	-.019	.022	.0002	.028	-.025	.0002	.046
18	.00008	-.0003	.0006	.00008	-.0003	.0006	.0008
19	-.0003	-.00007	.0005	-.00007	-.0003	.0005	.0007

B. Peel Test Models

The objective of the peel test models was to determine the K_I - K_{II} states at the liner-case interface which exists when the liner peels off. These states are interpreted as the fracture toughness of the liner-case bond, and are compared to the stress intensity factors arising from the rocket models. Thus, whether a bubble grows or not could be determined.

The peel test models incorporated the peel angle and mean peel load data, as shown in Figure 6. It became apparent in early model development that the values of K_I and K_{II} developed in the peel test models were not in a comparable range to the valves coming from the rocket models. In particular, the K_{II} valve, which represents a sliding motion, was much larger in the rocket models. As a result, comparison between the peel test results and the rocket results were hindered. This tendency became worse as the peel angle grew larger. For this reason it was decided to ignore the results of the peel tests with angles of 110° and 133°, and to concentrate upon the results of tests with the angles of 49°, 73° and 90°. The incompatibility of the stress intensity factor values from the rocket and peel test models indicated that the failure mechanism was different somehow, and dictates the need of smaller angle tests, or a different type of tests. This point is elaborated upon in Section V.

The load applied to the models was actually the mean peel load divided by ten. This was done to reduce the element distortion. Since the analysis was linear, all results obtained from the peel test models were multiplied by ten to obtain the full scale results. Plots of the original and deformed geometry of the peel test models are shown in Appendix B.

The following Figure 12 shows a typical peel test model. The Tables 11-13 give values of K_I and K_{II}, along with values of stress and strain at locations 1 and 2 near the crack tip. When the values of K_I and K_{II} from the peel tests did not lie in a comparable range to the rocket model results, it was decided to examine stress and strain near the crack tip. If a consistent failure stress or strain could be identified, then those values would be used for comparison values to determine whether the bubble would grow in the rocket models, and the K_I - K_{II} approach would be abandoned. This approach would require comparing the failure stress or strain level from the peel test models

to the stress or strain at the crack tip in the rocket models. A complete discussion of these results appears in the next section.

Location Guide For Stress and Strain
Peel Test Models
Peel Angle = 49 degrees

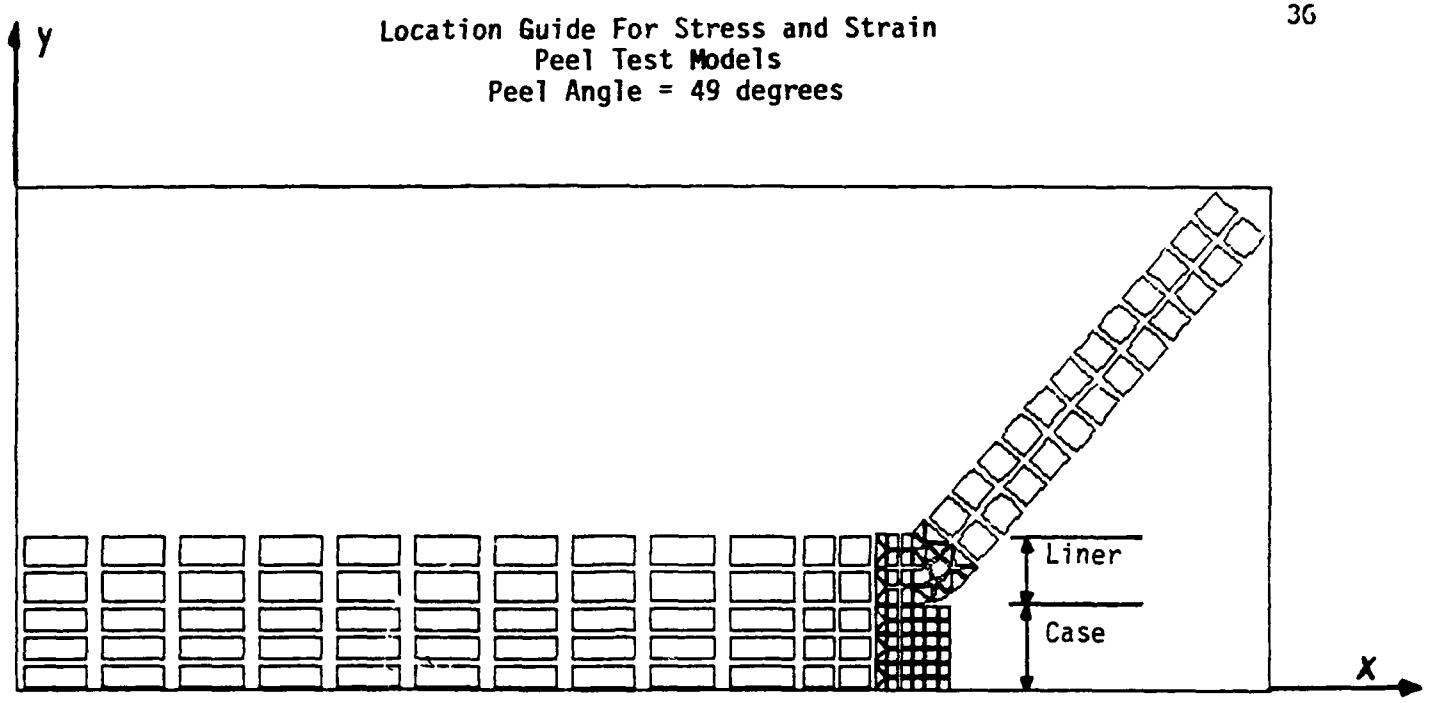

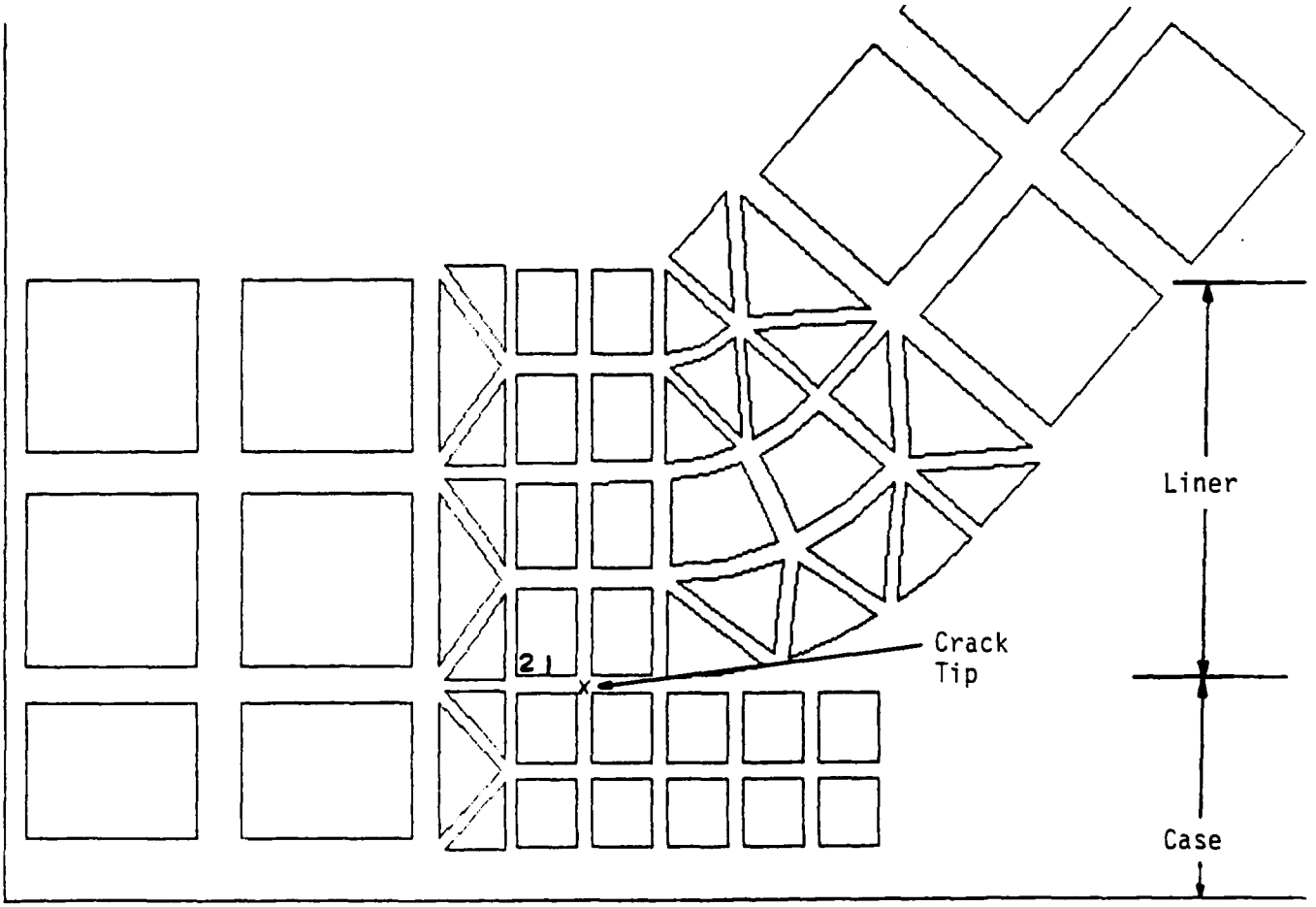

Figure 12

Table 11. Output Values From 49 Degree Peel Angle Model

K_I = 508.9 psi. √in K_{II} = 69.0 psi. √in

(all stress values in psi, positive denotes tensile value)

location	σ_x	σ_y	σ_z	σ_1	σ_2	σ_3	σ_{vm}
1	1710	1718	1710	2068	1360	1710	613
2	1132	1167	1132	1446	853	1132	514
	ε_x	ε_y	ε_z	ε_1	ε_2	ε_3	ε_{vm}
1	.00006	.010	0	.48	-.47	0	.82
2	.00004	.046	0	.42	-.38	0	.69

Table 12. Output Values From 73 Degree Peel Angle Model

K_I = 315.7 psi. √in K_{II} = 24.6 psi. √in

(all stress values in psi, positive denotes tensile value)

location	σ_x	σ_y	σ_z	σ_1	σ_2	σ_3	σ_{vm}
1	1065	1082	1065	1225	923	1065	262
2	710	739	710	859	589	710	234
	ε_x	ε_y	ε_z	ε_1	ε_2	ε_3	ε_{vm}
1	.00003	.022	0	.21	-.19	0	.35
2	.00002	.039	0	.20	-.16	0	.31

Table 13. Output Values From 90 Degree Peel Angle Model

K_I = 208.9 psi. √in K_{II} = -13.3 psi. √in

(all stress values in psi, positive denotes tensile value)

location	σ_x	σ_y	σ_z	σ_1	σ_2	σ_3	σ_{vm}
1	712	745	712	747	710	712	36
2	481	520	481	541	460	481	73
	ε_x	ε_y	ε_z	ε_1	ε_2	ε_3	ε_{vm}
1	.00001	.045	0	.047	-.0027	0	.048
2	.000003	.051	0	.081	-.029	0	.099

IV. DISCUSSION

This analysis depends upon two responses which occur as the pressurized bubble is formed. The first is the formation of stress and strain states within the propellant and case. The second is the development of stress singularities at the crack/bubble edge, characterized by the magnitude of the stress intensity factors. The failure scheme employed in this analysis was therefore a two parameter method. For the rocket models, the approach used was to determine a factor, which when multiplied by the applied pressure load, would cause either a specific stress or strain value to reach the failure value shown in Table 4. This factor was termed "failure factor." A similar factor was calculated for the stress intensity factors. The failure factor relative to the stress intensity factors would be the number, which when multiplied by the applied pressure load, would cause the K_I and K_{II} values to exceed the critical states mapped out by the peel tests. This load factor approach is valid in a linear analysis. For a particular model, which ever of these factors was the smaller would determine which process had reached "failure" first. Either the stress or strain would reach its failure value, indicating a rupture in the propellant or case, or the stress intensity factors would reach their critical values, indicating that the bubble would grow before the rocket case or propellant had failed.

A. Peel Test Models

The determination of the critical values of the stress intensity factors came from the peel test models, the results of which are shown in Tables 11-13. These values of K_I and K_{II} actually describe the strength of the case-liner bond. These values are graphed in Figure 13, along with the K_I and K_{II} values from each of the rocket models. The original idea was to have the peel test results map out a curve in K_I - K_{II} space, which would represent the critical values of K_I and K_{II} for crack/bubble growth.

Refering to Figure 13, it can be seen that the values from the peel test models do not lie in a comparable range with the rocket model results. The values of K_{II}, in particular, are much greater for the rocket models. Since K_{II} is the stress intensity which refers to sliding motion, this indicates that the crack/bubble in the rocket model is experiencing much more sliding

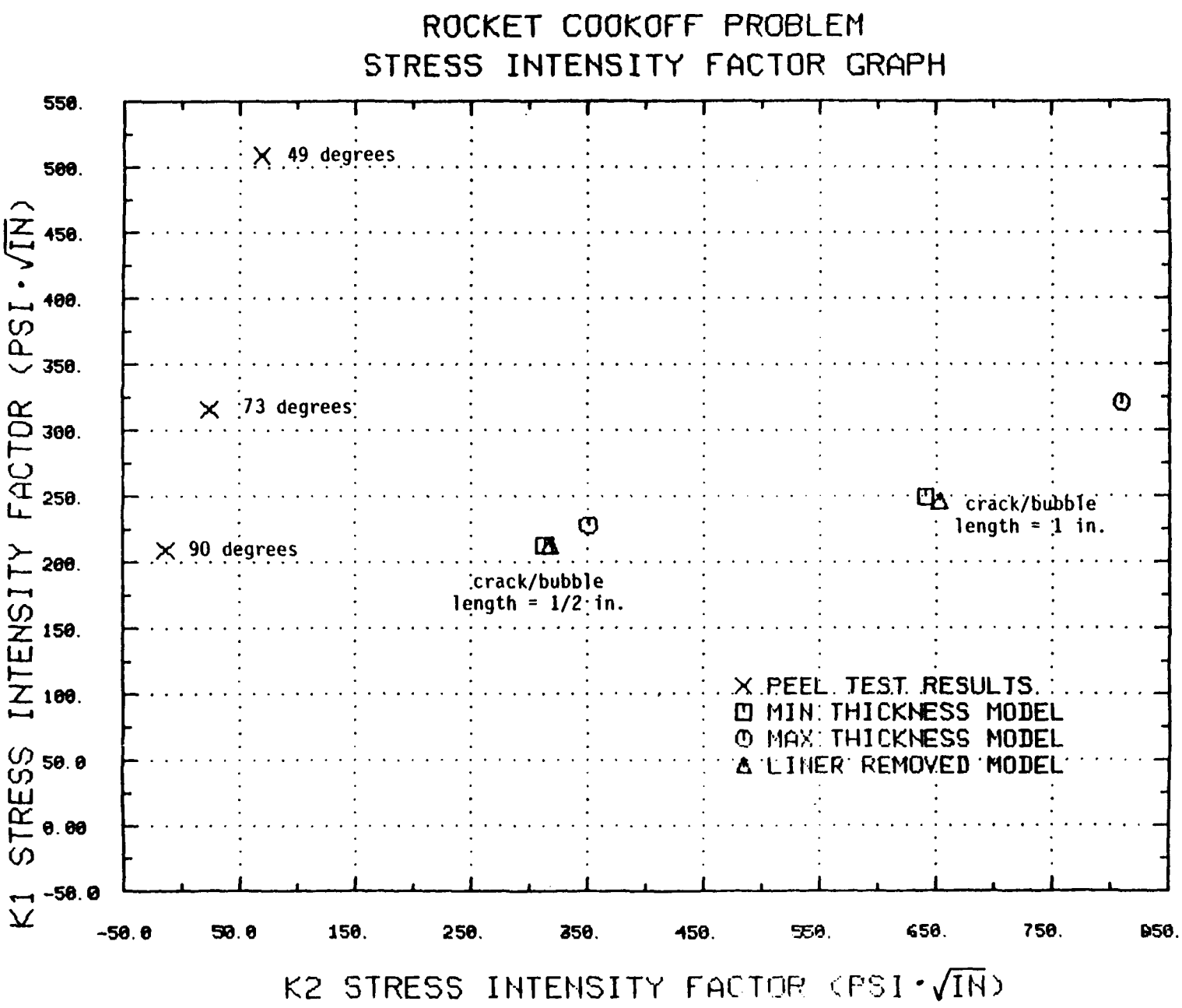
ROCKET COOKOFF PROBLEM
STRESS INTENSITY FACTOR GRAPH
K1 STRESS INTENSITY FACTOR (PSI·√IN)
K2 STRESS INTENSITY FACTOR (PSI·√IN)
550.
500.
450.
400.
350.
300.
250.
200.
150.
100.
50.0
0.00
-50.0
-50.0
50.0
150.
250.
350.
450.
550.
650.
750.
850.
49 degrees
73 degrees
90 degrees
crack/bubble
length = 1/2 in.
crack/bubble
length = 1 in.
X PEEL TEST RESULTS
MIN THICKNESS MODEL
MAX THICKNESS MODEL
LINER REMOVED MODEL

Figure 13

type motion than the peel tests are exhibiting. The peel test model results give larger K_{II} values as the peel angle gets smaller, but even at the smallest peel test angle (49°), the value of K_{II} is 60 psi $\sqrt{in}$, compared with values from 314 to 810 in the rocket models. Because stress intensity factors are dependent upon the stress fields which surround the singular point, these results indicate that the failure mechanisms occurring in the peel tests are different than those occurring in the rocket models. The basic reaction, liner peeling away from case, is the same, but the driving stress fields appear to be very different. Due to the incompatibility of the results on Figure 13, the use of the peel test models for determining the critical K_I - K_{II} curve was abandoned.

Another attempt was made to derive critical values from the peel test models. This approach was to examine the values of stress and strain, from Tables 11-13, which occur at points in the liner material next to the crack tip (labeled 1 and 2 on Figure 12). These locations in the peel test models would indicate the stress and strain magnitudes along the liner-case interface. Values at the crack tip itself were not used because the singularity exists there. If a consistent stress or strain value could be found among all the models, that value would be used as the critical value for crack initiation.

From an examination of the results in Tables 11-13, it can be seen that there is no consistent value among the different peel angles. All values are larger from the 49 degree model, and they get progressively smaller as the peel angle goes to 90 degrees. This response corresponds to the magnitude of the mean peel load, from Figure 6, which varies from 166 lb/in for the 49 degree test to 51.7 lb/in in the 90 degree test. It was expected that there should be some consistent values of stress or strain near the crack tip, because the materials are the same in all cases, but this is not borne out in the peel test models. It is felt that this inconsistency may be due to the fact that a linear analysis was performed, where in actual conditions the material behaves very nonlinearly.

The net results from the peel test models proved to be inapplicable for the bubble growth problem. Since a critical K_I - K_{II} curve, or a consistent critical stress or strain could not be identified, no failure criteria could be established to determine whether or not the crack would grow. This severely hindered the analysis and prevented any firm conclusions regarding

bubble growth. It did identify the complexity and difficulties encountered in the modeling of peel tests and demonstrated the inapplicability of the particular peel tests performed for determining case-liner bond failure in the cookoff environment.

B. Rocket Models

The values of stress and strain at various locations in the model are listed in Tables 5-10. The locations were chosen to give a representative description of the stress and strain state in the pressurized rocket model. There are no stresses or strains reported in the model as r becomes larger than the crack/bubble length, because the values become very small in that region. For the purpose of discussion, the minimum thickness model with the crack/bubble length of ½ inch will be examined first, and other models will be compared to it.

Referring to Figure 9, location 1, at the top or inner most portion of the propellant, is a likely point for failure initiation. Referring to Table 5, the stresses at that point are tensile, with a maximum value of 9.3 psi in the radial direction. This value gives a failure factor of 17.2, when divided into 160 psi from Table 4. The failure factor computed from the von Mises strain at location 1 is 19.1. The stresses form a similar pattern at location 8, but are reduced in magnitude. This type of trend indicates that the region of highest stress will be along the axis of symmetry, or adjacent to the crack/bubble. As one progresses down the axis of symmetry towards the cracktip, at locations 2-6, the state of stress changes from biaxial tension to triaxial compression. Locations 2 and 3 have smaller tensile stresses in the r and θ direction than location 1, but the compressive stress in the z direction increases. The result of this type of stress state is that the von Mises stress at locations 2 and 3 is higher than at location 1. At locations 4, 5 and 6, the magnitude of the compressive stresses increases further, giving maximum values from 74 to 100 psi. The von Mises stress at locations 4 and 5 are 66.7 and 63.0 respectively, much higher than the value of 8.9 at location 1.

If failure were based upon the magnitude of the principle stresses, then location 6 would be the failure point, due to principle stress 2 having the largest value, -100.2 psi. But it must be noted that location 6 is under a

state of triaxial compression. While the failure behavior of the propellant material is not completely understood, typically materials are not expected to fail in regions of triaxial compression. The von Mises stress at location 6 is 23.7 psi, due mainly to the difference in the z and r/θ components of stress.

If propellant failure were based upon maximum von Mises stress, then a region either near location 4 or location 11 would be the expected site of failure, due to the large (66.7 and 72.3 psi respectively) values there. Both of these points are also in states of triaxial compression, and they lie on the interior portions of the model, not near an edge. Failure from one of these points would require a tearing or opening from an interior point in the rocket propellant, and then propagation outwards. Since failures typically initiate from an edge, this does not seem to be a likely mode of failure.

After an examination of the stress states and magnitudes in the propellant, an engineering judgement of the situation resulted in identifying location 1 as the most likely propellant failure initiation point. The propellant and case behave much like plate structures fixed at the edges, and in such a case the failure initiation point would be location 1. Even though the stress magnitudes are higher at other locations in the propellant, they were mostly the result of triaxial compression states on the interior of the model, as described previously. Those location (2-6) are not expected to be failure initiation sites. Thorough material testing of the propellant would give results which could be used to substantiate these conclusions.

The propellant could also fail by reaching failure strain levels. The strain states in the models are also reported in Tables 5-10. The failure factor for location 1, when computed from the value of .21 given in Table 4 and the von Mises strain is 19.1. This value is higher than the failure factor (17.2) computed for the maximum stress, indicating that a stress failure criteria would be the deciding criteria for failure at location 1. This behavior is repeated throughout all models in this study. For this linear analysis, at least, failure can be determined from critical stress values only.

The stress and strain states for locations 8-11 were given to indicate the patterns into the model. In all cases, they show the stresses decreasing as you move farther into the model in the r direction. The stresses and strains at locations 12-17 were given to indicate the stress levels in the liner. In this analysis, the failure criteria for the liner was merely the

unbonding of the liner from the case material, determined by the stress intensity factors. The failure of the liner due to stress state could not be determined because no strength values for the liner material could be obtained. In spite of this, the liner would not be looked upon as a source for failure initiation of the rocket as a whole. The effect of what happens in the liner would not propagate into the case or propellant, except for the action of crack/bubble growth. Hence, only unbonding of the liner from the case was examined in this analysis. From an examination of Table 5, it can be seen that the stress levels in the liner are much higher near the crack tip than in the rest of the model. This type of behavior is expected near a stress singularity. Away from the singularity, the stresses in the liner attenuate quickly, as can be seen from an examination of the stresses at location 17.

Failure in the case is expected to initiate at location 7. This point reaches the highest stress levels (in tension) of any point in the case; geometrically this corresponds to location 1 in the propellant. The radial stress there reaches 11320 psi, giving a failure factor of 14.1. This factor is lower than the factor at location 1 (17.2), indicating that the case would rupture before the propellant would. That situation would be true only if the failure factor for the stress intensity factors at the crack tip was sufficiently large (> 14.1) such that the case failure would occur before crack growth. For longer crack/bubble lengths, as described next, the situation just discussed reverses itself. When the model with a crack/bubble length of 1 inch is examined, the failure factor for the propellant is lower than that for the case.

Table 14 has been constructed for all the rocket models. Since failure is defined to initiate at locations 1 and 7, for the propellant and case respectively, Table 14 gives the maximum radial stresses and failure factors for locations 1 and 7 in all models. The radial stresses are the maximum tensile stresses at these locations. The stress results are also graphed in Figures 14 and 15 for the propellant and case, respectively.

The minimum thickness propellant model with a crack/bubble length of 1 inch will be compared to the results from the previously described ½ inch crack/bubble length model. Referencing Table 6 and Table 14, it can be seen that the stress/strain pattern is very similar to the model with the shorter crack/bubble, but the stress/strain magnitudes are higher. In particular, the

Table 14. Rocket Model Radial Stresses and Failure Factors

Propellant Thickness	Crack/Bubble Length (in)	Location 1 Stress (psi)	Location 1 Failure Factor	Location 7 Stress (psi)	Location 7 Failure Factor
Minimum	½	9.3	17.2	11320	14.1
Minimum	1	50.0	3.2	35500	4.5
Maximum	½	0.7	228.6	11840	13.5
Maximum	1	5.0	32.0	37890	4.2
Minimum (some liner removed)	½	9.7	16.5	11410	14.0
Minimum (some liner removed)	1	52.8	3.0	35620	4.5

maximum radial stress at location 1 in the propellant jumps to 50.0 psi, a five fold increase. The stress at location 7 in the case jumps three fold to 35,500 psi from 11,320 psi. However, as previously mentioned, the failure factor is now lower in the propellant when compared to the case, indicating that failure would occur in the propellant first, at location 1. This tendency would be expected to continue as the crack/bubble length increases. Therefore, in the minimum thickness models, if the crack/bubble length were to increase much past ½ inch, the failure would be expected to initiate at the innermost (in bore) portion of the propellant.

Comparing the maximum thickness propellant model with a crack/bubble length of ½ inch to the minimum thickness model with the same crack/bubble length, it can be seen that the stresses are much lower at locations 1, 2, 3, 8, 9 and 10. The stresses at locations near the crack/bubble region are nearly the same. The overall stress/strain pattern, however, is very similar. The maximum radial stress at location 1 is only 0.7 psi, while at location 7 it is 11,840 psi. As expected, increasing the propellant thickness has reduced the possibility of failure occurring in the propellant. The failure factor for the case at location 7 is 13.5, a little lower than the value from the minimum thickness model at the same location (14.1). Increasing the propellant thickness has slightly increased the stress levels in the case.

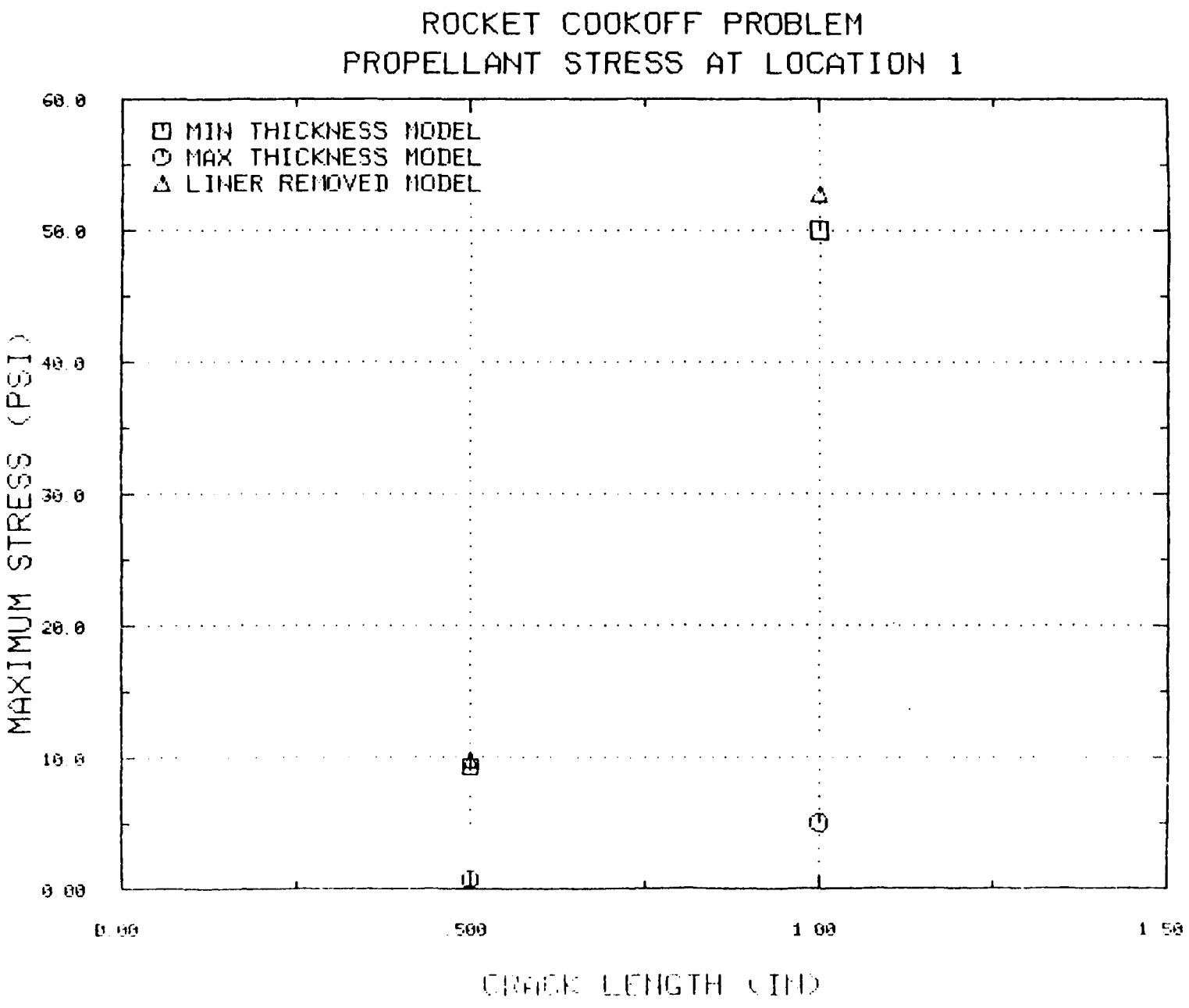
ROCKET COOKOFF PROBLEM
PROPELLANT STRESS AT LOCATION 1
MIN THICKNESS MODEL
MAX THICKNESS MODEL
LINER REMOVED MODEL
60.0
50.0
40.0
30.0
20.0
10.0
0.00
MAXIMUM STRESS (PSI)
0.00
.500
1.00
1.50
CRACK LENGTH (IN)

Figure 14

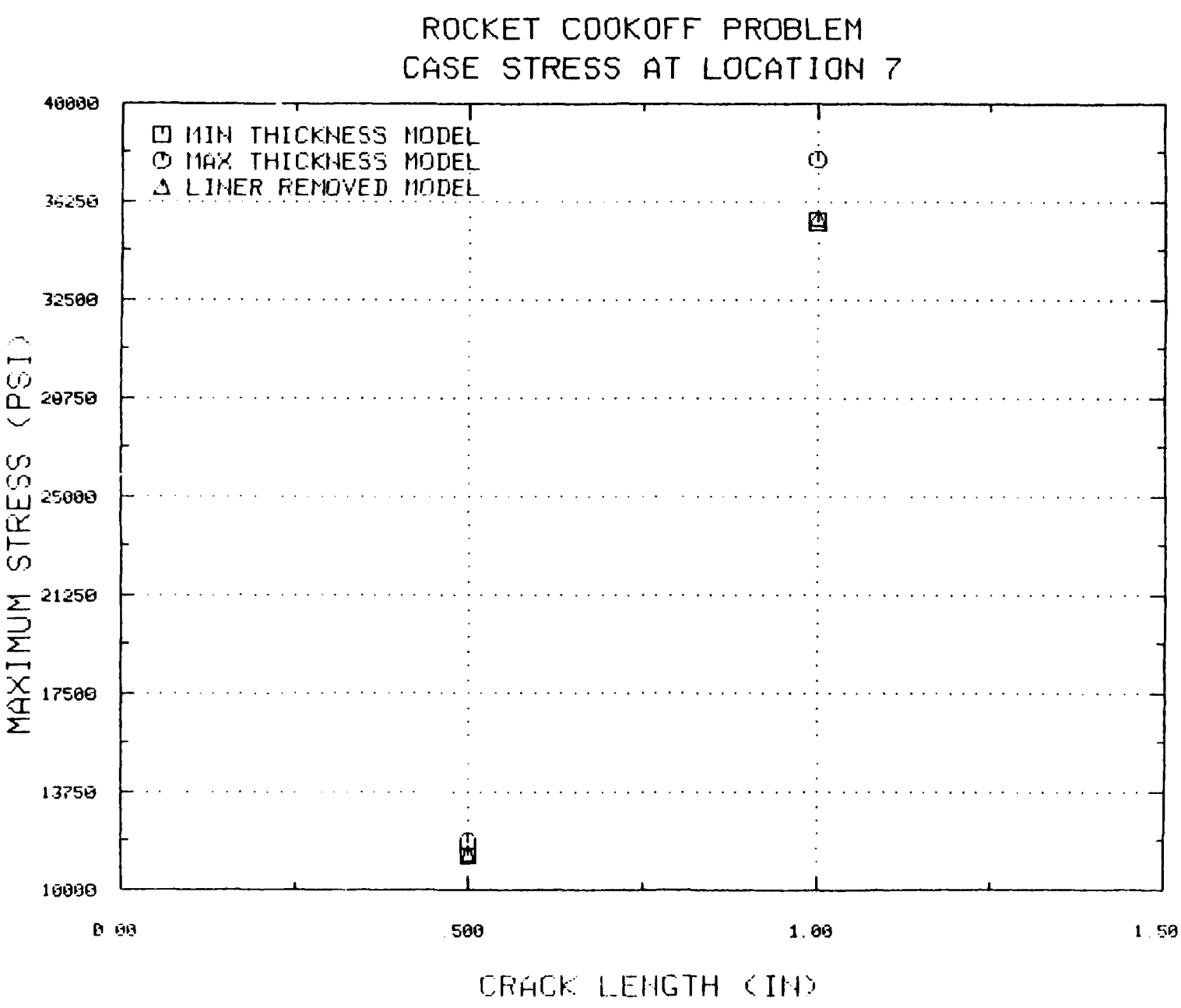
ROCKET COOKOFF PROBLEM
CASE STRESS AT LOCATION 7
MIN THICKNESS MODEL
MAX THICKNESS MODEL
LINER REMOVED MODEL
40000
36250
32500
20750
25000
21250
17500
13750
10000
MAXIMUM STRESS (PSI)
0.00
.500
1.00
1.50
CRACK LENGTH (IN)

Figure 15

When the crack/bubble length is increased to 1 inch in the maximum thickness model, the stress pattern is again very similar to the minimum thickness models. As in the previous case, the stress magnitudes at locations away from the crack/bubble are reduced, when compared to the minimum thickness model with a crack/bubble length of 1 inch. Stresses near the crack/bubble are nearly the same, however. The maximum radial stress at location 1 is still small, 5.0 psi, but the stress at location 7 is 37,890 psi. So, for the maximum thickness propellant models, the failure factor for the case is much lower than in the propellant, indicating that the case would fail much earlier than the propellant.

In the cases run where some liner elements were removed in order to simulate loss of liner, the stresses at the failure initiation locations increase slightly. This can be seen in Table 14. Both of the models with some liner removed had the minimum thickness propellant, so they will be compared to minimum thickness model results with similar crack/bubble lengths. For the cases with a ½ inch crack/bubble, the maximum radial stress at location 1 increase from 9.3 to 9.7 psi when some liner elements are removed. At location 7, the stress increases from 11,320 to 11,410 psi. The general stress/strain pattern is very similar, with slight increases in most of the propellant, and slightly lower stresses near the crack/bubble tip in the models with some liner removed. For the models with a 1 inch crack/bubble length, the stress increases at location 1 and 7 are 50.0 to 52.8 and 35,500 to 35,620 psi, respectively. The results show that the behavior of the model with some liner removed is nearly identical to the models with all liner elements. Therefore, even though the amount of liner degraded into gas is an unknown, its effect upon the stress state in the propellant and case appears to be minimal.

To summarize, the stresses increase at the expected failure initiation points as the crack/bubble length is increased. For the minimum thickness propellant models with a crack/bubble length of ½ inch, failure is more likely to occur in the case. When the crack/bubble length is increased to 1 inch or longer, failure is more likely to occur in the propellant. For the maximum thickness propellant models, the failure initiation point is expected to be in the case, for all lengths of crack/bubble. Removing some of the liner elements has a minimal effect upon the stresses generated in the propellant and case.

The limitations of this analysis should be noted here also. The flat plate analysis is a simplified version of the three dimensional rocket motor, and would give valid results only when bubble diameters are small compared to the diameter of the rocket. That is why the maximum crack/bubble length investigated in this analysis was 1 inch. The linear analysis was performed because biaxial stress/strain material test data were not available for use in a nonlinear model. It is felt that the propellant material actually behaves in a nonlinear fashion. The case material is expected to be highly heated in the cookoff event. The high temperature effect upon the case may cause it to soften, and the material will go plastic before failure, both of which would likely cause non-linear material response. Due to the insulating effect of the pyrolysized gas, the propellant is expected to avoid these types of effects. The degree of nonlinearity will determine how valid or invalid the linear model performed here is. If the propellant and case stress-strain path to failure is fairly linear, then the results from this analysis should be reasonable. The lack of high temperature strength values for the propellant, liner and liner-case interface caused all the failure criteria to be based upon room temperature values. This discrepancy is probably the largest approximation used in this analysis. At the temperatures expected in the cookoff event, the strength of the case, propellant and the liner-case interface may be reduced greatly. This may not affect the strength of the propellant at the in-bore location 1, due to a lack of heat transfer to that location; but for the steel case, it would change the failure factors computed.

V. RECOMMENDATIONS

These recommendations are intended to provide the supporting data necessary to improve the cookoff rocket structural analysis reported here.

Since the propellant and liner material are rubber-like, and are expected to behave in a nonlinear stress-strain manner, material mechanical testing should be performed to characterize the propellant and possibly the liner. These tests should be done in an incremental manner, in order to describe the stress-strain path. Tests should also be done under biaxial tension, in order to derive constants for a nonlinear analysis. Ideally, these tests should be performed under a range of temperatures, up to temperatures where cookoff is expected to occur (300 - 400°F).

In order to obtain improved results for the liner-case bond strength, blister type tests should be performed with the proper liner and case materials. These type of tests should have bond failures in a very similar manner to the failure hypothesized in this analysis. This consistency should allow the determination of a critical K_I - K_{II} curve, or a critical pressure or stress value for use in determining crack/bubble growth. These tests should also be performed under a range of temperatures, up to the expected cookoff values.

In order to improve the numerical simulation, a nonlinear code such as TEXLESP or MARC should be used in further analysis. The nonlinear analysis will be substantially more expensive, but will give results which should be closer to the actual conditions. The current versions of TEXLESP would be hindered by their lack of a crack tip node and crack elements, but these elements are available in codes such as MARC. Three dimensional models should also be constructed and run, to determine how much variation exists with the simpler, less expensive flat plate models. The amount of variation will determine whether sufficient accuracy can be obtained with the flat plate model.

REFERENCES

1. CPIA Solid Propellant Manual, March 1979.

2. Geyer, W. H. and B. Saltzman, Rocket Motor Case-to-Insulation Peel Strength in the Cookoff Environment, NWCTM5075, July 1983.

3. Telephone conversation with Wayne Geyer, Naval Weapons Center, China Lake, CA, March 1986.

4. Telephone conversation with Randy James, Anatech, La Jolla, CA, March 1986.

5. American Society for Metals, Handbook Number One, Eighth Edition, 1961.

6. Fung, M. L., T. Casper, T. Hicks, R. Vetter, Thermal Modeling of Insulator/Liner, NWCTP 6336, August 1982.

7. Burton, J. D. and B. C. Harber, Application of Fracture Mechanics to Predicting Failures in Solid Propellants, AFRPL-TR-70-62, May 1970.

APPENDIX A

This appendix contains the plots of the initial and deformed geometry of the different rocket models. The stresses and stress intensity factors from these runs are reported in Section III.A. For each model, there is a plot of the undeformed geometry, a full scale plot of the deformed geometry, and an enlargement of the deformed crack tip region. For the models with some liner elements removed, a plot of the undeformed crack tip region is also included. The scale on all of the deformed graphs is 1.0.

Undeformed Geometry

Propellant Thickness = minimum

Crack Length = 0.5 in.

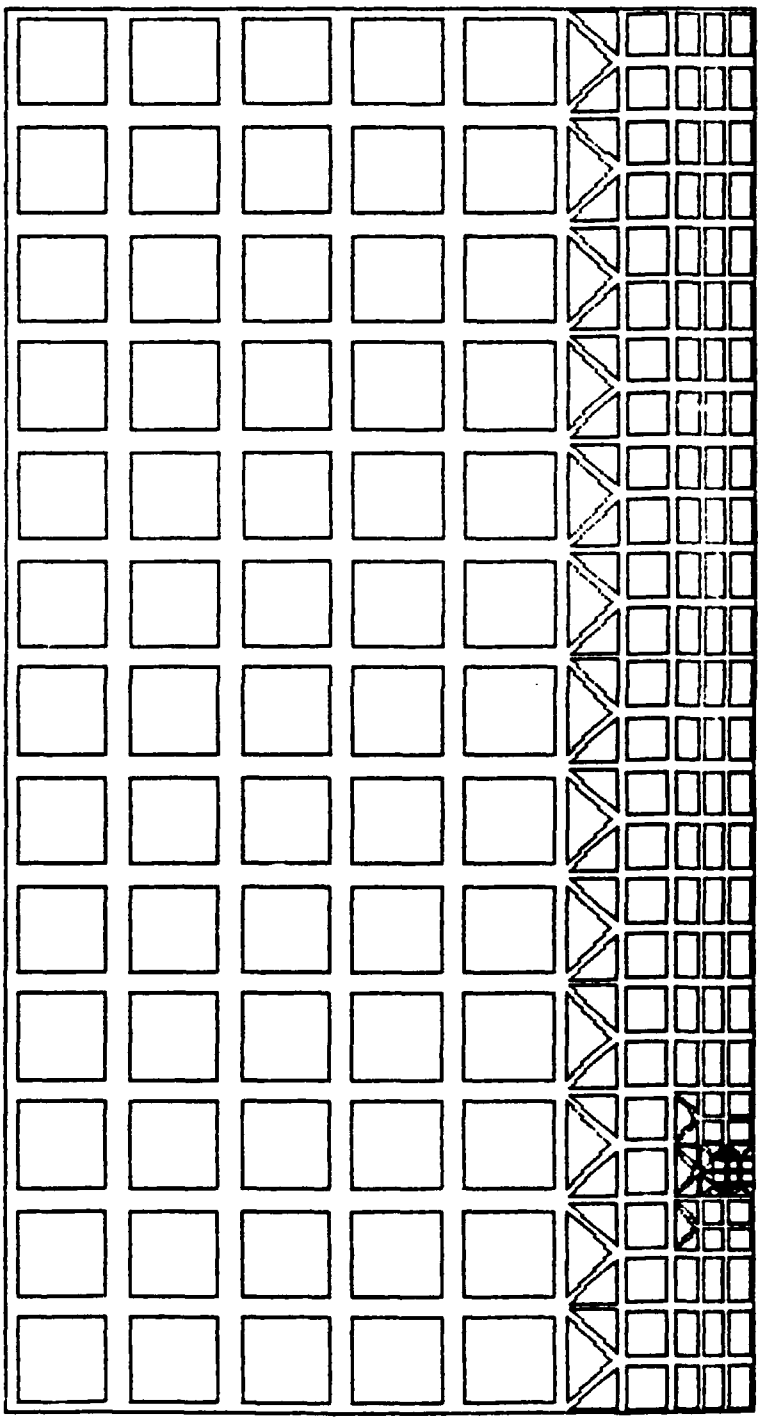

FIGURE A1

Deformed Geometry

Propellant Thickness = minimum

Crack Length = 0.5 in.

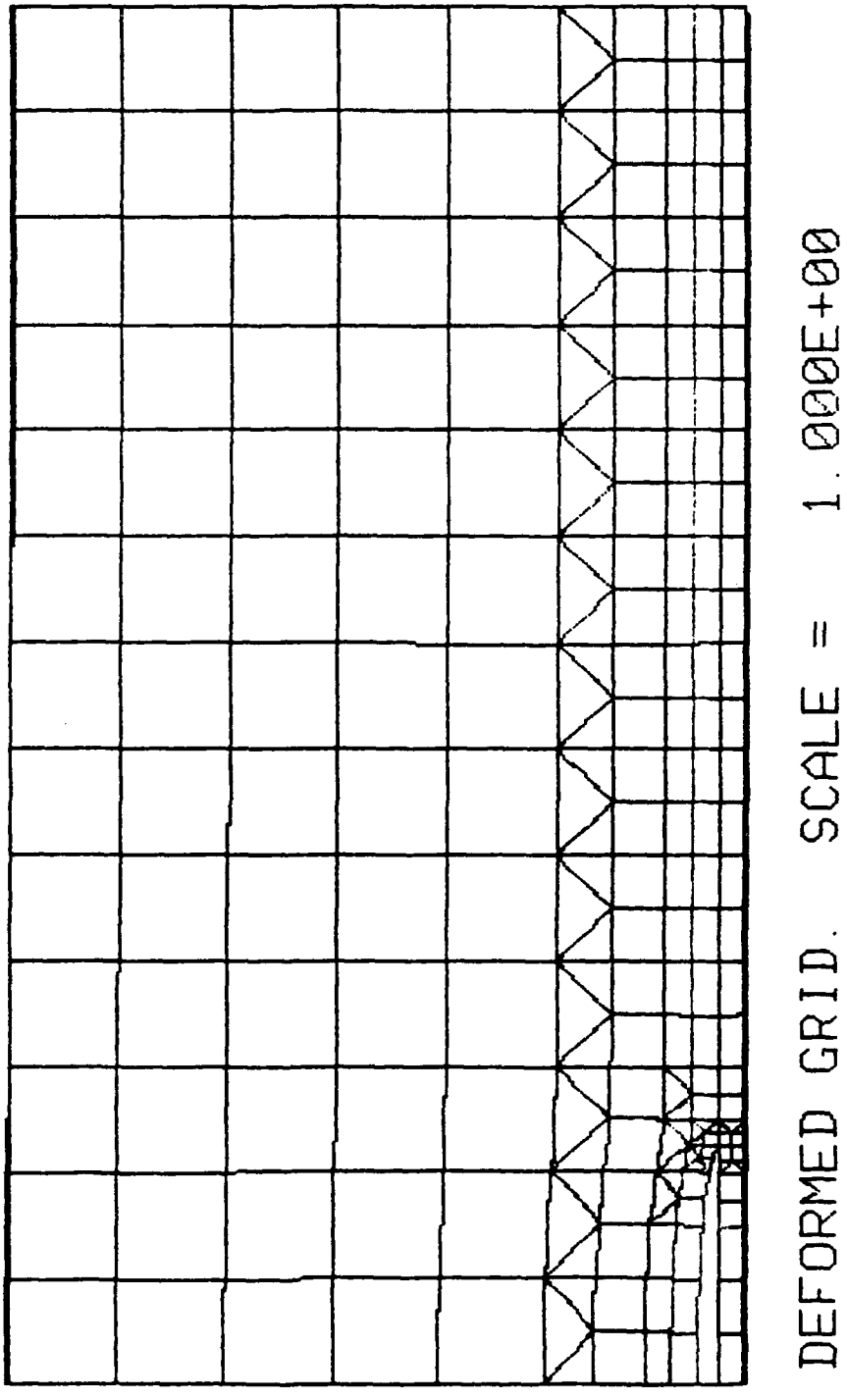

FIGURE A2

Deformed Close-up

Propellant Thickness = minimum

Crack Length = 0.5 in.

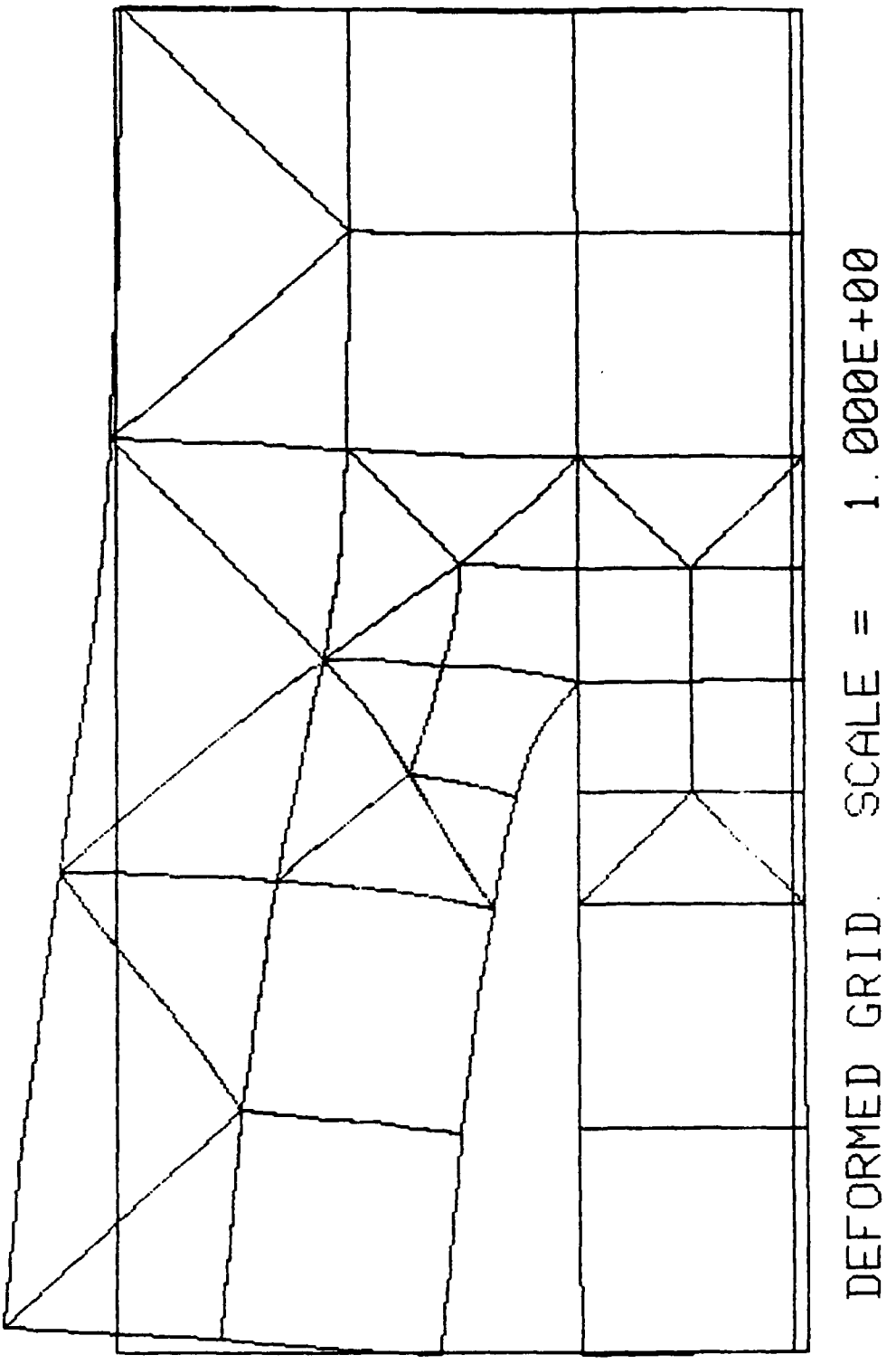

FIGURE A3

Undeformed Geometry

Propellant Thickness = minimum

Crack Length = 1.0 in.

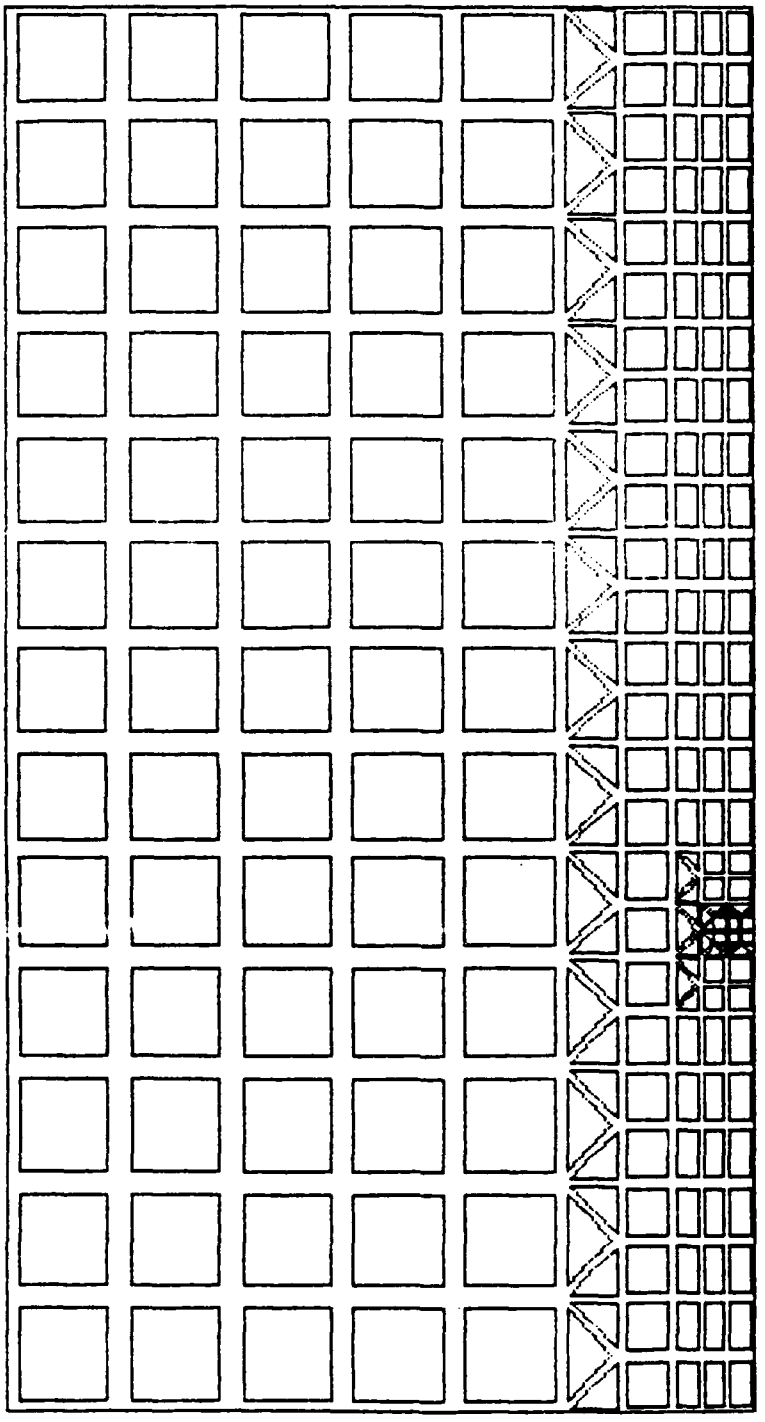

FIGURE A4

Deformed Geometry

Propellant Thickness = minimum

Crack Length = 1.0 in.

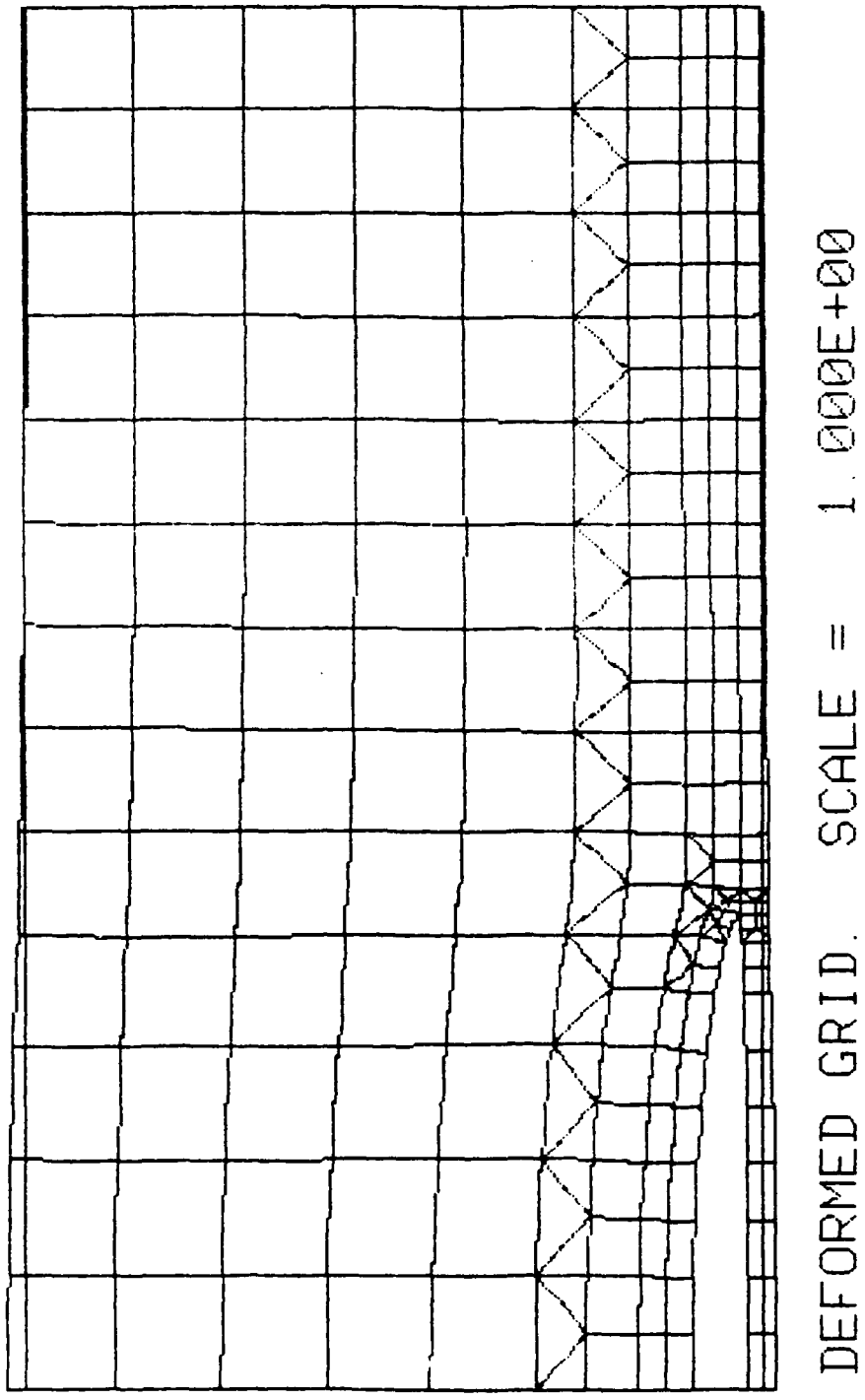

FIGURE A5

Deformed Close-up

Propellant Thickness = minimum

Crack Length = 1.0 in.

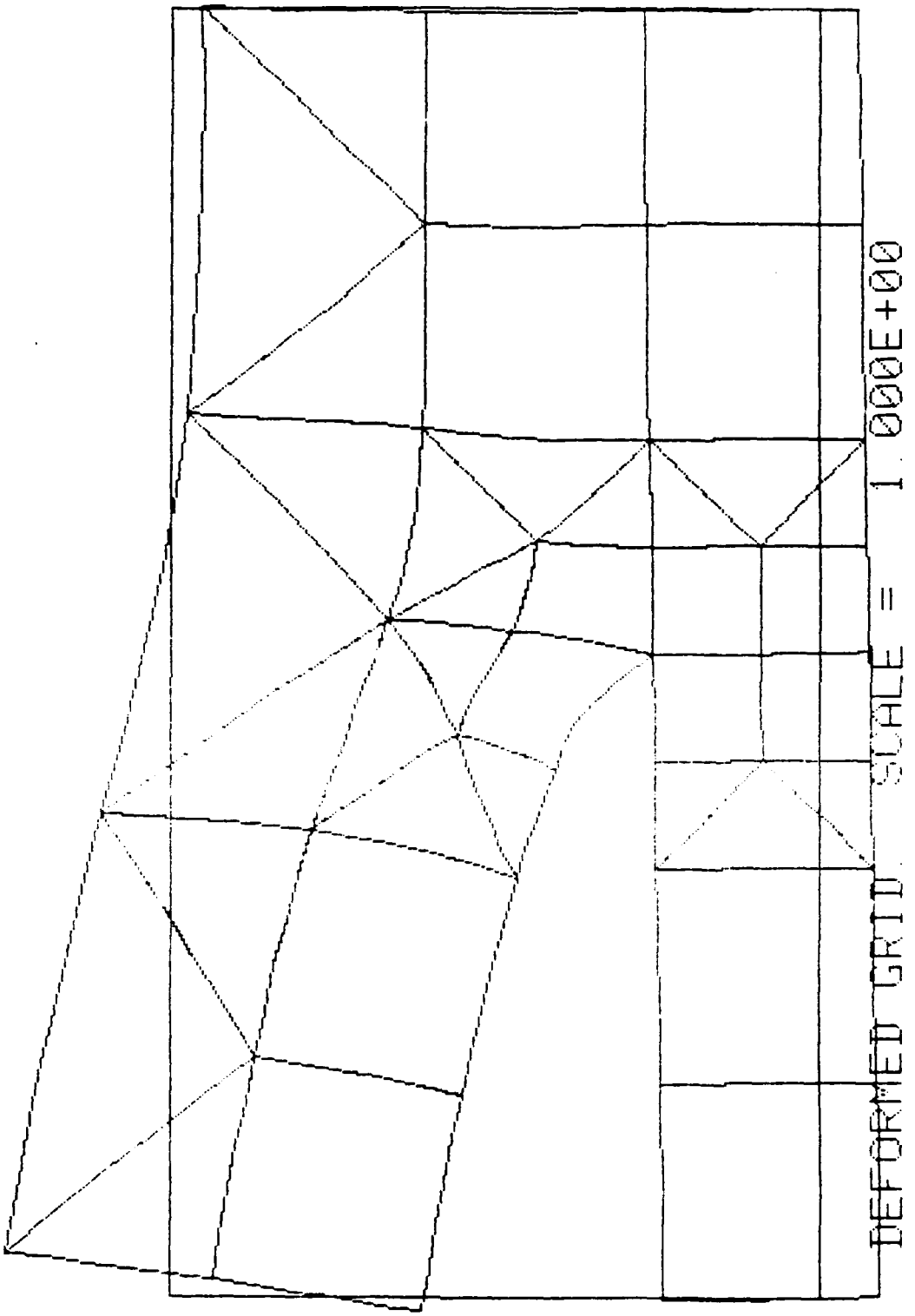

FIGURE A6

Undeformed Geometry

Propellant Thickness = maximum

Crack Length = 0.5 in.

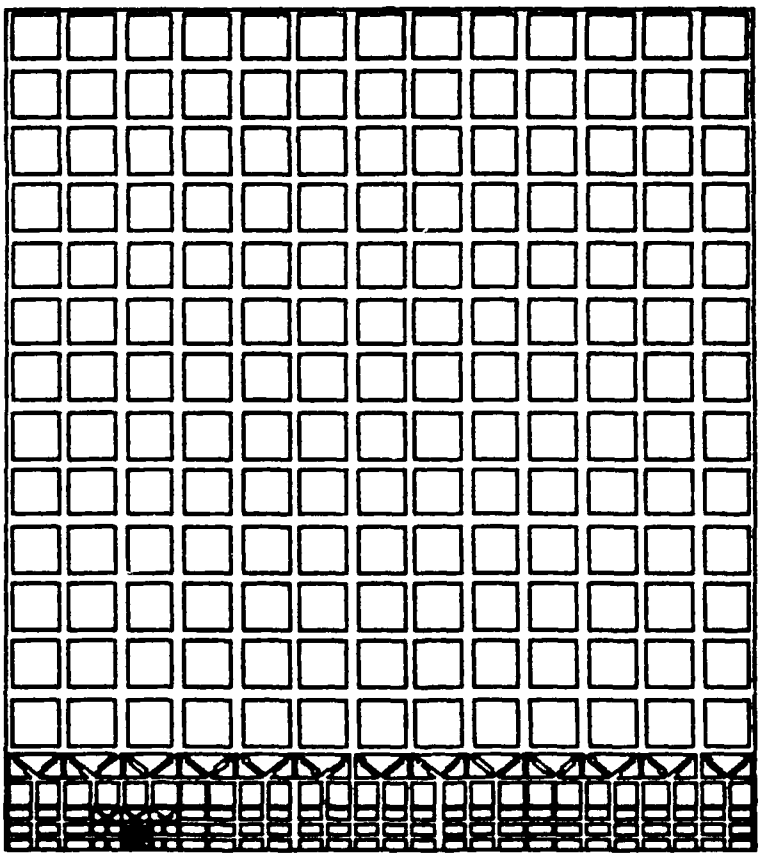

ELEMENTS

FIGURE A7

Deformed Geometry

Propellant Thickness = maximum

Crack Length = 0.5 in.

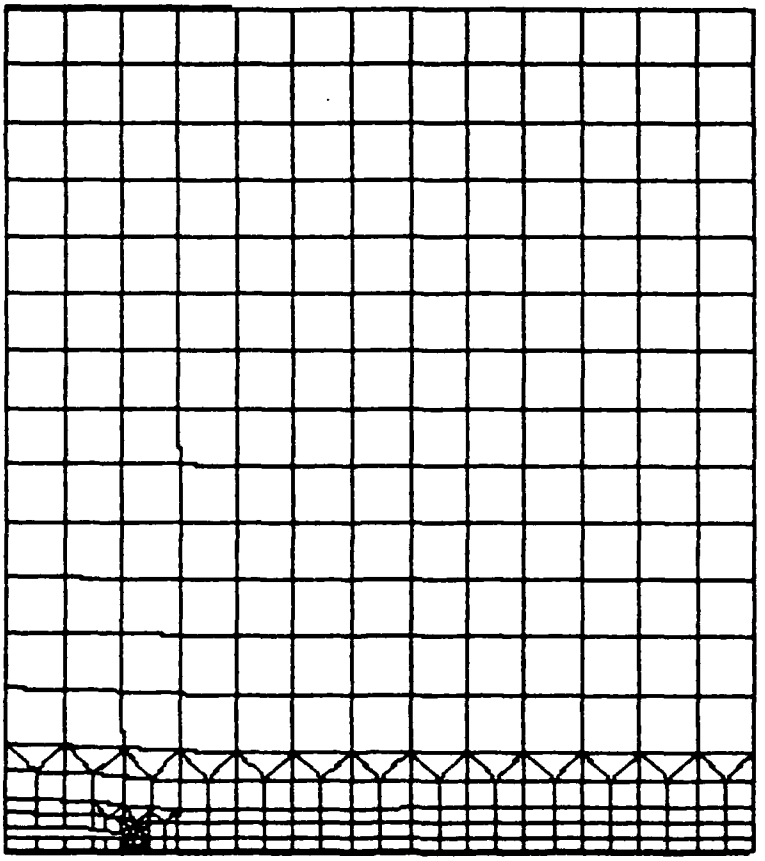

DEFORMED GRID. SCALE = 1.1

FIGURE A8

Deformed Close-up

Propellant Thickness = maximum

Crack Length = 0.5 in.

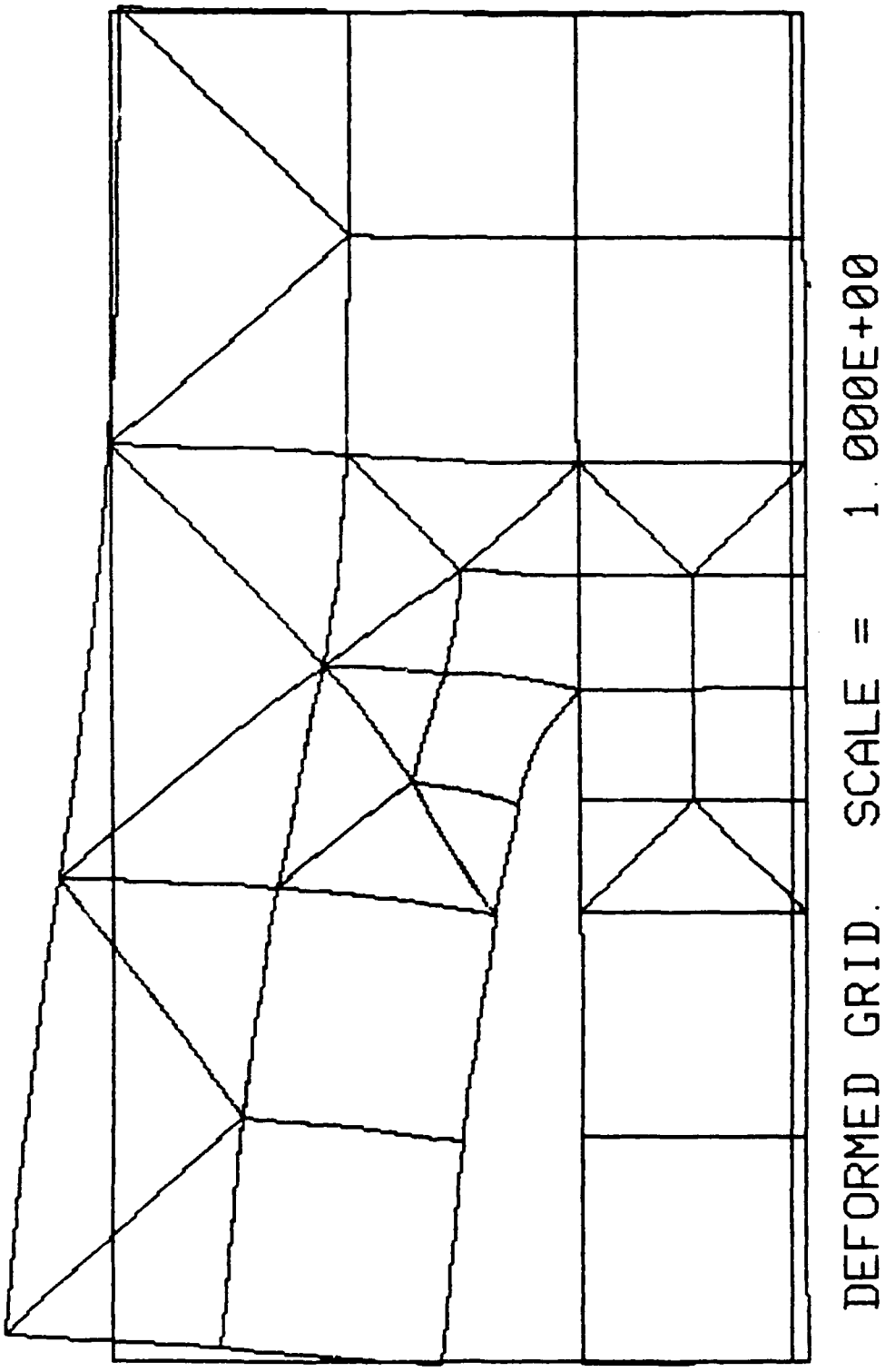

FIGURE A9

Undeformed Geometry

Propellant Thickness = maximum

Crack Length = 1.0 in.

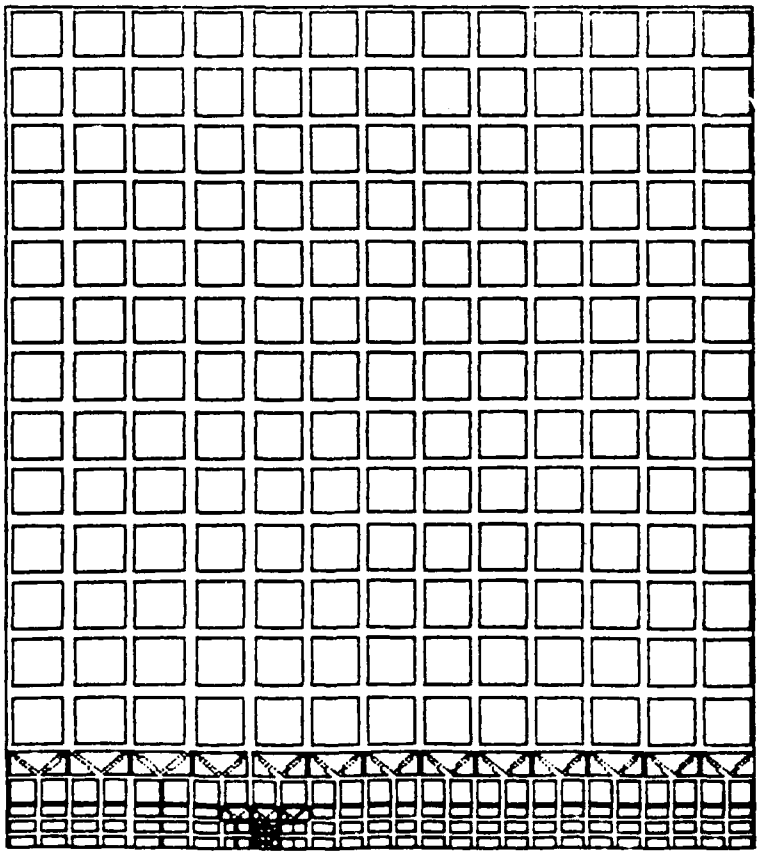

ELEMENTS

FIGURE A10

Deformed Geometry

Propellant Thickness = maximum

Crack Length = 1.0 in.

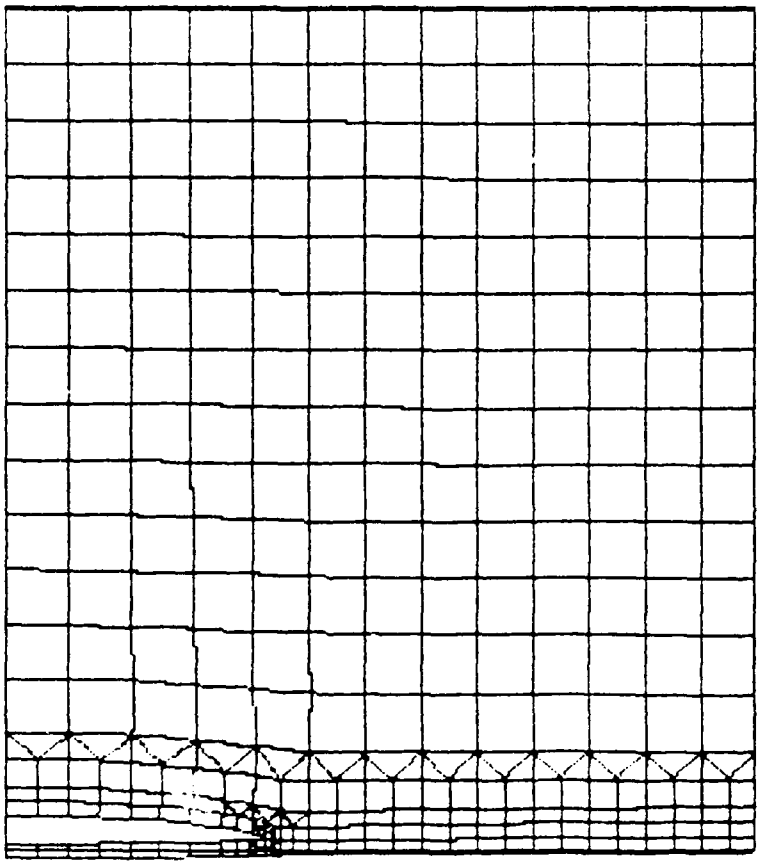

FIGURE A11

Deformed Close-up

Propellant Thickness = maximum

Crack Length = 1.0 in.

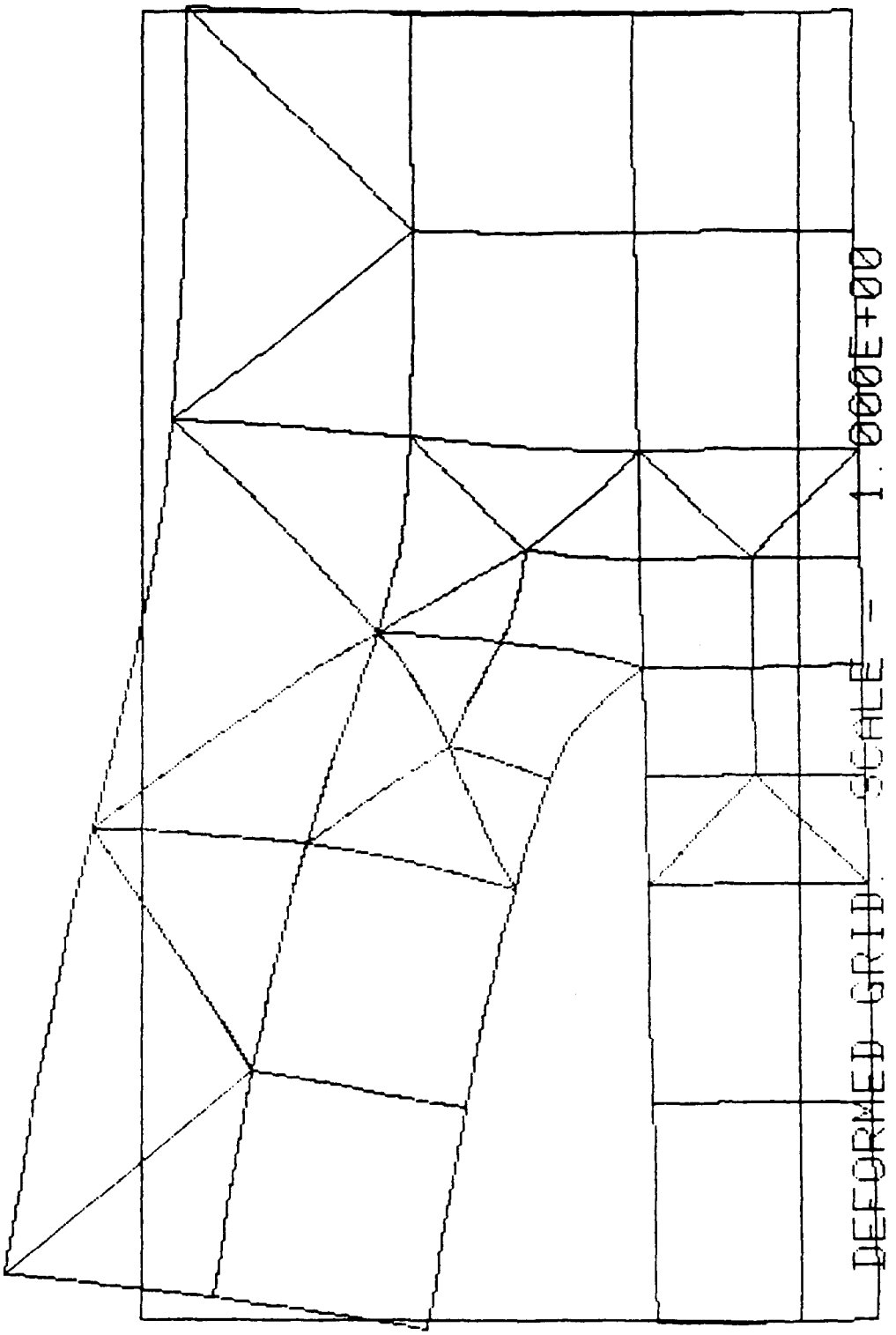

FIGURE A12

Undeformed Geometry
Some Liner Removed

Propellant Thickness = minimum

Crack Length = 0.5 in.

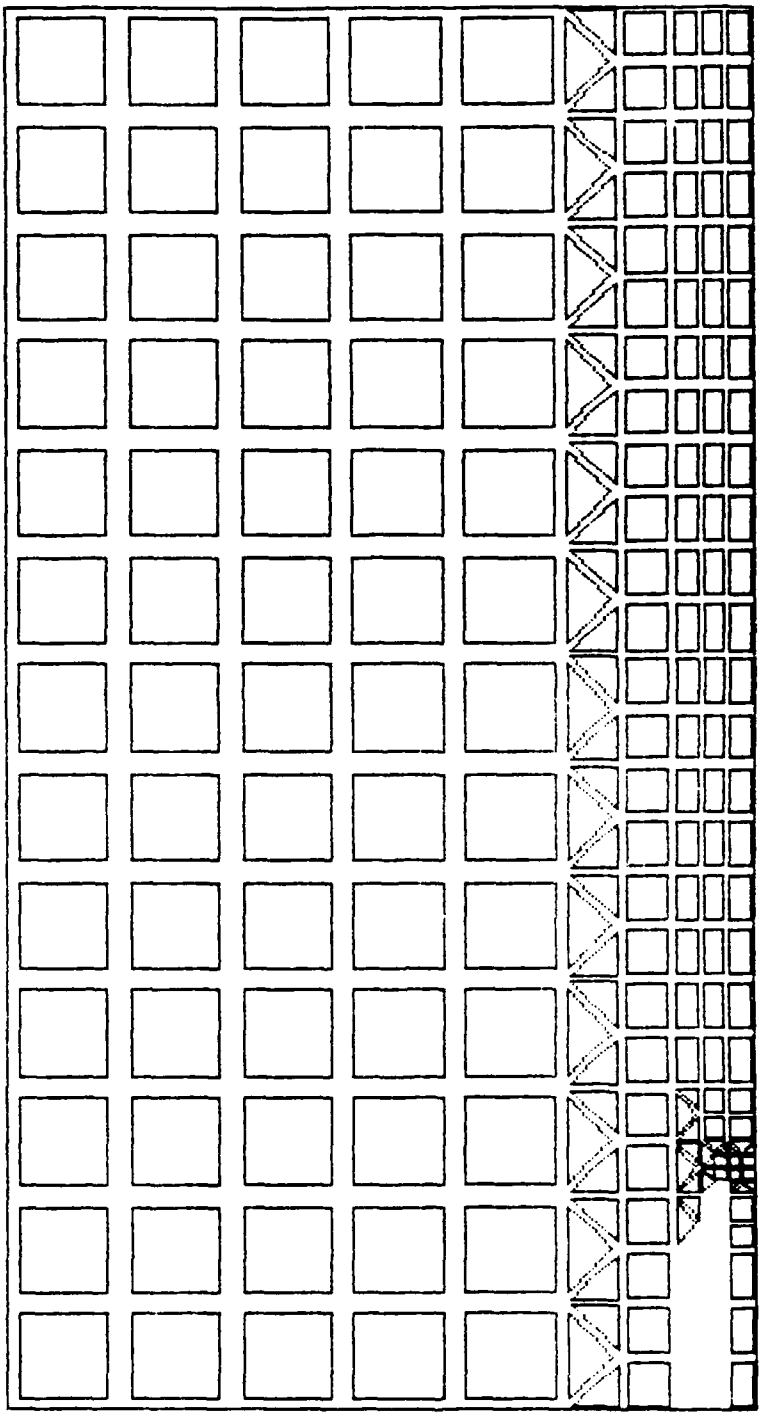

FIGURE A13

Undeformed Geometry Close-up
Some Liner Removed

Propellant Thickness = minimum

Crack Length = 0.5 in.

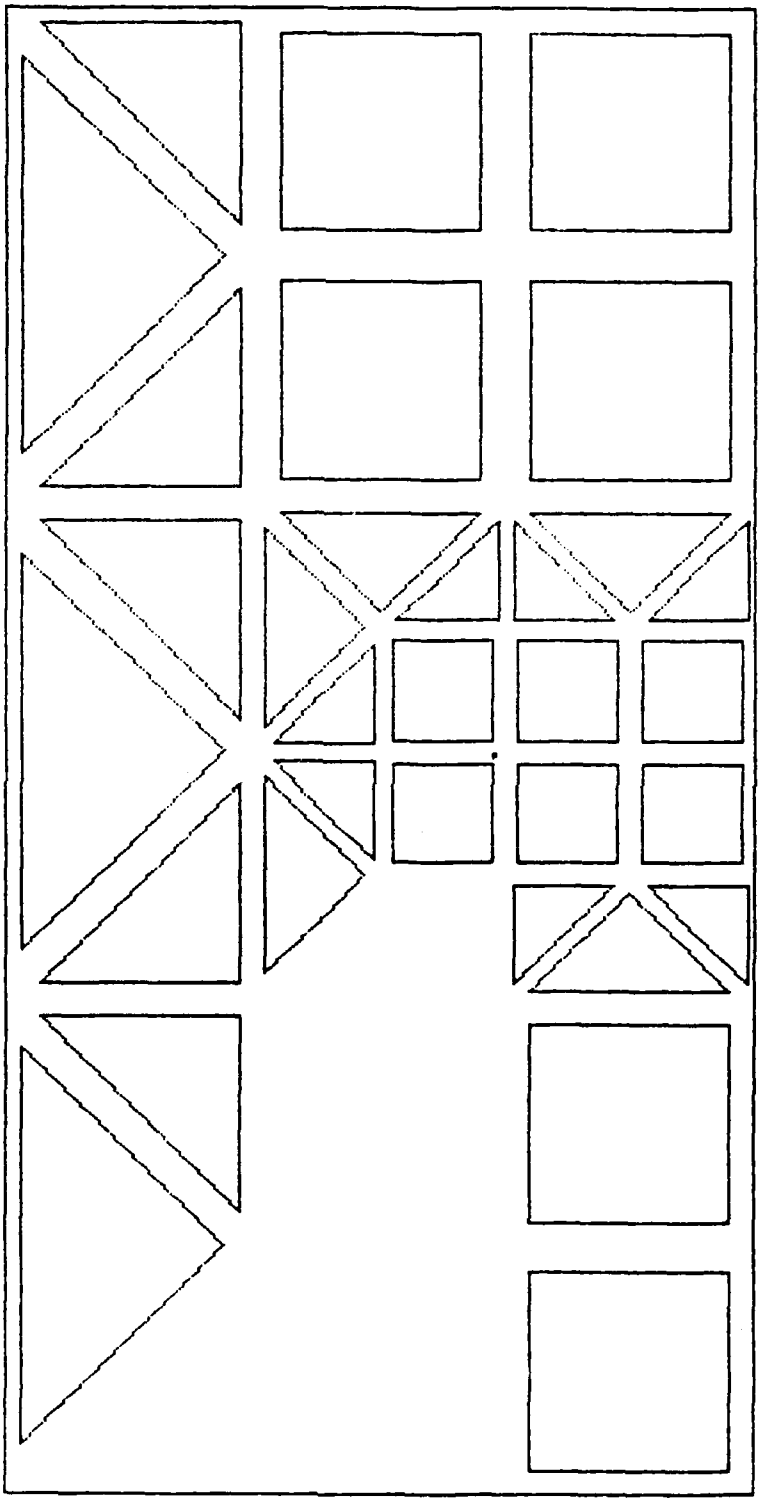

FIGURE A14

Deformed Geometry
Some Liner Removed

Propellant Thickness = minimum

Crack Length = 0.5 in.

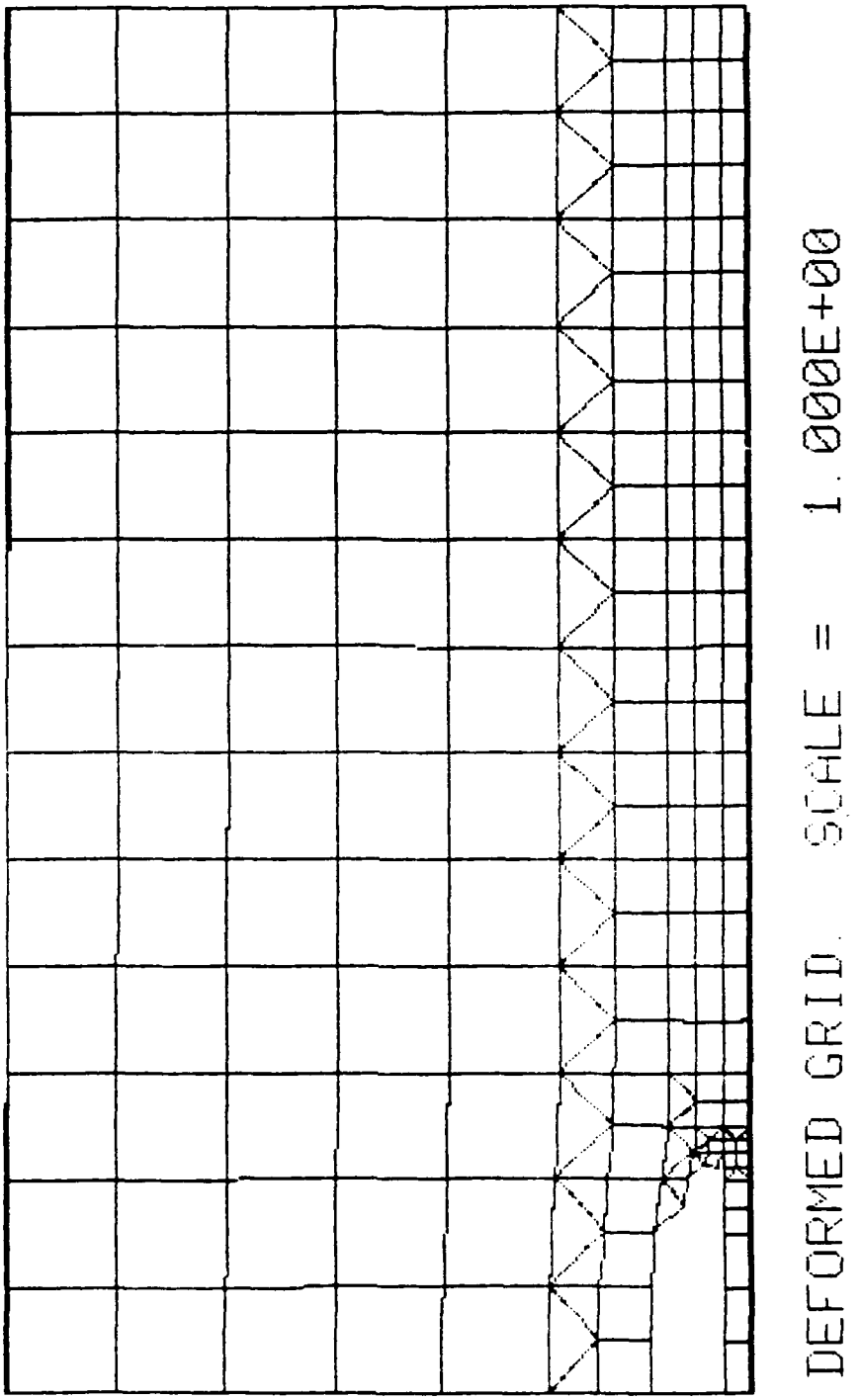

FIGURE A15

Deformed Close-up
Some Liner Removed

Propellant Thickness = minimum

Crack Length = 0.5 in.

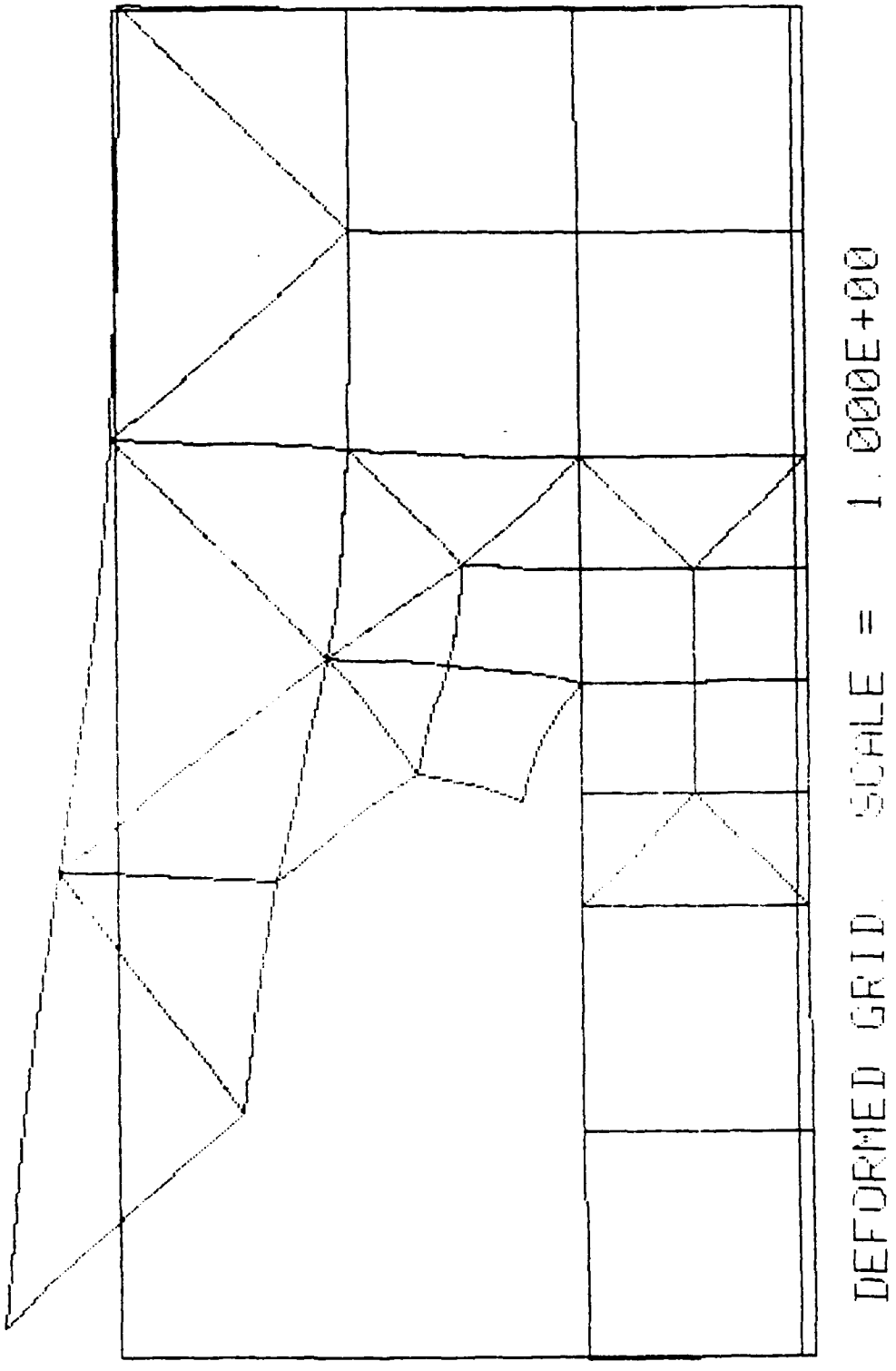

FIGURE A16

Undeformed Geometry
Some Liner Removed

Propellant Thickness = minimum

Crack Length = 1.0 in.

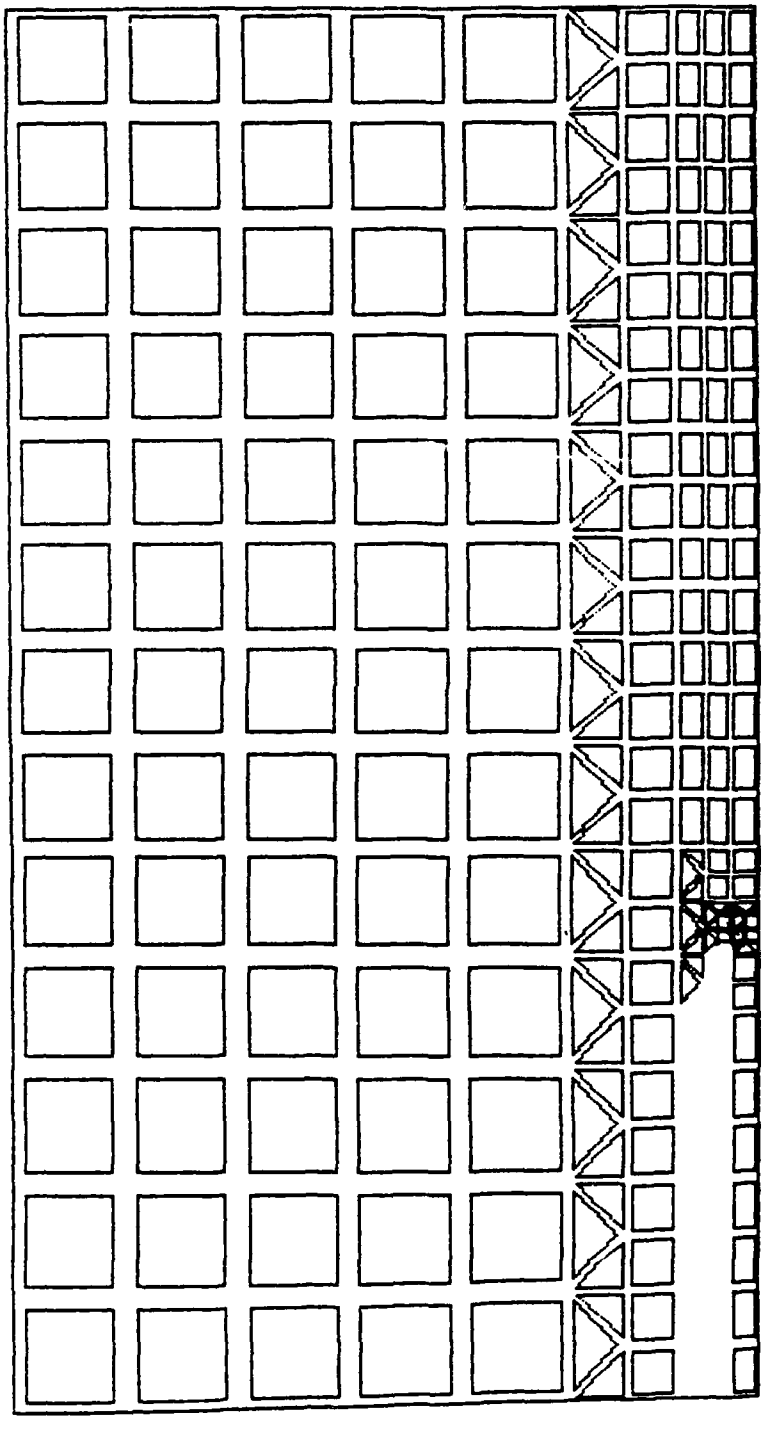

FIGURE A17

Undeformed Geometry Close-up
Some Liner Removed

Propellant Thickness = minimum

Crack Length = 1.0 in.

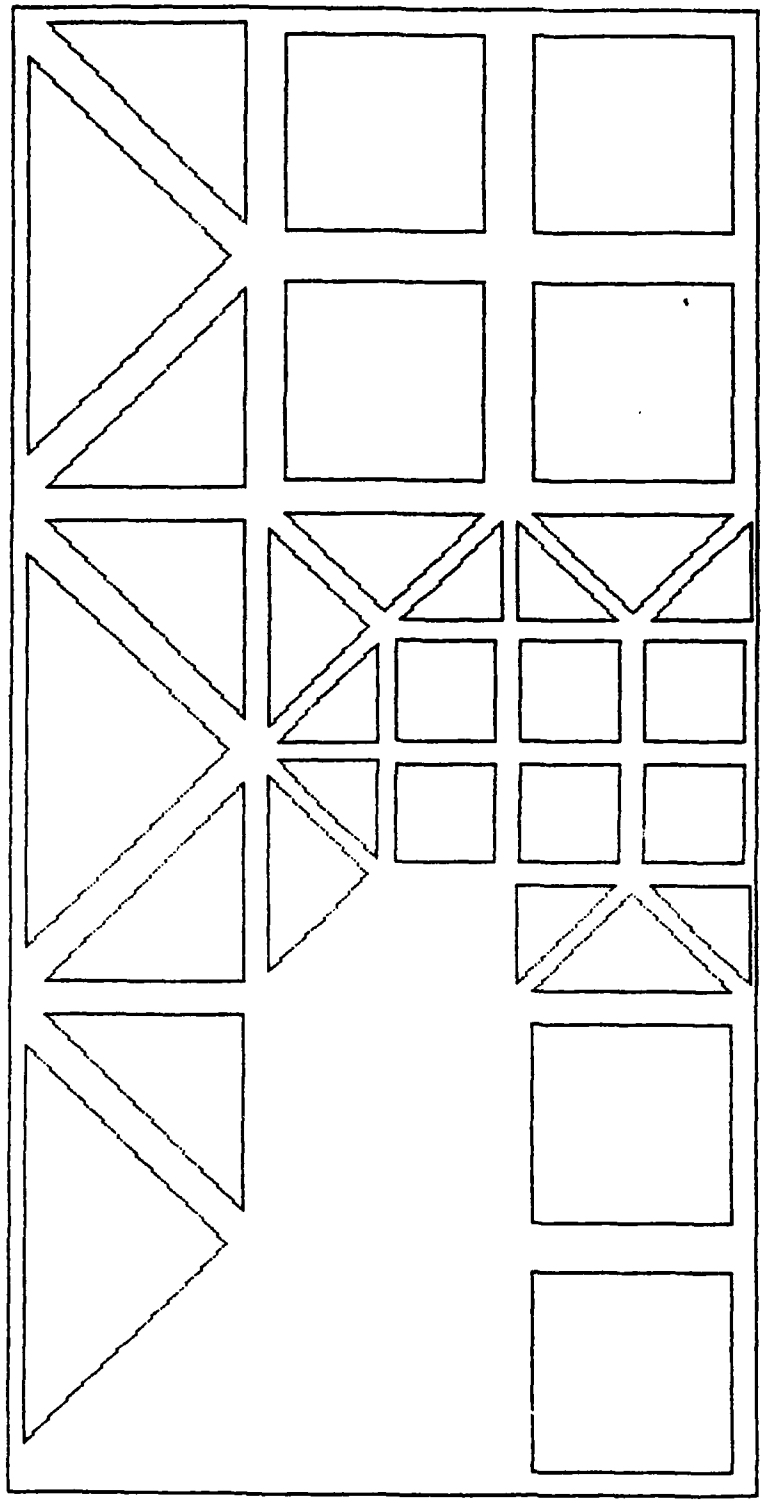

FIGURE A18

Deformed Geometry
Some Liner Removed

Propellant Thickness = minimum

Crack Length = 1.0 in.

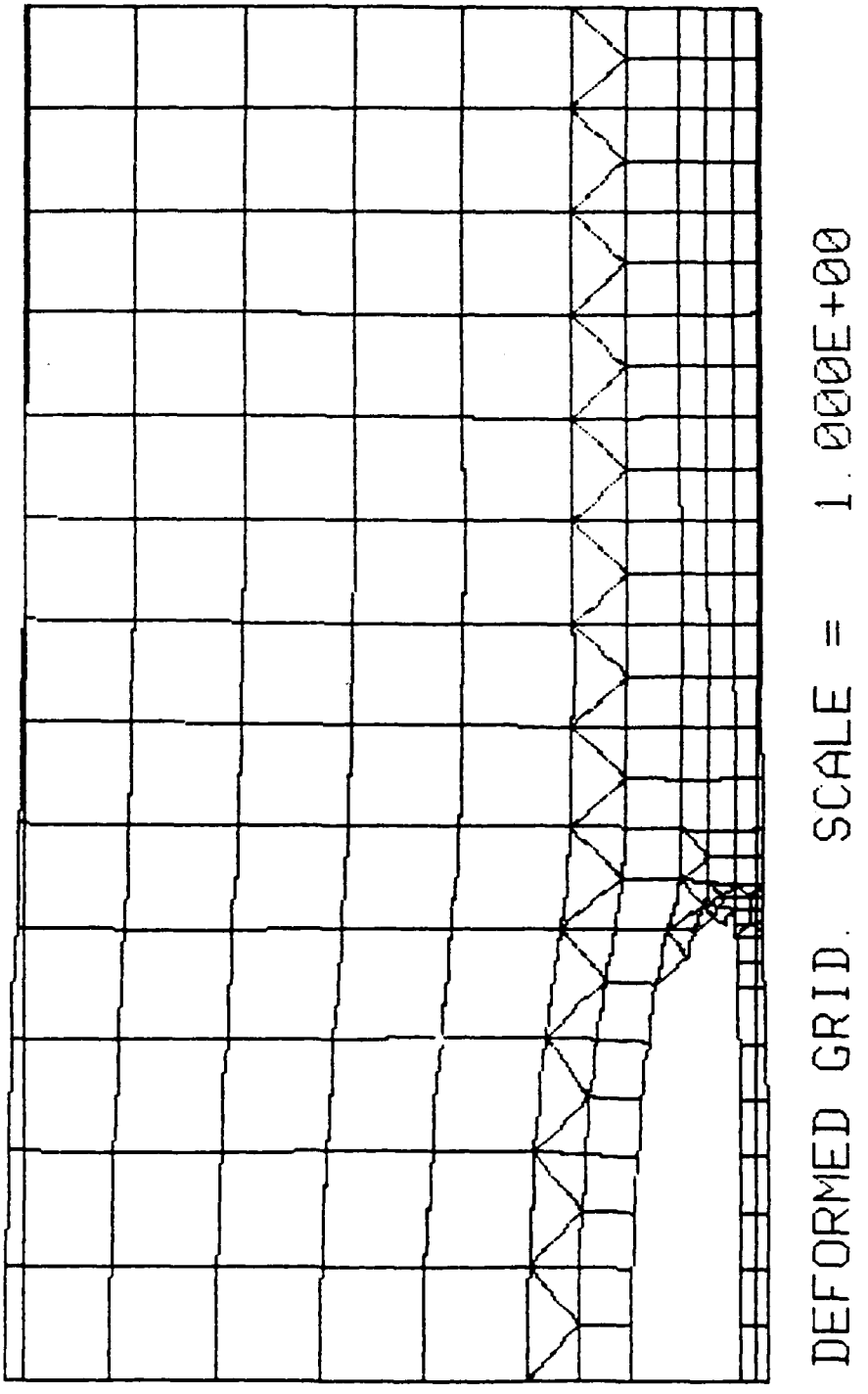

FIGURE A19

Deformed Close-up
Some Liner Removed

Propellant Thickness = minimum

Crack Length = 1.0 in.

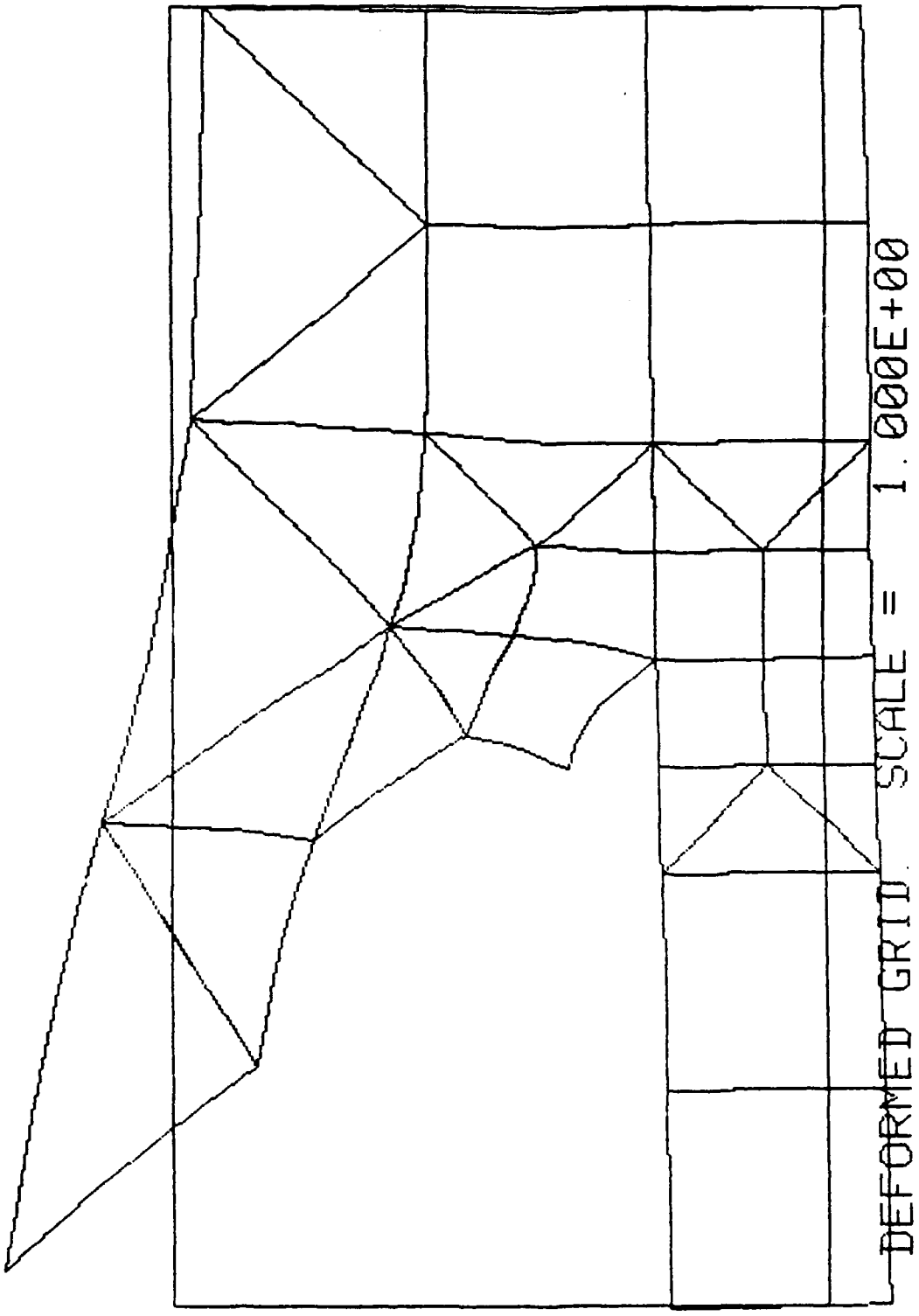

FIGURE A20

APPENDIX B

This appendix contains the plots of the initial and deformed geometry for each angle of the peel test models (49°, 73°, 90°). The stresses, strains, and stress intensity factors from these runs are reported in Section III.B. For each model, there is a plot of the undeformed geometry, a full scale plot of the deformed geometry, and an enlargement of the deformed crack tip region. The scale on all of the deformed graphs is 1.0.

Undeformed Geometry

Peel Angle = 49°

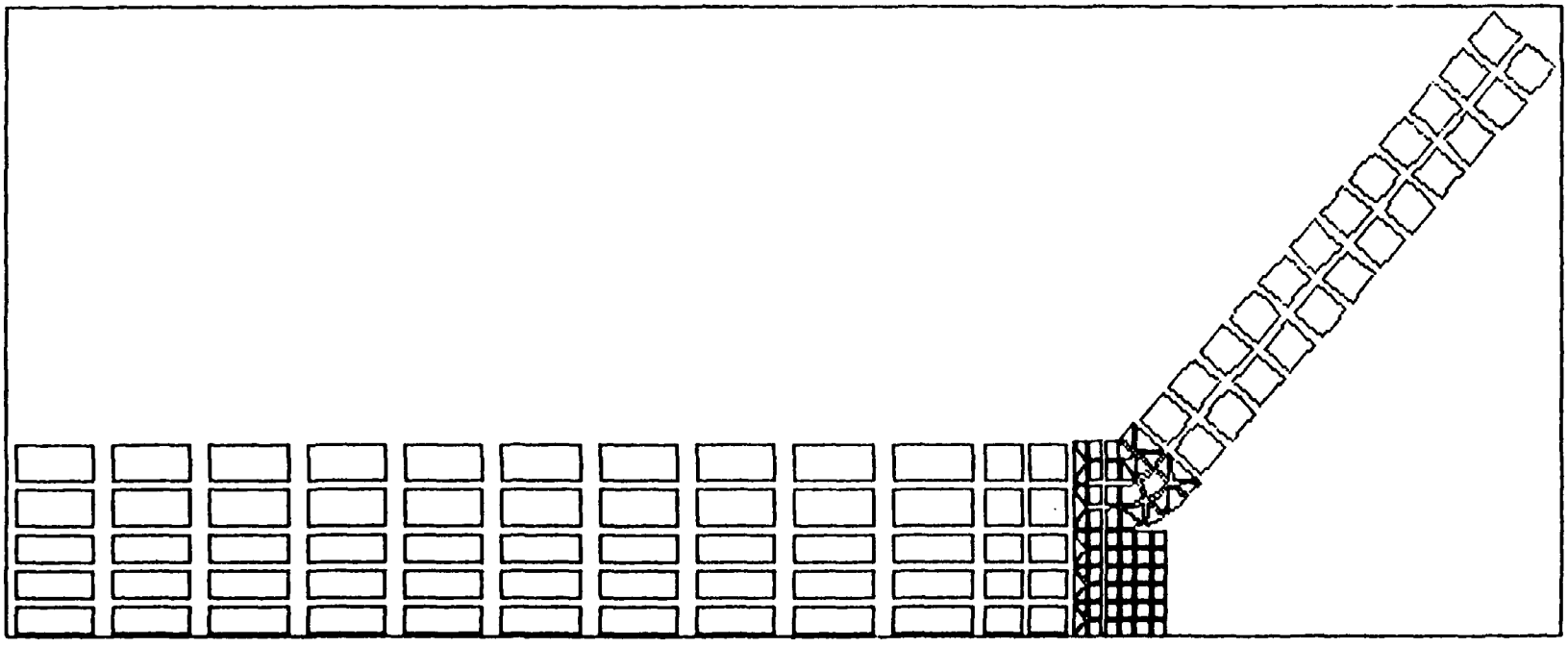

FIGURE B1

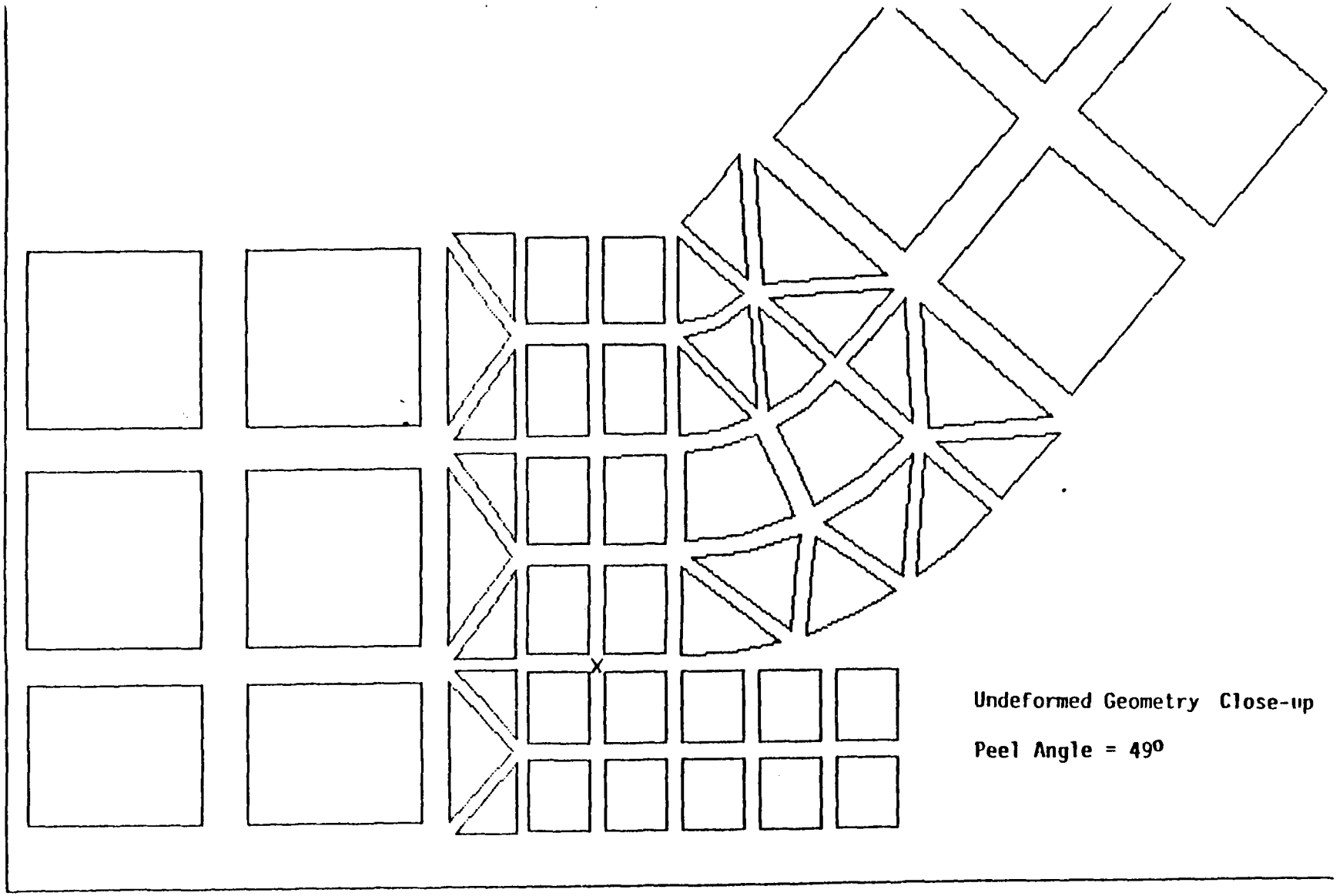

FIGURE B2

Deformed Geometry

Peel Angle = 49°

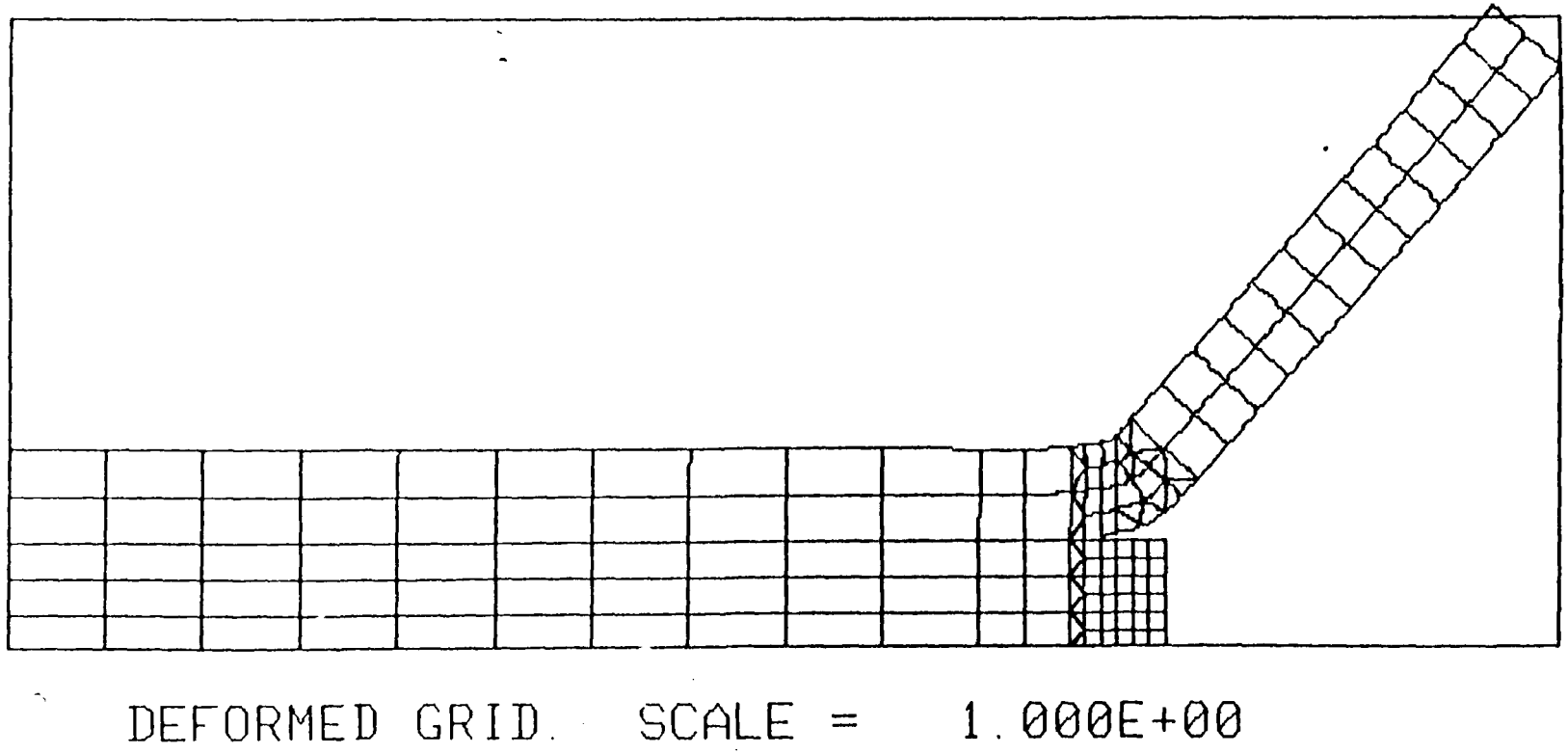

FIGURE B3

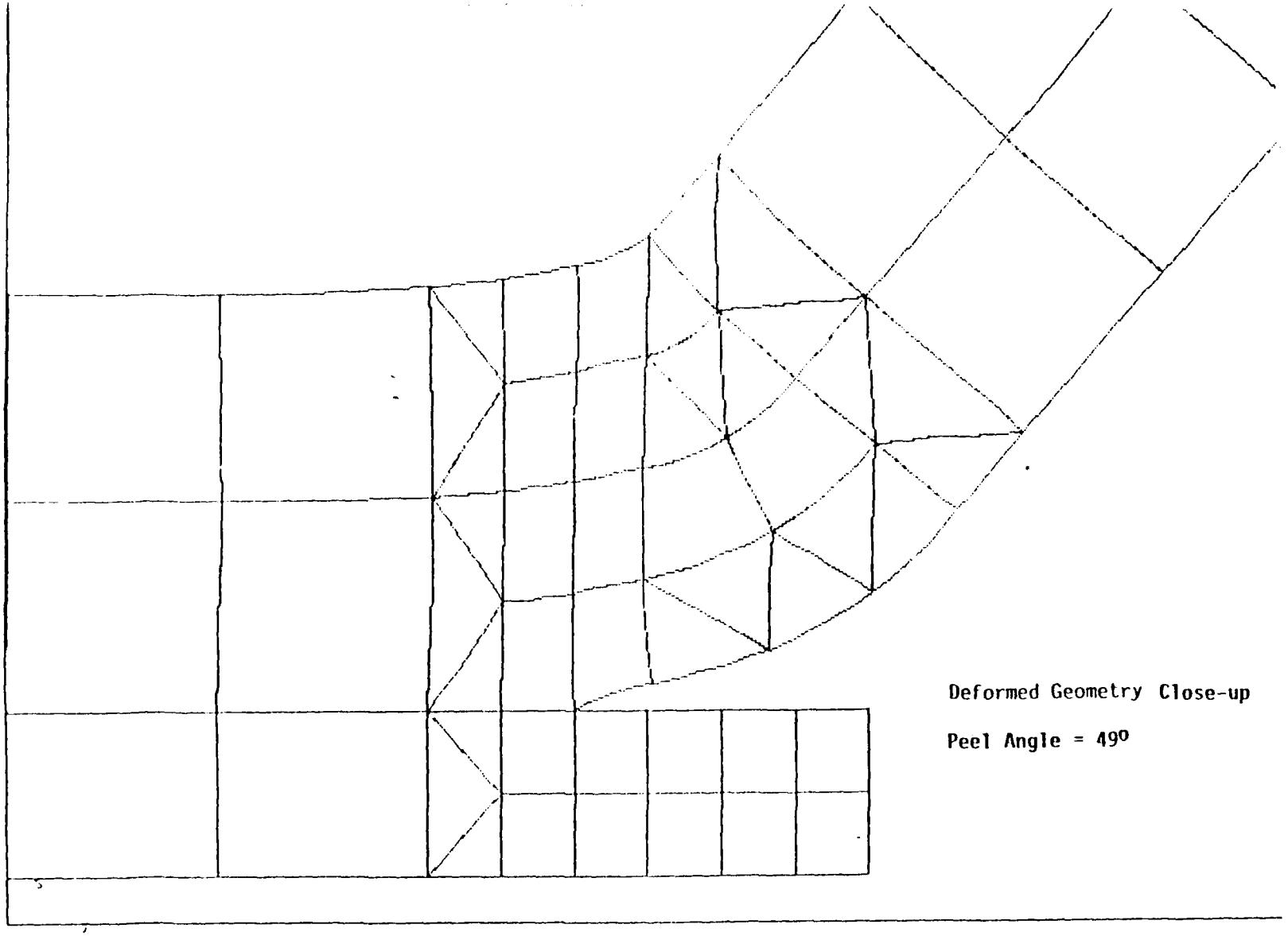
Deformed Geometry Close-up
Peel Angle = 49°
DEFORMED GRID SCALE = 1.000E+00

FIGURE B4

Undeformed Geometry

Peel Angle = 73°

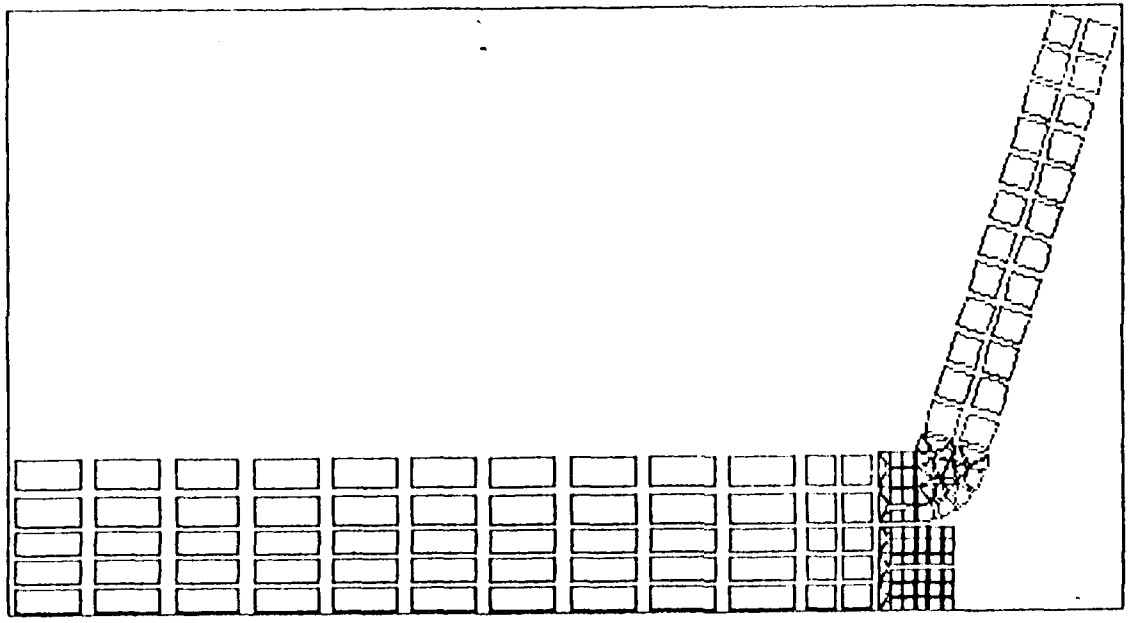

FIGURE B5

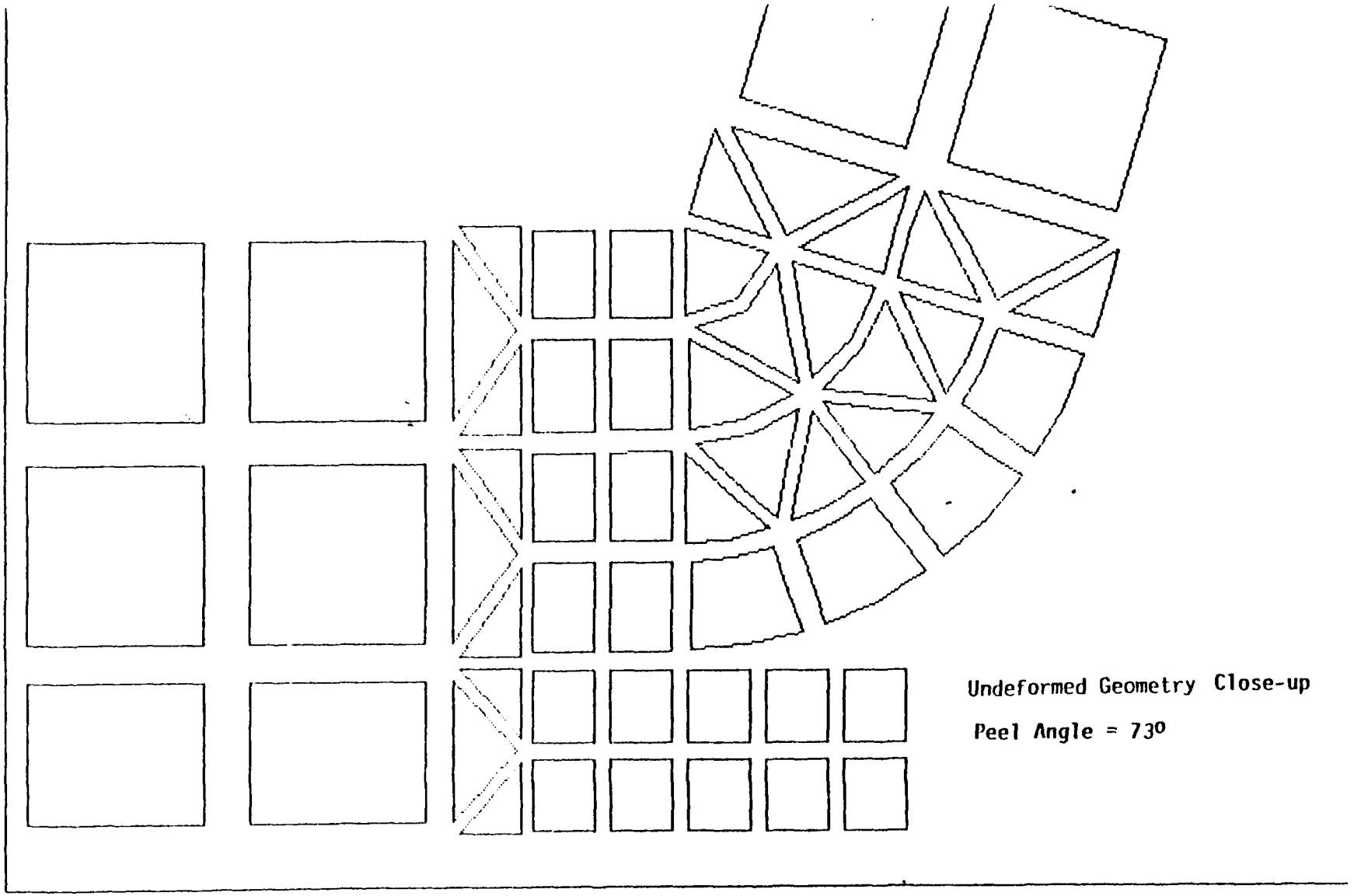

FIGURE B6

Deformed Geometry

Peel Angle = 73°

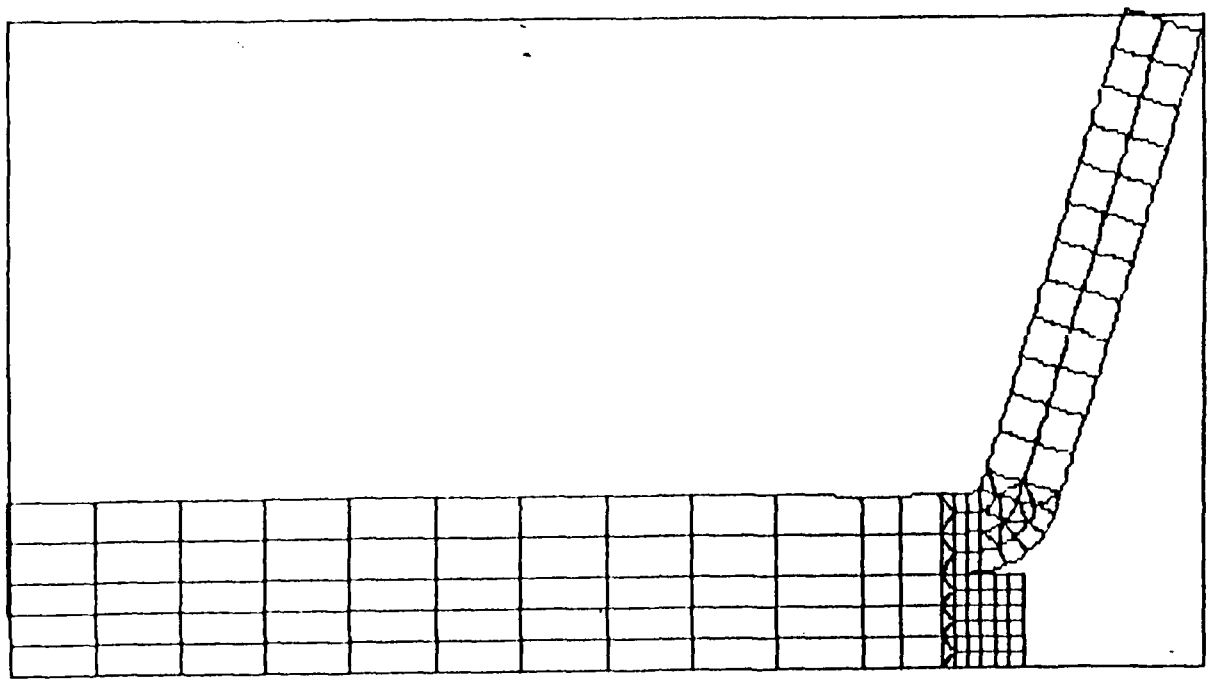

FIGURE B7

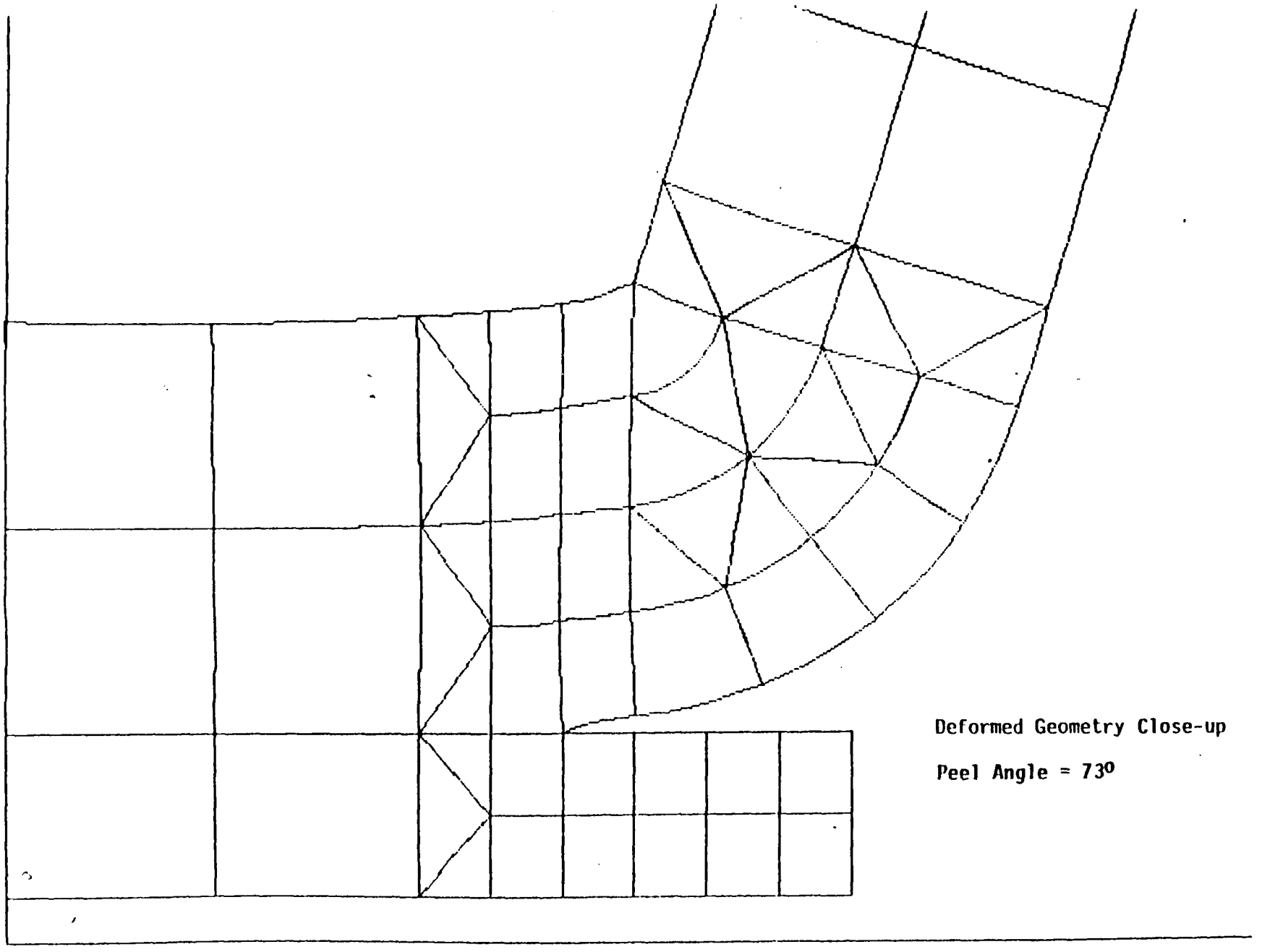
Deformed Geometry Close-up
Peel Angle = 73°
DEFORMED GRID. SCALE = 1.000E+00

FIGURE B8

Undeformed Geometry

Peel Angle = 90°

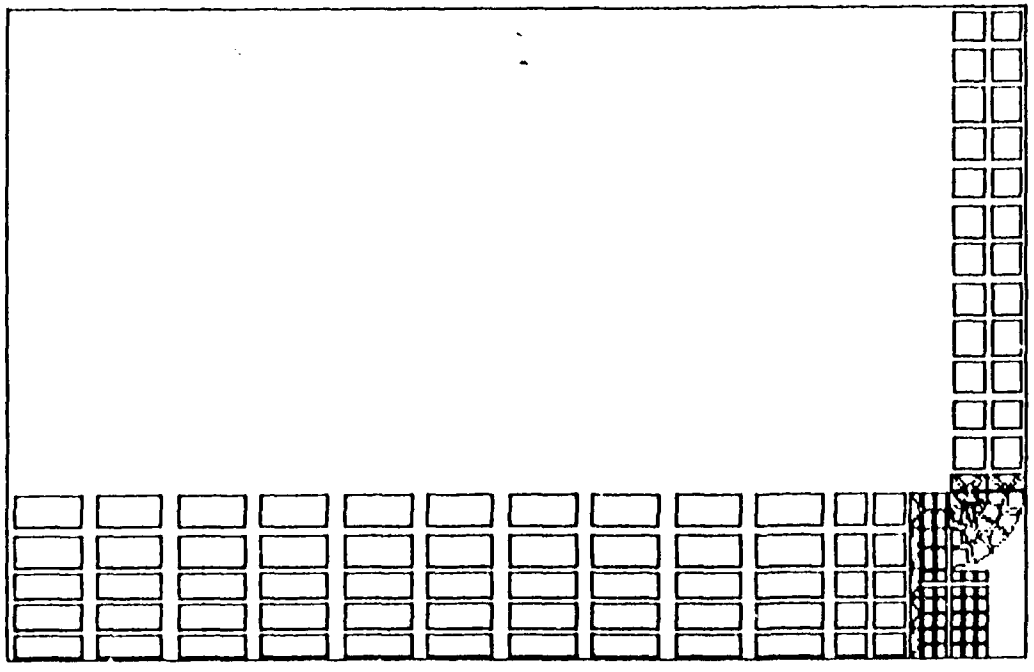

FIGURE B9

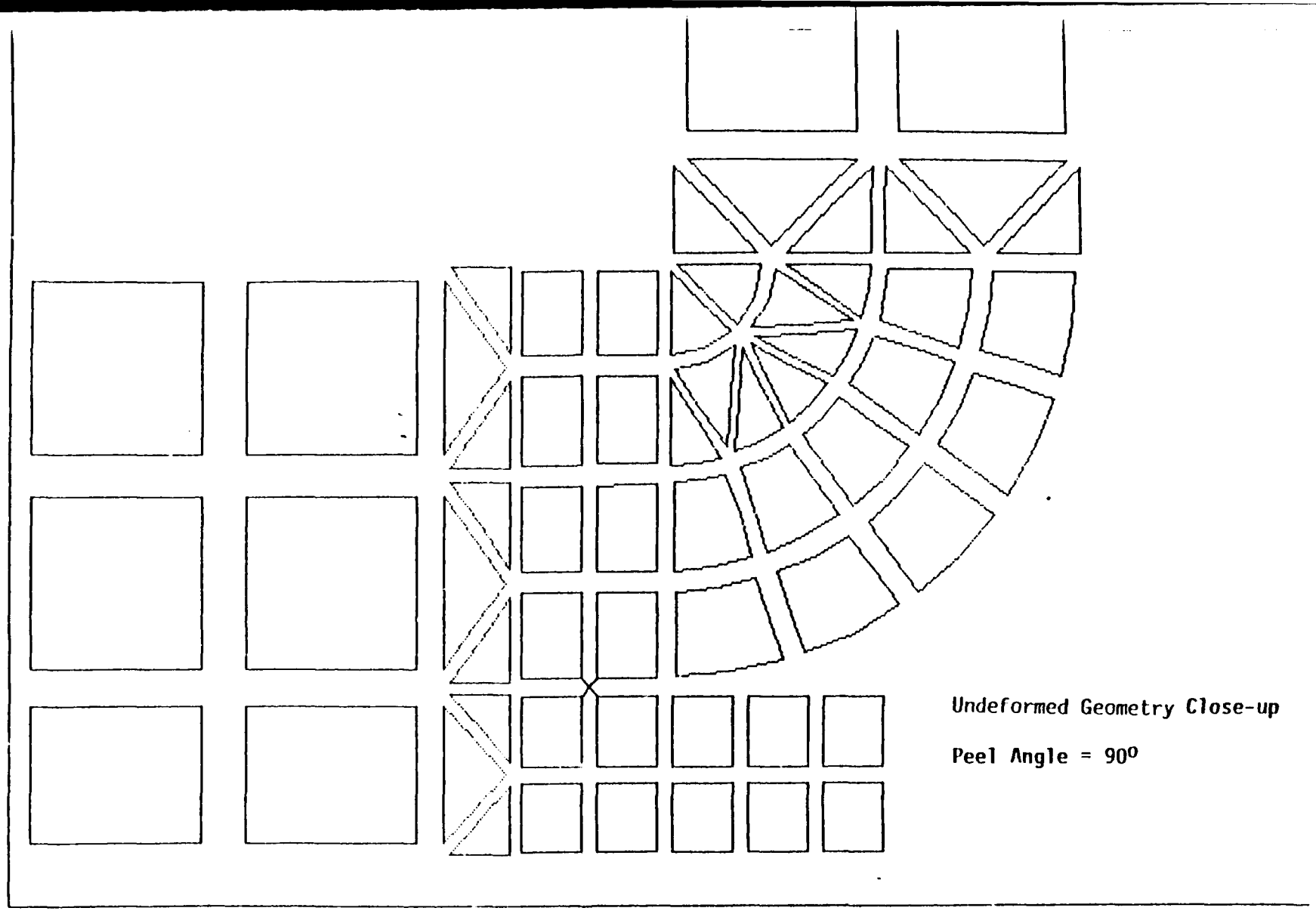

FIGURE B10

Deformed Geometry

Peel Angle = 90°

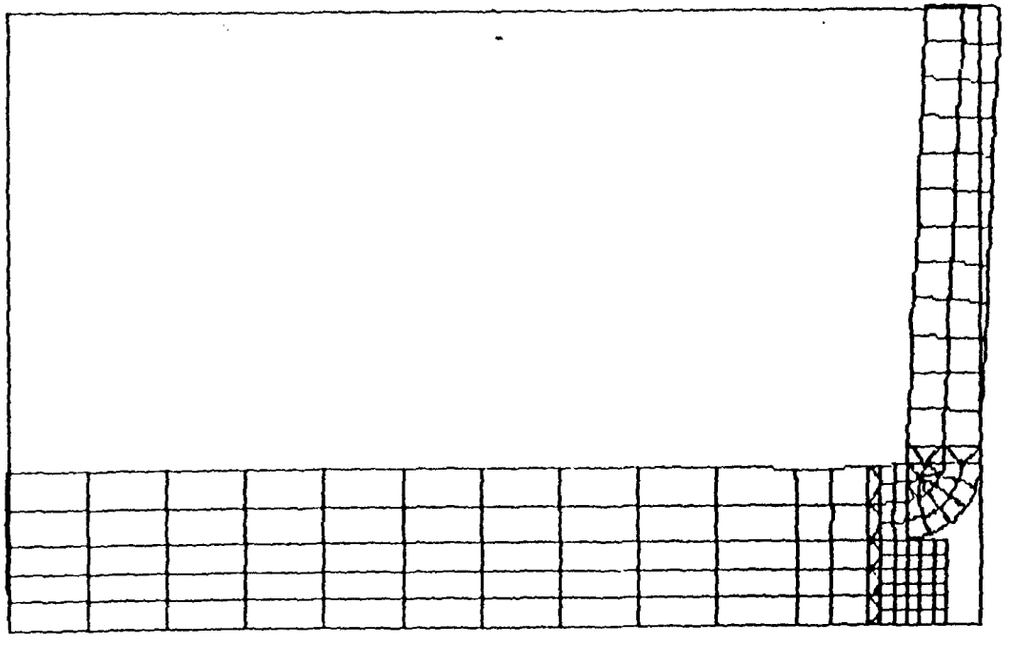

FIGURE B11

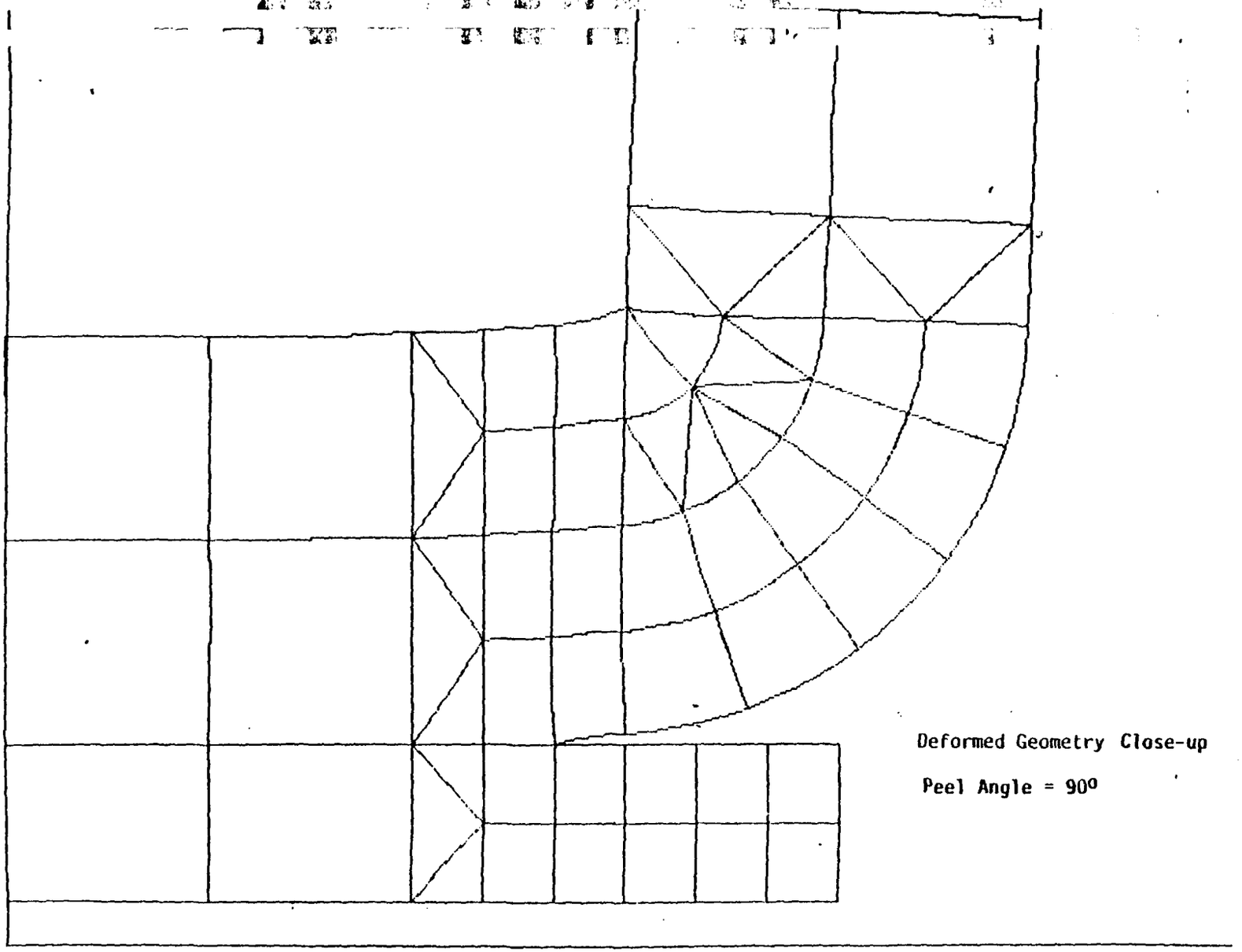

DEFORMED GRID. SCALE = 1.000E+00

FIGURE B12